ON THE USE OF TIME AND CORRELATION WINDOWS FOR NON-PARAMETRIC SPECTRAL ANALYSIS

A thesis presented for the degree of Doctor of Philosophy in the Department of Engineering, University of Warwick, by

P.M. Obene., B.Sc(Hons).

December 1990

Contents

Acknowledgements.

I would like to thank my supervisor, Professor J.L. Douce, for his technical, consistent and continual guidance throughout the period of research leading to this thesis.

I would like to thank Mr. Alan Hulme for his assistance with some of the computing aspects of the project.

Many thanks are due also to Dr. Mike. Chappell for his advice in some of the mathematical theorems derived, Mr. Tom Judge, Miss. Kay Garbett, Mr. Peter Gosling and Mr. Andrew Jones for their assistance in proof reading this thesis.

The research programme was funded by the Science and Engineering Research Council.

Summary.

Design of time and correlation windows for non-parametric frequency response estimates.

The thesis deals with problems that arise in the field of spectral analysis due to finite observations of input and output records. In particular, it is concerned with the method of applying time and correlation windows in spectral analysis procedures to obtain non-parametric frequency response estimates of open-loop time invariant systems.

The thesis reviews and develops the sources of error that arise when frequency response techniques are applied directly to windowed records of input and output data to estimate the frequency response of open loop systems.

Having identified the cause of these errors, methods of eliminating or reducing them are studied. The techniques introduced, which are believed to be novel, involve the use of differing time windows for the input and output data records. Rather than the use of previously developed and ad-hoc symmetrical windows, it is shown that windows can be designed on the basis of some specified criterion such as maximum square coherence or minimum mean square error.

Another method of window selection is based on minimum a priori knowledge of the system characteristics which leads to further improvement in the frequency response estimates. These **Least Mean Square Error Windows**, are solved numerically and are shown to be superior to conventional, classical windows developed in the past.

Window carpentry and modelling of power spectral data

Careful mathematical modelling is always required in the design of modern suspension bridges, as these models are used to predict free vibrations and excitation responses. However, in order to validate any assumption made in the modelling and accuracy of the model parameters, full scale testing procedures need to be undertaken. From the spectrum of measured ambient responses of such large structures, it is necessary to determine the damping factor, resonant frequency and amplitude for each resonance.

Such high Q systems have very sharp spectral peaks and any smoothing; by splitting into segments or by smoothing over frequencies of estimates obtained from a single realisation, removes important fine spectral details.

By analysis and experiment, tests on known similar models show that least squares fitting on the windowed unsmoothed estimates reduces bias in the spectral estimates. It is also be shown that least squares fitting on the unsmoothed cumulative spectra further reduces this bias.

Both procedures, applied to ambient response data from the Humber suspension bridge, are found to differ consistently from earlier results. In particular estimates of damping factor are shown to be very much smaller than those based on smoothed spectral density measurements.

List of symbols

As far as possible the following conventions have been followed :-

Lower case variables denote time signals, $x(t)$, $y(t)$, and upper case denote their Fourier Transforms.

$\hat{}$ over a variable denotes an estimated or unsmoothed value, e.g. $\hat{g}(t)$

$\bar{}$ over a variable denotes a smoothed value, e.g. $\bar{G}(j\omega)$

$\hat{c}_{xx}(\tau)$, $\hat{c}_{yy}(\tau)$, $\hat{c}_{xy}(\tau)$: – Biased input, output and cross covariance functions.

$E[\ ]$: – Expectation operator.

f : – frequency.

$g(t)$: – System impulse response.

$G(j\omega)$: – System frequency response.

$K_x(t,t_1), K_y(t,t_1)$: – Input and output window kernel.

L : – Number of data segments in estimate.

$n(t)$: – Noise signal.

$P_{xx}(\omega)$, $P_{yy}(\omega)$, $P_{xy}(\omega)$: – Input, output and cross power spectrum of open – loop time invariant system.

$r_{xx}(\tau)$, $r_{yy}(\tau)$, $r_{xy}(\tau)$: – Input, output and cross correlation functions of open – loop time invariant system.

$\bar{R}_{xx}(f)$, $\bar{R}_{yy}(f)$, $\bar{R}_{xy}(f)$: – Smoothed input, output and cross power spectrum of windowed sample covariance functions.

s : – Laplace operator.

t : – Time.

T : – Record length.

$w_x(t)$, $w_1(t)$: – Window on the input time function.

$w_y(t)$: – Window on the output time function.

$w_{xx}(t)$, $w_{11}(t)$: – Window on the input correlation function.

$w_{xy}(\tau)$, $w_{12}(\tau)$: – Window on the cross correlation function.

$w_{yy}(\tau)$: – Window on the output correlation function.

$x(t)$: – System input signal.

$y(t)$: – System output signal.

τ : – Argument in correlation function.

$\Phi_{xx}(\omega)$, $\Phi_{yy}(\omega)$, $\Phi_{xy}(j\omega)$: – Input, output and cross power spectrum of open – loop time invariant system.

$\Phi_{ee}(\omega)$: – Error power spectrum of closed – loop system.

$\Phi_{ec}(j\omega)$: – Cross power spectrum between error and output of closed – loop system.

$\Phi_{re}(j\omega)$: – Cross power spectrum between reference and output of closed – loop system.

$\Phi_{re}(j\omega)$: – Cross power spectrum between reference and error of closed – loop system.

Chapter 1

Introduction

This thesis deals with problems that arise in the field of spectral analysis due to finite observation records of input-output time series when using non-parametric estimation methods. In particular it is concerned with the method of applying time windows in the spectral analysis procedure, to obtain frequency response estimates of open-loop time invariant systems. The new procedures discussed are presented with careful mathematical and qualitative reasoning.

The purpose of this chapter is to present some background information and essential procedures on the subject of non-parametric spectral analysis. An in depth explanation into the historical and theoretical evaluation can be found in [1]. Section (1.1) presents from basic principles the definition of an open-loop frequency response function. Section (1.2) provides a brief historical perspective of non-parametric spectral analysis and gives a qualitative description on the effects of unavoidable windowing which occurs in the spectral estimation procedures. Section (1.3), presents recent developments on the analysis of the statistical errors of frequency response estimates due to short length observations and forms the basic motivation of the work undertaken in this thesis. Finally section (1.4) contains a summary of the contents in the thesis.

1.1 The Open-loop frequency response function.

In a wide variety of physical problems a vector of inputs $\{ x_1(t), x_2(t), \cdots, x_k(t) \}$ is fed into some stable system producing a vector of outputs $\{ y_1(t), y_2(t), \cdots, y_k(t) \}$, where t represents time. By solving the differential equations relating inputs and outputs, it is possible to express the outputs as a function of all past inputs.

For small fluctuations and a single input $x(t)$ and output $y(t)$ the differential equation may be linearised to give an estimate in the form

$$y(t) = \int_0^\infty g(u)x(t-u)du + n(t). \tag{1.1}$$

Equation (1.1) is called a **linear dynamic equation** in continuous time and in engineering applications $g(t)$ is called the **impulse response** of the system. The term $n(t)$, is a noise term which in practice is assumed to be uncorrelated with the output. This term may also include quadratic and higher terms omitted by this linear approximation [2]

There exists many non-parametric methods for estimating $g(t)$ [3] such as

(1) Impulse-Response Analysis,

(2) Step-Response Analysis,

(3) Sine-Wave Testing,

(4) Correlation Methods.

In the presence of output noise, such methods may become significantly unreliable. In the assumption that $x(t)$ and $y(t)$ are statistically stationary time series and the noise term is uncorrelated with the input, then on multiplying throughout equation (1.1) by $x(t-\tau)$ and taking expectations,

$$r_{xy}(\tau) = \int_0^\infty g(t)r_{xx}(\tau - t)dt \tag{1.2}$$

where $r_{xx}(\tau)$ and $r_{xy}(\tau)$ are the respective auto correlation function of the input and

cross correlation function between the input and output. In practice these quantities can only be estimated and the impulse response $g(t)$ may be estimated by solving the integral equation (1.2). Mapping these correlation functions into the frequency domain by taking Fourier transforms gives,

$$\Phi_{xy}(j\omega) = \int_{-\infty}^{\infty} r_{xy}(\tau)\exp(-j\omega\tau)d\tau \tag{1.3}$$

and

$$\Phi_{xx}(\omega) = 2\int_{0}^{\infty} r_{xx}(\tau)\cos(\omega\tau)d\tau \tag{1.4}$$

which denote respectively the **cross power spectrum** and the **input power spectrum** of the system. Finally the ratio between equation (1.3) and (1.4) is the **frequency response estimate** of the open-loop system

$$\hat{G}_{xy}(j\omega) = \frac{\Phi_{xy}(j\omega)}{\Phi_{xx}(\omega)}.$$

1.2 Time windows in spectral analysis.

In non-parametric spectrum estimation there exists much literature on the use of time limited window functions and their effects on the resolution and statistical errors of the estimates [4, 5, and 6]. The two well known methods of power spectrum and frequency response estimation are :

(1) the **Indirect method** in which the correlation functions of the process are estimated, weighted by a selected lag window (the Fourier transform of which is called a spectral window) and Fourier transformed.

(2) the **Direct method** in which the spectrum of the process first weighted by a time window (the Fourier transform of which is called a frequency window) is estimated and smoothed over sections to reduce variance.

These time windows have been chosen to be real, symmetrical, and well behaved functions that have frequency counterparts which exhibit certain desirable leakage reduction properties. In general the width of the window is said to control the trade off between bias and variability [3].

Since Cooley and Tukey's introduction of the FFT (1965) [7], the direct method (commonly known as segmental averaging) has become the more popular of the two methods. However the shortening of the effective record in the segmenting process leads to increase in bias but reduces variability due to the resulting smoothed estimate.

The method of overlapping segments introduced by Welch [8] (1967) in some cases reduces variability further but results in lack of frequency resolution and added correlation between segments.

There are two fundamental parameters that critically affect the performance of any spectral estimation technique. They are the length of the available data record of the stationary random process, and the effective frequency resolution required.

In practice, various window functions are used which are generally unrelated to the data or random process being analysed and unless one performs good window carpentry excessive side lobe leakage may be introduced into the estimate.

The basic idiom on the subject of windowing is that the weight given to any individual value should be a function of its variance. That is, the more uncertainty there is about the data point the less weight it should be given.

As a direct consequence, time windows have been designed so that their weights are maximum at the center of the data, whilst allowing for uncertainty gradually cause a reduction of weight at the beginning and end of the records [9]. It is not quite clear why data at the centre has less uncertainty, however justification can be given to this statement if it is argued that undesirable end (or transient) effects are predominant towards the beginning and end of these records. This decay rate however is objective and in practice, leakage suppression is achieved by using well shaped computationally simple windows, such as the Hanning.

1.3 Statistics of the frequency response estimate.

This section reviews the sources of error which arise when frequency response techniques are applied directly to short records of input and output data, to estimate the frequency response of open loop systems.

The errors correspond to bias and variance in the resulting estimates. The magnitude of these separate terms can be evaluated in terms of the excitation, the system characteristics and time window applied to the input and output records.

A method evaluating the statistics of the measured frequency response has been successfully developed by **Douce** and **Balmer** [10 and 11]. Their motivation stems from consideration of the difference between the observed signal and that of an equivalent periodic signal based on the record.

In relation to an open loop system, the analysis considers an input signal $x(t)$ for $-\infty \leq t \leq T$ and an equivalent periodic input $x_r(t)$ such that

$$x_r(nT + t) = x(t) \quad \text{for} \quad n = -\infty, \cdots, -1, 0,$$

where T is the record length of the signal. Under these conditions, $x_r(t) = x(t)$ over the duration $0 \leq t \leq T$. However, the resulting outputs from the system

$$y_r(t) - y(t) = h(t),$$

are not the same. This 'transient' $h(t)$ is such that $h(t) \to 0$ as $t \to \infty$ and is described as containing two terms :-

(i) $h_0(t)$, the response due to the input signal $x(t)$ prior to time $t = 0$,

(ii) $h_T(t)$, the response for $t > T$ due to the input signal $x(t)$ prior to $t = T$.

General properties of the transients and possible methods of reduction is documented in [10].

The bias in the estimate is defined as

$$G_b(j\omega) = E\ [\ \hat{G}(j\omega)\ ] - G(j\omega).$$

For this special case it was shown in [11] to be evaluated using

$$E\ [\ \hat{G}(j\omega)\ ] = E\ [\ \frac{\hat{\Phi}_{xy}(j\omega)}{\hat{\Phi}_{xx}(\omega)}\ ] = \frac{E\ [\ \hat{\Phi}_{xy}(j\omega)\ ]}{E\ [\ \Phi_{xx}(\omega)\ ]}$$

and the variance in the estimate was found to be

$$Var\ [\ \hat{G}(j\omega)\ ] = K_0(\frac{E\ [\ \hat{\Phi}_{yy}(\omega)\ ]}{E\ [\ \Phi_{xx}(\omega)\ ]} + |\ G_b(j\omega)\ |^2)$$

where

$$K_0 = \begin{cases} \frac{1}{L-2} & \text{for } \omega = 0 \\ \frac{1}{L-1} & \text{for } \omega \neq 0 \end{cases} \tag{1.5}$$

and L is the number of segments over which $x(t)$ and $y(t)$ are averaged.

Finally the combination of bias and variance leads to the mean square error of the estimate

$$mse\ [\ \hat{G}(j\omega)\ ] = |\ G_b(j\omega)\ |^2 + Var\ [\ \hat{G}(j\omega)\ ].$$

1.4 Contents of thesis.

Chapter (2) investigates the effects of windows on finite record lengths of observation for evaluation of power spectral and frequency response estimates, with attention given to newly proposed window carpentry procedures. The term window carpentry is used essentially to describe its shape and sharpness. The majority of work undertaken in this chapter has been either introduced by the author or extended from previous work. A detailed content of contributions made by the author will be given in the introduction

of the chapter.

Having developed the basic principles of window carpentry, a new mathematical formulation is presented in chapter (3) which allows for the design of these time correlation windows based on apriori knowledge of the system characteristics. These **Least mean square error windows** are found to be a solution of integral equation pairs and in particular the Fredholm equation of the second kind.

In chapter (4), these windows are applied to simulated realisations of input output records. It is shown that the least mean square error windows leads to significant improvements in the resultant frequency response estimates when compared to conventional windows used in the past.

Chapter (5) deals with problems encountered in the power spectral analysis of the Humber suspension bridge ambient response data. It is found that with such high Q systems that have very sharp spectral peaks, any smoothing by splitting into segments or smoothing over frequencies, leads to unacceptable bias in the model parameters. The bias is known to be particularly significant in the estimation of damping associated with the individual spectral peaks. A procedure is adopted by which the whole record length weighted initially by an appropriate choice of time window, is Fourier transformed. This allows for maximum detail and minimum bias in the spectrum. Estimates of the model parameters are found to be further improved by curve fitting over the smoother integral raw spectrum.

Finally chapter (6) concludes this thesis by presenting, briefly, other research work by the author with a recommendation for further work that needs to be undertaken in this field.

1.5 References for chapter (1).

[1] **Special issue.** : 'Spectral estimation'. Proc,IEEE.,September 1982.

[2]. **G.M.Jenkins** : 'An Example of the Estimation of a linear open loop Transfer function'. Technometrics, vol.5, No.2, pg 227,May 1963.

[3]. **L.Ljung:** 'System identification: Theory for the user'. Prentice-Hall information and system sciences series. 1987.

[4] **Geckinli. N.C. and Yavuz. D.,:** ' Discrete Fourier transforms and its application to power spectra estimation'.Elsevier 1983.

[5] **Blackman. R.B. and Tukey. J.W.,:** 'The measurement of power spectra'. Dover Publications Inc. New York 1958.

[6] **Harris. F.J.,:** 'On the use of windows for harmonic analysis with the discrete Fourier transform'. Proc,IEEE,vol 66,No.1,January 1978.

[7] **Cooley. J.W. and Tukey. J.W.,:** 'An algorithm for machine calculation of complex Fourier series'. Math. Comp., vol 19, pp 297-301, April 1965.

[8] **Welch. P.D.,:** 'The use of fast Fourier transform for the estimation of power spectra: A method based on time averaging over short, modified periodograms'. IEEE,Trans.,vol AU-15,pp 70-73,June 1967.

[9] **Kay. S.M. and Marple. S.L.,:** 'Spectral analysis - A modern Perspective'. Proc. IEEE., vol 69, No.11,pp 1380-1419, November 1981.

[10] **Douce. J.L. and Balmer. L.,:** 'The statistics of frequency response estimates'. Proc,IEE., vol 137,Pt.D,No 5,September 1990.

[11] **Balmer. L.,:** 'Short term spectral estimation with applications'. Ph.D. Thesis,University of Warwick,1986.

Chapter 2

Window carpentry.

2.1 Introduction.

This chapter investigates the effects of both windows and finite record length on the estimation of the frequency response of linear time-invariant open-loop systems. Comparison is made between a range of conventional windows, and their effect on the frequency response estimates is studied for different lengths of observation time T. The departure is made from conventional window carpentry by defining a more generalised trigonometric sum type window in order to study the effects of differing window shapes on the spectral estimates.

2.2 Summary of contents in chapter (2).

Section (2.3) defines the expected value of the measured frequency response function in terms of steady state correlation functions and the input-output time windows applied to the record before spectral analysis. An exact relationship between windows on the time function and windows on the correlation function is also derived.

Section (2.4) introduces a new class of time window function which encompasses the majority of classical time windows. This window is termed a trigonometric sum type, as

it is formulated from the summation of cosine terms whose amplitudes and phase are determined by the coefficients applied at each summation.

Section (2.5) uses the theory derived in (2.4) to define two classical window families.

In section (2.6), these window families are used to study the effects of differing window types on the expected value of the measured frequency response function as defined in section (2.3). Specific examples of input-output observations in section (2.7) are given, in order to compare the frequency response estimates derived for the differing time windows and some conclusions are made.

Finally in section (2.8), further conclusions are drawn by studying the effects of asymmetrical input-output time windows on the bias and coherence of the measured frequency response functions.

Throughout this chapter, simulation studies and qualitative arguments are used to verify assumptions made in the analysis.

2.3 Measured frequency response function.

With reference to figure (2.1), $x(t)$ and $y(t)$ are the input and output signals obtained from a linear time invariant system. Prior to analysis, the signals are windowed by their respective time window functions $w_x(t)$, $w_y(t)$ and the constraint of finite record is introduced by requiring $w_x(t)$ and $w_y(t)$ to have zero values outside the range $0 \leq t \leq T$.

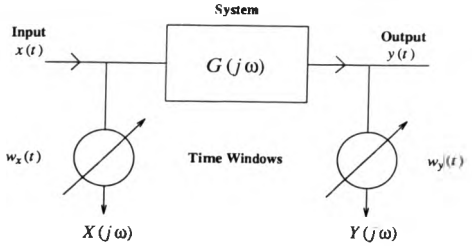

Figure 2.1: **Open-loop identification scheme.**

Conventionally such time windows satisfy the conditions

(1) $w(T/2) = 1$,

(2) $w(t) = w(T-t)$,

(3) $w(t) = 0$, for $0 < t$ and $t > T$.

The short term Fourier transform of the measured input is given by

$$X(j\omega) = \int_0^T x(t) w_x(t) \exp(-j\omega t) dt.$$

Similarly the short term Fourier transform of the output from the system is given by

$$Y(j\omega) = \int_0^T y(t) w_y(t) \exp(-j\omega t) dt$$

From the above two equations, the raw cross spectrum is defined by

$$\hat{\Phi}_{xy}(j\omega) = \frac{1}{T} X^*(j\omega) Y(j\omega) \qquad (2.1)$$

where * denotes a complex conjugate.

The expected value of equation (2.1) is

$$E\,[\,\hat{\Phi}_{xy}(j\omega)\,] = \frac{1}{T}\int_0^T \int_0^T r_{xy}(t_2 - t_1) w_x(t_1) w_y(t_2) \exp\{-j\omega(t_2 - t_1)\} dt_1 dt_2.$$

Assuming that $x(t)$ and $y(t)$ are statistically stationary, by setting $\tau = t_2 - t_1$ and $t = t_1$,

$$E\,[\,\hat{\Phi}_{xy}(j\omega)\,] = \frac{1}{T}\int_0^T w_y(t)\Big(\int_{-t}^{0} + \int_0^{T-\tau}\Big) r_{xy}(\tau) w_x(t-\tau) \exp(-j\omega\tau) d\tau dt.$$

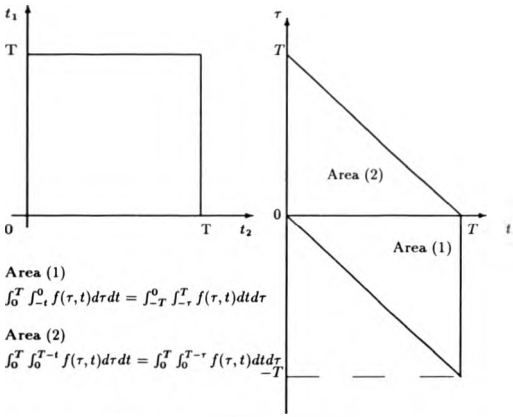

Area (1)
$\int_0^T \int_{-t}^{0} f(\tau,t) d\tau dt = \int_{-T}^{0} \int_{-\tau}^{T} f(\tau,t) dt d\tau$

Area (2)
$\int_0^T \int_0^{T-t} f(\tau,t) d\tau dt = \int_0^T \int_0^{T-\tau} f(\tau,t) dt d\tau$

Figure 2.2: Transformation of co-ordinates for the measured cross spectrum.

From the transformation in figure (2.2) we obtain

$$E\left[\hat{\Phi}_{xy}(j\omega)\right] = \frac{1}{T}\int_{-T}^{T} r_{xy}(\tau) w_{xy}(\tau)\exp(-j\omega\tau)d\tau \tag{2.2}$$

where

$$w_{xy}(\tau) = \begin{cases} \frac{1}{T}\int_0^{T-\tau} w_x(t)w_y(t+\tau)dt & \text{for } \tau \geq 0 \\ \\ \frac{1}{T}\int_{|\tau|}^{T} w_x(t)w_y(t+\tau)dt & \text{for } \tau \leq 0. \end{cases} \tag{2.3}$$

Similar expressions are obtained for $w_{xx}(\tau)$, $E\left[\hat{\Phi}_{xx}(j\omega)\right]$ and $w_{yy}(\tau)$, $E\left[\hat{\Phi}_{wy}(j\omega)\right]$ by changing the appropriate subscripts in equations (2.2) and (2.3). Equation (2.3) gives an explicit analytical relationship between windows on the time function and their corresponding windows on the correlation function. In practice $w_{xy}(\tau)$ is normalised such that the position of maximum weight is unity, and in order to strictly adhere to this, the constant $1/T$ in equation (2.3) is replaced by

$$\frac{1}{\int_0^T w_x(t)w_y(t)dt}.$$

To prevent confusion, we will at this stage note the distinction between windows on the time and correlation function. When specified with single subscripts, windows such as $w_x(t), w_y(t)$ and $w_1(t)$, will strictly imply windows on the time function defined over the time index $0 \leq t \leq T$. Those with double subscripts, will imply windows on the correlation function defined over the time index $-T \leq t \leq T$.

From the measured spectral densities, the least square estimate of the frequency response function is given by

$$\hat{G}_{xy}(j\omega) = \frac{X^*(j\omega)Y(j\omega)}{X^*(j\omega)X(j\omega)} = \frac{\hat{\Phi}_{xy}(j\omega)}{\hat{\Phi}_{xx}(j\omega)}, \tag{2.4}$$

if the estimate is based on one segment.

For estimates averaged over L segments, each of length T, the system frequency response function is represented by

$$\overline{G}_{xy}(j\omega) = \frac{\frac{1}{L}\sum_{i=1}^{L} X^*(j\omega)Y(j\omega)}{\frac{1}{L}\sum_{i=1}^{L} X^*(j\omega)X(j\omega)} = \frac{\overline{\Phi}_{xy}(j\omega)}{\overline{\Phi}_{xx}(j\omega)}. \tag{2.5}$$

2.4 Spectral windows.

The effects of windowing the time functions before spectral estimation are well documented [2,3]. The design of such windows aims at the minimisation of the undesirable side lobes, whilst maintaining the bandwidth of the main lobe acceptable. Windows such as the Hanning and Hamming have been adopted in the past, and their bandwidths are said to be an index of the range over which the smoothing operation is effectively extended [3].

2.4.1 A class of window function.

Extensive catalogues of time windows along with their suggested uses in different spectral estimation procedures have been documented [2,4]. However, the implementation of these options is still considered somewhat vague and confusing to the practical engineer.

A new function that encompasses the majority of these windows will be termed a **Trigonometric sum type window** and is defined by

$$w_1(t) = \sum_{k=-m}^{m} \alpha_k \cos(a_k t + b_k) \tag{2.6}$$

where

$$a_k = \begin{cases} \frac{-k\pi}{2U} & \text{for} \quad U \geq T/2 \\ \\ \frac{-k\pi}{2(T-U)} & \text{for} \quad U \leq T/2, \end{cases}$$

The parameter $b_k = -a_k U$ and the vector α

$$\{\alpha_{-m}, \alpha_{-m+1}, \cdots, \alpha_0, \cdots, \alpha_{m-1}, \alpha_m\}$$

of length $2m + 1$ can take any arbitrary real values. The above specification gives a maximum weight at time U and allows for this weight to fall towards zero at $t = 0$ and $t = T$.

Conventionally the restriction

$$w_1(0) = w_1(T) = 0$$

is given to these windows. For the Trigonometric sum type window, this is not necessary as such factors will be based on the coefficients α and the position of maximum weight U.

For classical windows, the position of maximum weight is fixed such that $U = T/2$. The significant difference between Trigonometric sum type and classical windows is that U is a allowed to vary over the duration of the observation period

$$0 \leq U \leq T.$$

On applying (2.6) to conventional window carpentry, this function will be subject to the constraints

$$\sum_{k=-m}^{m} \alpha_k = 1.0,$$

$$\alpha_k = \alpha_{-k},$$

$$\alpha_k \geq 0,$$

$$U = T/2,$$

$$0 \leq t \leq T.$$

By defining a new vector σ such that $\sigma_0 = \alpha_0$, and $\sigma_k = 2\alpha_k$ for $k > 0$, equation (2.6) simplifies to

$$w_1(t) = \sigma_0 + \sum_{k=1}^{m} \sigma_k \cos(\Omega_k t - k\pi/2) \tag{2.7}$$

where $\Omega_k = k\pi/T$.

The equivalent window on the correlation function is derived from equation (2.3) by evaluating

$$\begin{aligned}
&\sigma_0^2 \int_0^{T-\tau} dt \\
&+ \sigma_0 \sum_{k=1}^{m} \sigma_k \int_0^{T-\tau} \cos(\Omega_k t - k\pi/2) dt \\
&+ \sigma_0 \sum_{k=1}^{m} \sigma_k \int_0^{T-\tau} \cos(\Omega_k t + \Omega_k \tau - k\pi/2) dt \\
&+ \sum_{k=1}^{m} \sigma_k \sum_{j=1}^{m} \sigma_j \int_0^{T-\tau} \cos(\Omega_k t - k\pi/2) \cos(\Omega_j t + \Omega_j \tau - k\pi/2) dt,
\end{aligned}$$

and leads to

$$\begin{aligned}
w_{11}(\tau) = V\sigma_0^2(T-\tau) \;&+\; V \sum_{k=1}^{m} \frac{\sigma_k}{\Omega_k} \left\{ \sin(\tfrac{k\pi}{2} - \Omega_k \tau) + \sin(\tfrac{k\pi}{2}) \right\} \\
&+\; V \sum_{j=1}^{m} \sum_{k=1}^{m} \Upsilon(\sigma_k, \sigma_j, k, j, \tau)
\end{aligned} \tag{2.8}$$

where $\Omega_i = i\pi/T$,

$$\frac{1}{V} \;=\; \sigma_0^2 T + 2 \sum_{k=1}^{m} \frac{\sigma_k}{\Omega_k} \sin(\frac{k\pi}{2}) + \sum_{j=1}^{m} \sum_{k=1}^{m} \Upsilon(\sigma_k, \sigma_j, k, j, 0)$$

$$\begin{aligned}
\Upsilon(\sigma_k, \sigma_j, k, j, \tau) \;&=\; \frac{\sigma_k \sigma_j}{2(\Omega_k - \Omega_j)} \left\{ \sin(\tfrac{\pi(k-j)}{2} - \Omega_k \tau) + \sin(\tfrac{\pi(k-j)}{2} + \Omega_j \tau) \right\} \\
&+\; \frac{\sigma_k \sigma_j}{2(\Omega_k + \Omega_j)} \left\{ \sin(\tfrac{\pi(k+j)}{2} - \Omega_k \tau) + \sin(\tfrac{\pi(k+j)}{2} - \Omega_j \tau) \right\}
\end{aligned}$$

for $k \neq j$, and

$$\Upsilon(\sigma_k, \sigma_j, k, j, \tau) = \frac{\sigma_k^2}{2}\left\{ (T-\tau)\cos(\Omega_k \tau) - \sin(\Omega_k \tau - k\pi)/\Omega_k \right\}$$

for $k = j$.

2.5 Some classical windows.

In this section some classical windows are introduced in the form of the trigonometric sum type windows described in section (2.4.1). The trigonometric sum type coefficients for the Blackman, Hanning, and Papoulis windows are given to justify the ease with which such windows can be generally implemented and a more detailed study of the Hanning and Papoulis windows chosen for analysis.

2.5.1 Hanning window family.

Such a window results when $\sigma = \{\rho, 0, 1-\rho\}$. Applying this substitution, equation (2.7) gives

$$w_1(t) = \rho + (1-\rho)\cos(\omega_0 t + \pi) \tag{2.9}$$

where

$$0.5 \leq \rho \leq 1.0, \quad \text{and} \quad \omega_0 = 2\pi/T.$$

For clarity, and as in [4], the word 'exact' is used to describe the window that leads to the condition

$$w_1(0) = w_1(T) = 0.$$

For this condition, the exact Hanning is defined in equation (2.9) when $\rho = 1/2$. We will also denote the word 'minimum' to describe the window that leads to the greatest reduction of the side lobe levels.

The equivalent spectral window for a Do-nothing (or rectangular window) on the time function is defined by the Dirichlet kernel

$$W_d(\omega) = \exp(\frac{j\omega}{2})\frac{\sin(\frac{\omega T}{2})}{\frac{\omega T}{2}},$$

for the Hanning family of spectral windows, can be represented as a sum of three Dirichlet kernels

$$W_h(\omega) = \rho W_d(\omega) + \frac{1}{2}(1-\rho)[W_d(\omega - \frac{2\pi}{T}) + W_d(\omega + \frac{2\pi}{T})]$$

as in figure (2.3). Since the three side lobes are in phase opposition, summation leads to a reduction in the side lobe amplitudes. A minimum side lobe is achieved when

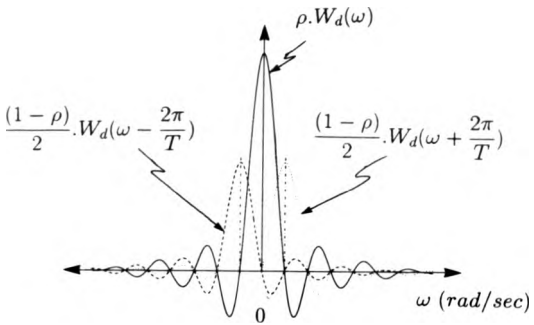

Figure 2.3: **Transform of Hanning type windows as a sum of three Dirichlet kernels.**

$\rho = 0.5385$(4dp) and although should be strictly termed minimum Hanning, is commonly known as the **Hamming window**.

The equivalent window on the correlation function is derived from equation (2.8) and leads to :-

$$w_{11}(\tau) = \frac{1}{(A_1 + A_2)} \left\{ \ (1 - \frac{|\tau|}{T})(A_1 + A_2 \cos(\omega_0 \tau)) + A_3 \sin(\omega_0 \mid \tau \mid) \ \right\} \qquad (2.10)$$

where

$$A_1 = \rho^2, A_2 = \frac{(1-\rho)^2}{2}, A_3 = \frac{(5\rho - 1)(1-\rho)}{4\pi}.$$

2.5.2 Minimum bias windows for high resolution spectral estimates.

It is important to note the analysis developed by Papoulis [6] as a means to justify the selection of this window type. For convenience we shall call this the **Papoulis family of windows**. The author believes this family of windows to be the best out of all conventional windows when comparison is made from a statistical viewpoint. Its selection is significant in that is yields minimum bias in spectral estimates and will therefore be reviewed in this thesis.

Consider the correlation window subject to the constraints

$$w_{11}(\tau) = w_{11}(T - \tau) \ \text{ for } \ \mid \tau \mid < T, \ w_{11}(\tau) = 0, \ \text{ for } \ \mid \tau \mid > T,$$

where

$$w_{11}(0) = \frac{1}{2\pi} \int_{-\infty}^{\infty} W_{11}(\Omega) d\Omega = 1.$$

The bias due to windowing the power spectrum $S(\Omega)$ is

$$\frac{1}{2\pi} \int_{-\infty}^{\infty} S(\Omega - y) W_{11}(y) dy - S(\Omega) \approx \frac{S''(\Omega)}{4\pi} \int_{-\infty}^{\infty} y^2 W_{11}(y) dy.$$

The object thus is to determine $W_{11}(\Omega)$ so as to minimise the term

$$M_2 \equiv \int_{-\infty}^{\infty} \Omega^2 W_{11}(\Omega) d\Omega,$$

where M_2 is the second moment of the spectral window $W_{11}(\Omega)$.

On the assumption that this spectrum has a continuous second derivative and that T is sufficiently large so that an acceptable level of variance is obtained, it is found that the determination of such an optimum window is equivalent to evaluating a time window $w_1(t)$ that minimises the integral

$$\int_{-\infty}^{\infty} \Omega^2 \mid W_1(\Omega) \mid^2 d\Omega.$$

Such a condition leads to the Euler equation

$$\frac{d^2 w_1(t)}{dt^2} + \lambda w_1(t) = 0$$

and has a solution

$$w_1 = (\frac{2}{T})^{1/2} \sin(\frac{\pi t}{T}), \quad \text{for} \quad 0 \leq t \leq T,$$

with an equivalent correlation window

$$w_{11}(\tau) = \frac{1}{\pi} \mid \sin(\frac{\pi \tau}{T}) \mid + (1 - \frac{\mid \tau \mid}{T}) \cos(\frac{\pi \tau}{T}).$$

This general window type, $\sigma = \{(1-\rho), \rho\}$, gives a time window of the form

$$w_1(t) = (1-\rho) + \rho \sin(\omega_0 t) \tag{2.11}$$

where $0 \leq \rho \leq \frac{1}{2}$, and $\omega_0 = \pi/T$.

The equivalent window on the correlation function is

$$w_{11}(\tau) = \frac{1}{A_1/\pi + A_2 + A_3}\frac{A_1}{\pi} + (1 - \frac{|\tau|}{T})(A_2 + A_3\cos(\omega_0\tau)) + \frac{A_3}{\pi}\sin(\omega_0|\tau|)$$

where $A_1 = 4\rho(1-2\rho)$, $A_2 = (1-2\rho)^2$, and $A_3 = 2\rho^2$.

In the special case when $\rho = \frac{1}{2}$, this window is proved by Papoulis to result in minimum bias for high resolution spectral estimate [6]. Figures (2.4) and (2.5) show examples of some classical time and correlation windows. Table (2.1) gives the trigonometric sum type coefficients of these windows as defined by equation (2.6).

——— Exact Papoulis window; -.-.-.-.- Exact Blackman window.

. . . . . Exact Hanning window; - - - - - - Papoulis window ($\rho = \frac{1}{4}$).

..... Hamming window.

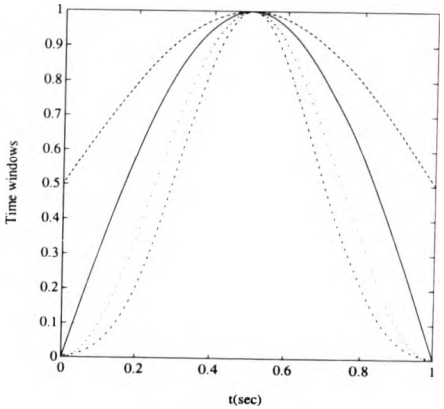

Figure 2.4: **Some classical time windows.**

——— Exact Papoulis window: -.-.-.-.- Exact Blackman window.

. . . . . Exact Hanning window: - - - - - - Papoulis window ($\rho = \frac{1}{4}$).

..... Hamming window.

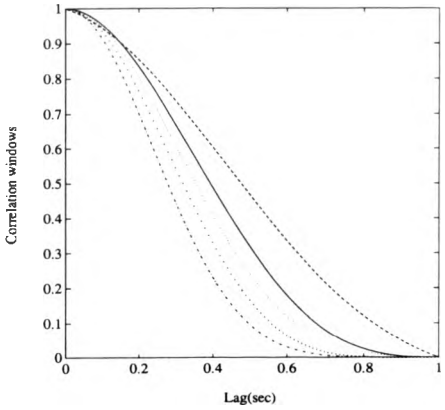

Figure 2.5: Equivalent windows on the correlation function.

Classical windows	σ_0	σ_1	σ_2	σ_3	σ_4	σ_5	σ_6
Do-nothing	1						
Exact Papoulis	0	1					
Exact Hanning	0.5	0	0.5				
Hamming	0.539	0	0.461				
Exact Blackman	0.423	0	0.498	0	0.081		
3-term minimum Blackman-Harris	0.450	0	0.494	0	0.056		
4-term Blackman-Harris	0.402	0	0.497	0	0.094	0	0.007
4-term minimum Blackman-Harris	0.359	0	0.488	0	0.141	0	0.012

Table 2.1: **Trigonometric sum type representation of some classical windows.**

2.6 The effects of windows on the spectral estimate.

In this section, the effect of finite record lengths on the expected value of the measured frequency response and the squared coherence function will be studied. Where possible an attempt will be made to obtain expressions that are totally dependent on the systems correlation functions. In cases where the analysis is deemed too complicated, specific but generalised examples through numerical methods will be presented. Such situations arise when evaluating frequency response and coherence estimates for windows that do not have positions of maximum weight at $U = T/2$.

Explicit and approximate derivation of the spectral estimates for the Hanning and Papoulis family of windows can be achieved for systems that are subjected to theoretical white noise and have record lengths greater than the magnitude of the system settling times.

The general expression for the expected value of the measured frequency response is given by

$$E\,[\,\hat{G}_{xy}(j\omega)\,] = \frac{E\,[\,\hat{\Phi}_{xy}(j\omega)\,]}{E\,[\,\Phi_{xx}(\omega)\,]}$$

where

$$E\ [\ \hat{\Phi}_{xx}(\omega)\ ] = 2\int_0^T w_{xx}(\tau) r_{xx}(\tau)\cos(\omega\tau)d\tau,$$

and

$$E\ [\ \hat{\Phi}_{xy}(\omega)\ ] = \int_{-T}^{T} w_{xy}(\tau) r_{xy}(\tau)\exp(-j\omega\tau)d\tau,$$

The analysis for a given white noise input with no intentional windowing is studied in [1] and will be briefly reviewed.

In this special case

$$w_{xx}(\tau) = w_{xy}(\tau) = w_{yy}(\tau) = 1 - \frac{|\tau|}{T}$$

As in [1], the expected value of the measured spectrum for an input signal of constant power spectral density Φ is

$$E\ [\ \hat{\Phi}_{xx}(\omega)\ ] = \int_{-T}^{T}(1 - \frac{|\tau|}{T})\ .\ \Phi\ .\ \delta(\tau)\ .\ \exp(-j\omega\tau)d\tau = \Phi.$$

For white noise input the expected value of the measured cross correlation function

$$r_{xy}(\tau) = \Phi\ .\ g(\tau)$$

is similarly substituted to give

$$E\ [\ \hat{\Phi}_{xy}(j\omega)\ ] = \Phi.\int_0^T (1 - \frac{|\tau|}{T})g(\tau)\exp(-j\omega\tau)d\tau$$

and these equations lead to the expected value of the measured frequency response

$$E\ [\ \hat{G}_{xy}(j\omega)\ ] = \int_0^T (1 - \frac{|\tau|}{T})g(\tau)\exp(-j\omega\tau)d\tau.$$

Two features in this expression lead to bias in the estimate.

(1) The finite value of the upper limit of integration,

(2) The second term within the brackets which leads to non-zero contribution.

When the period of observation is much greater then the settling time of the system, the upper limit of integration can be effectively replaced by infinity. This leads to an approximate expression for the expected value of the measured frequency response

$$\begin{aligned} E\ [\ \hat{G}_{xy}(j\omega)\ ] &= \int_0^\infty g(\tau)\exp(-j\omega\tau)d\tau - \frac{1}{T}\int_0^\infty \tau g(\tau)\exp(-j\omega\tau)d\tau \\ &= G(j\omega) - \frac{j}{T}\frac{dG(j\omega)}{d\omega}. \end{aligned}$$

Thus in the case of no direct windowing of the input-output record, the bias in the expected value of the measured frequency response can be said to be perpendicular to the locus of the true frequency response function $G(j\omega)$ on the complex plain with a clockwise rotation of magnitude $(1/T)\mid dG(j\omega)/d\omega \mid$ [1].

2.6.1 Asymptotic effects of Hanning window on the spectral estimates.

Here we use the term asymptotic to imply that the observation time T is much larger than the settling time of the system. If this condition is maintained, the substitution $T = \infty$ in the limits of integration can be implemented to obtain an estimate.

Expected value of measured output power spectrum.

For white noise input $\Phi_{xx}(\omega) = \Phi$.

For the above assumption,

$$E\ [\ \hat{\Phi}_{yy}(\omega)\ ] \approx 2\int_0^\infty r_{yy}(\tau)w_{yy}(\tau)\cos(\omega\tau)d\tau$$

Recalling from equation (2.10), the expression derived for Hanning on the correlation

function

$$w_{11}(\tau) = \frac{1}{(A_1 + A_2)} \left\{ (1 - \frac{|\tau|}{T})(A_1 + A_2\cos(\omega_0\tau)) + A_3\sin(\omega_0 \mid \tau \mid) \right\} \tag{2.12}$$

Defining

$$C_{yy}(\omega) = \int_0^\infty r_{yy}(\tau)\cos(\omega\tau)d\tau, \quad \text{and} \quad S_{yy}(\omega) = \int_0^\infty r_{yy}(\tau)\sin(\omega\tau)d\tau$$

as the expected cosine and sine transforms of the output auto correlation function leads to five terms in the evaluation of equation (2.12).

These terms are :-

Term (1)

$$2A_1 \int_0^\infty r_{yy}(\tau)\cos(\omega\tau)d\tau = 2A_1 C_{yy}(\omega).$$

Term (2)

$$2A_2 \int_0^\infty r_{yy}(\tau)\cos(\omega_0\tau)\cos(\omega\tau)d\tau$$

$$= A_2 \int_0^\infty r_{yy}(\tau)\cos(\{\omega + \omega_0\}\tau)d\tau + A_2 \int_0^\infty r_{yy}(\tau)\cos(\{\omega - \omega_0\}\tau)d\tau$$

$$= A_2\{C_{yy}(\omega + \omega_0) + C_{yy}(\omega - \omega_0)\}.$$

Term (3)

$$-\frac{2A_1}{T} \int_0^\infty \tau.r_{yy}(\tau)\cos(\omega\tau)d\tau = -\frac{2A_1}{T}\frac{dS_{yy}(\omega)}{d\omega}$$

where $S_{yy}(\omega)$ is the fourier sine transform of the output auto-correlation function.

Term (4)

$$-\frac{2A_2}{T} \int_0^\infty \tau.r_{yy}(\tau)\cos(\omega_0\tau)\cos(\omega\tau)d\tau$$

$$= -\frac{A_2}{T} \int_0^\infty \tau.r_{yy}(\tau)\cos(\{\omega + \omega_0\}\tau)d\tau - \frac{A_2}{T} \int_0^\infty \tau.r_{yy}(\tau)\cos(\{\omega - \omega_0\}\tau)d\tau$$

$$= -\frac{2A_2}{T}\frac{dS_{yy}(\omega+\omega_0)}{d(\omega+\omega_0)} - \frac{2A_2}{T}\frac{dS_{yy}(\omega-\omega_0)}{d(\omega-\omega_0)}.$$

Term (5)

$$2A_3\int_0^\infty r_{yy}(\tau)\sin(\omega_0\tau)\cos(\omega\tau)d\tau$$

$$= A_3\int_0^\infty r_{yy}(\tau)\sin(\{\omega+\omega_0\}\tau)d\tau + A_3\int_0^\infty r_{yy}(\tau)\sin(\{\omega-\omega_0\}\tau)d\tau$$

$$= A_3\{S_{yy}(\omega+\omega_0) - S_{yy}(\omega-\omega_0)\}$$

where

$$A_1 = \rho^2, A_2 = \frac{(1-\rho)^2}{2}, A_3 = \frac{(5\rho-1)(1-\rho)}{4\pi}.$$

Finally combining all the terms,

$$\begin{aligned} E\,[\,\hat{\Phi}_{yy}(\omega)\,] &= 2A_1\Phi C_{yy}(\omega) - \frac{2A_1\Phi}{T}\frac{dS_{yy}(\omega)}{d\omega} \\ &+ A_2\Phi C_{yy}(\omega+\omega_0) + A_3\Phi S_{yy}(\omega+\omega_0) - \frac{2A_2\Phi}{T}\frac{dS_{yy}(\omega+\omega_0)}{d(\omega+\omega_0)} \\ &+ A_2\Phi C_{yy}(\omega-\omega_0) - A_3\Phi S_{yy}(\omega-\omega_0) - \frac{2A_2\Phi}{T}\frac{dS_{yy}(\omega-\omega_0)}{d(\omega-\omega_0)}. \end{aligned} \tag{2.13}$$

Expected value of measured cross power spectrum.

For white noise input, the effects of a Do-nothing window on the expected value of the measured frequency response has already been described. The analysis will now be extended to the Hanning family (which includes the Do-nothing, for $\rho = 1$).

The expected value of the measured cross spectrum is

$$E\,[\,\hat{\Phi}_{xy}(j\omega)\,] \approx \Phi\int_0^\infty w_{xy}(\tau)g(\tau)\exp(-j\omega\tau)d\tau,$$

if it is again assumed that the record length T is sufficiently large in comparison to the

settling time of the system.

Using sin and cosine identities

$$\sin(\omega_0 t) = \frac{-j}{2}[\exp(s_0 t) - \exp(-s_0 t)],$$

$$\cos(\omega_0 t) = \frac{1}{2}[\exp(s_0 t) + \exp(-s_0 t)],$$

where $s_0 = j\omega_0$ and the integral substitutions

$$\int_0^\infty t f(t) \exp(-st) dt = -\frac{d}{ds} F(s),$$

$$\int_0^\infty \cos(\omega_0 t) f(t) \exp(-st) dt = \frac{1}{2}[F(s - s_0) + F(s + s_0)],$$

$$\int_0^\infty t \cos(\omega_0 t) f(t) \exp(-st) dt = -\frac{1}{2T}[\frac{dF(s - s_0)}{d(s - s_0)} + \frac{dF(s + s_0)}{d(s + s_0)}]$$

where $s = j\omega$, leads to an approximation to the expected value of the measured cross power spectrum.

$$\begin{aligned} E\,[\,\hat{\Phi}_{xy}(j\omega)\,] &= A_1 \Phi[G(j\omega) - \frac{1}{T}\frac{dG(j\omega)}{d\omega}] \\ &+ \frac{\Phi}{2}[G(j\{\omega + \omega_0\})(A_2 + jA_3) - \frac{jA_2}{T}\frac{dG(j\{\omega + \omega_0\})}{d(\omega + \omega_0)}] \\ &+ \frac{\Phi}{2}[G(j\{\omega - \omega_0\})(A_2 - jA_3) - \frac{jA_2}{T}\frac{dG(j\{\omega - \omega_0\})}{d(\omega - \omega_0)}], \end{aligned} \tag{2.14}$$

where $\omega_0 = 2\pi/T$.

For the Hanning family of windows, equations (2.13) and (2.14) are approximations

to the expected value of the measured output and cross power spectral estimates for an open-loop time invariant system that is subjected to a white noise input of constant power Φ. These expressions are functions of

(1) The record length T.

(2) The Hanning windows coefficients A_1, A_2, and A_3.

(3) The system characteristics.

Such expressions are new and allow for a more precise observation when studying the effects of varying the record length, window parameters, and system characteristics on the frequency response and coherence estimates.

The expected value of the measured frequency response and square coherence functions are :-

$$E\ [\ \hat{G}_{xy}(j\omega)\ ] = \frac{E\ [\ \hat{\Phi}_{xy}(j\omega)\ ]}{\Phi}$$

and

$$E\ [\ \bar{\gamma}^2_{xy}(j\omega)\ ] = \frac{1}{\Phi}\frac{|\ E\ [\ \hat{\Phi}_{xy}(j\omega)\ ]\ |^2}{E\ [\ \hat{\Phi}_{yy}(\omega)\ ]}$$

2.6.2 Asymptotic effects of Papoulis windows on the spectral estimates.

Similar consideration of this window type leads to :-

$$\begin{aligned} E\ [\ \hat{\Phi}_{yy}(\omega)\ ] &= \Phi(\frac{A_1}{\pi} + A_2)C_{yy}(\omega) - \Phi\frac{2A_2}{T}\frac{dS_{yy}(\omega)}{d\omega} \\ &+ \Phi A_3\{C_{yy}(\omega+\omega_0) + \frac{1}{\pi}S_{yy}(\omega+\omega_0) - \frac{1}{T}\frac{dS_{yy}(\omega+\omega_0)}{d(\omega+\omega_0)}\} \\ &+ \Phi A_3\{C_{yy}(\omega-\omega_0) - \frac{1}{\pi}S_{yy}(\omega-\omega_0) - \frac{1}{T}\frac{dS_{yy}(\omega-\omega_0)}{d(\omega+\omega_0)}\} \end{aligned} \tag{2.15}$$

and

$$
\begin{aligned}
E\,[\,\hat{\Phi}_{xy}(j\omega)\,] \;=\; & \Phi[(\frac{A_1}{\pi}+A_2)G(j\omega)-\frac{A_2}{T}\frac{dG(j\omega)}{d\omega}] \\
+\; & \frac{A_3\Phi}{2}[G(j\{\omega+\omega_0\})(1+\frac{j}{\pi})-\frac{1}{T}\frac{dG(j\{\omega+\omega_0\})}{d(\omega+\omega_0)}] \\
+\; & \frac{A_3\Phi}{2}[G(j\{\omega-\omega_0\})(1-\frac{j}{\pi})-\frac{1}{T}\frac{dG(j\{\omega-\omega_0\})}{d(\omega-\omega_0)}],
\end{aligned}
\tag{2.16}
$$

where $\omega_0 = 2\pi/T$, $A_1 = 4\rho(1-2\rho)$, $A_2 = (1-2\rho)^2$, $A_3 = 2\rho^2$ and $0 \le \rho \le 1/2$.

2.7 Example (1).

Two examples illustrate the previous work.

We first consider the effects of the Hanning and Papoulis window families in conjunction with a second order transfer function defined by a resonant frequency w_n and damping factor ζ. Analysis shows that ρ is a function of T when minimum square error criterion is chosen, and that as $T \to \infty$, the window satisfies the condition

$$w_1(t) = w_1(T-t).$$

We then examine the effect of non-white noise input by considering a first order filter system. Comparison is made between Do-nothing, exact Hanning and exact Papoulis windows.

2.7.1 Second order system subject to white noise input.

The transfer function chosen is

$$G(s) = \frac{w_n s}{(s^2 + 2\zeta w_n s + w_n^2)}$$

with the parameter values $\zeta = 0.2$ and $w_n = 0.2$. The impulse response of this system is

$$g(t) = \frac{w_n}{2c}[\, a\exp(-at) - b\exp(-bt)\,]$$

where

$$a = \zeta + c, b = \zeta - c, \text{ and } c = w_n\sqrt{\zeta^2 - 1}.$$

The cross correlation function between input (of constant power Φ) and output is given by

$$r_{xy}(\tau) = \Phi \cdot g(\tau)$$

and the auto-correlation function of the output is

$$\begin{aligned} r_{yy}(\tau) &= \int_0^\infty g(t)g(t+\tau)dt \\ &= \frac{w_n^2}{8c^2}\{a\exp(-a\tau)(1-\frac{b}{\zeta}) + b\exp(-b\tau)(1-\frac{a}{\zeta})\}. \end{aligned}$$

For this system arrangement the respective cosine, sine and derivative of the sine transforms are :-

$$C_{yy}(\omega) = \frac{w_n^2}{4c^2}(\frac{a^2 d}{a^2+\omega^2} + \frac{b^2 e}{b^2+\omega^2}),$$

$$S_{yy}(\omega) = \frac{w_n^2}{4c^2}(\frac{a.d.\omega}{a^2+\omega^2} + \frac{b.e.\omega}{b^2+\omega^2})$$

and

$$\frac{dS_{yy}(\omega)}{d\omega} = \frac{w_n^2}{4c^2}(\frac{a.d(a^2-\omega^2)}{(a^2+\omega^2)^2} + \frac{b.e(b^2-\omega^2)}{(b^2+\omega^2)^2}).$$

Substitution into equation (2.14) and (2.13) lead to the expected value of the measured output and cross power spectrum for the Hanning family of windows. Substitution in (2.16) and (2.15) will lead to a similar expression for the Papoulis family of windows.

Figure (2.6) is an impulse response representation of the system under investigation. Figures (2.7) and (2.8) compare expectations of frequency response functions at $T = 150$ and $T = 300$ for the Do-nothing, exact Hanning ($\rho = 0.5$) and exact Papoulis ($\rho = 0.5$) windows.

Figures (2.9) and (2.10) present square coherence plots for the above windows at $T = 150$ and $T = 300$. Finally figures (2.11), (2.12) and (2.13) compare bias squared at $T = 150$, $T = 300$ and $T = 3000$.

In all cases, the exact Papoulis window yields the smallest bias in the resulting frequency response estimate. As a measure of variance in the estimate, the coherence plots also show Papoulis to be superior. The exact Hanning was found not to be a good estimator of the bias when T is of the same length as the system settling time. However, for large T (> 150), the resulting frequency response gave results comparable to the exact Papoulis window.

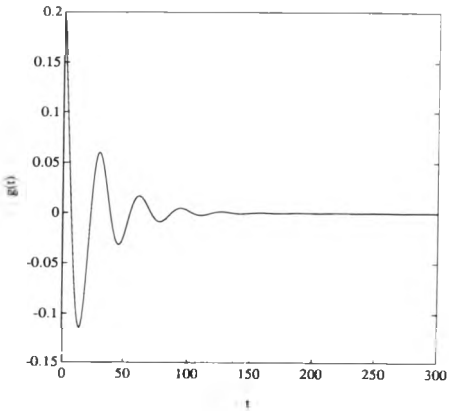

Figure 2.6: Impulse response of

$G(s) = s.w_n/(s^2 + 2\zeta w_n s + w_n^2), \zeta = 0.2, \quad w_n = 0.2.$

——— True value.

-.-.-.-.- Exact Papoulis window ($\rho = \frac{1}{3}$).

- - - - - - Exact Hanning window ($\rho = \frac{1}{2}$).

..... Do-nothing window.

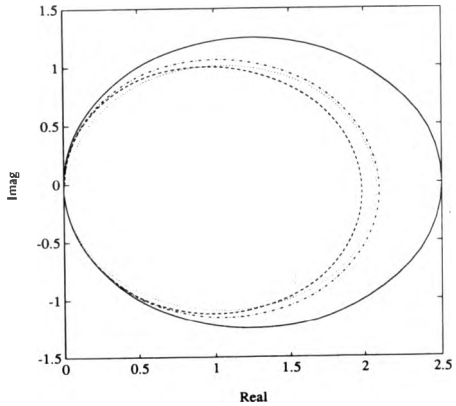

Figure 2.7: Expected value of measured frequency response. Second order transfer function for $T = 150$.

——— True value.

-.-.-.-.- Exact Papoulis window ($\rho = \frac{1}{3}$).

- - - - - - Exact Hanning window ($\rho = \frac{1}{3}$).

..... Do-nothing window.

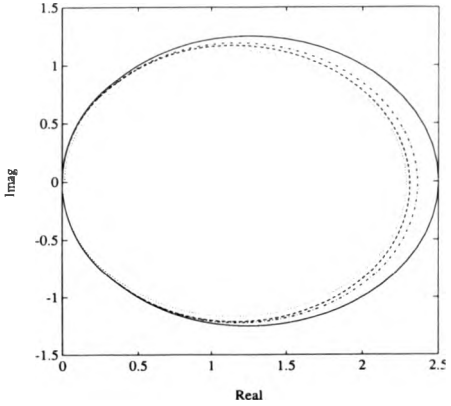

Figure 2.8: **Expected value of measured frequency response. Second order transfer function for $T = 300$.**

-.-.-.-.- Exact Papoulis window ($\rho = \frac{1}{2}$).

- - - - - - Exact Hanning window ($\rho = \frac{1}{2}$).

..... Do-nothing window.

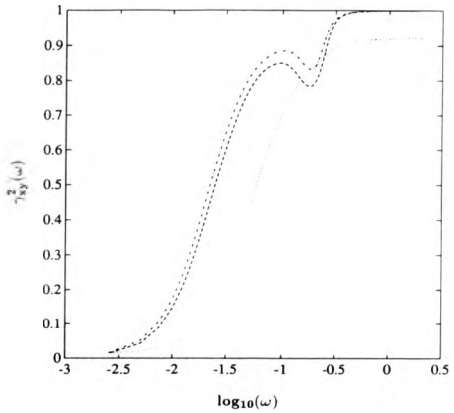

Figure 2.9: Square coherence of second order transfer function for $T = 150$.

-.-.-.-.- Exact Papoulis window ($\rho = \frac{1}{2}$).

- - - - - - Exact Hanning window ($\rho = \frac{1}{2}$).

..... Do-nothing window.

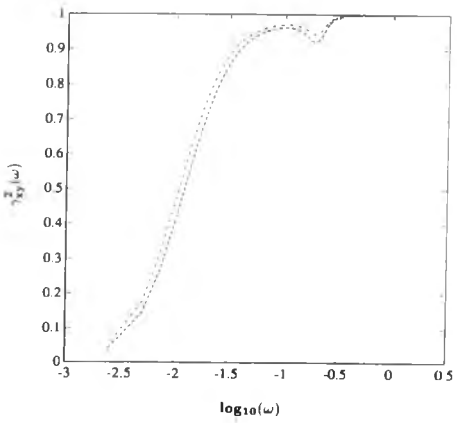

Figure 2.10: Square coherence of second order transfer function for $T = 300$.

-.-.-.-.- Exact Papoulis window ($\rho = \frac{1}{2}$).

- - - - - - Exact Hanning window ($\rho = \frac{1}{2}$).

..... Do-nothing window.

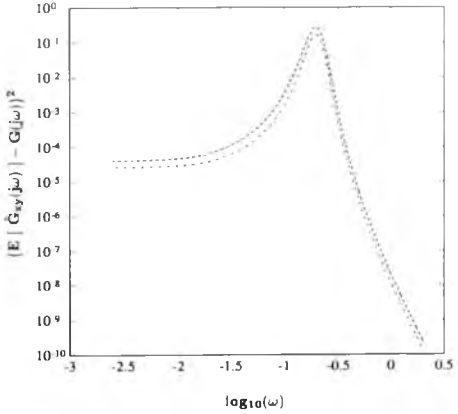

Figure 2.11: **Square of bias for second order transfer function for $T = 150$.**

-.-.-.-.- Exact Papoulis window ($\rho = \frac{1}{3}$).

- - - - - - Exact Hanning window ($\rho = \frac{1}{3}$).

..... Do-nothing window.

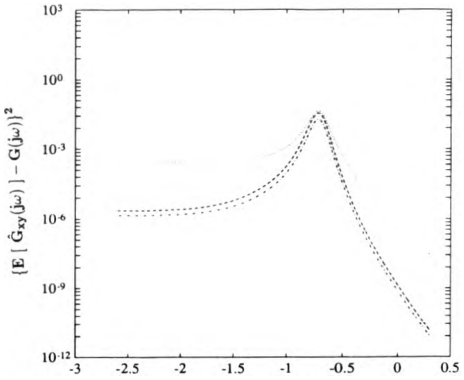

Figure 2.12: **Square of bias for second order transfer function for $T = 300$**

-.-.-.-.- Exact Papoulis window ($\rho = \frac{1}{2}$).

- - - - - - Exact Hanning window ($\rho = \frac{1}{3}$).

..... Do-nothing window.

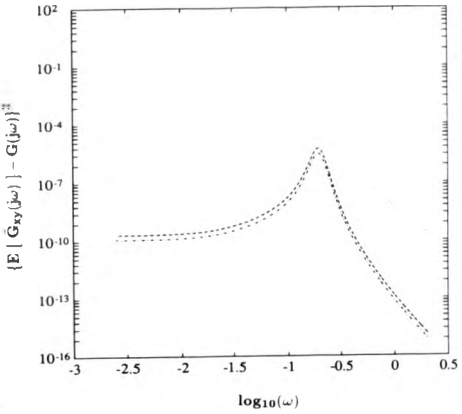

Figure 2.13: Square of bias for second order transfer function for $T = 3000$.

From the view point of minimising the bias, if $T \neq \infty$, the exact Hanning and exact Papoulis are in fact suboptimum windows. Minimising the bias can be justified if the assumption is made that the record length is sufficiently long to allow for enough smoothing over segments to reduce variance in the frequency response estimate.

Under such conditions, the optimum for these class of windows can be evaluated by minimising the integral square of the bias between the true $G(j\omega)$ and $\hat{G}_{xy}(j\omega)$ obtained by varying ρ over the range $0.5 \leq \rho \leq 1$ for the Hanning family and $0.0 \leq \rho \leq 0.5$ for the Papoulis family.

This is implemented by using a Matlab optimisation routine "fmin.m". Figure (2.14) and (2.15) compare frequency responses between optimum Hanning, optimum Papoulis and exact Papoulis windows at $T = 150$ and $T = 300$.

It is observed that the superior estimates based on these optimum windows are concentrated at parts of the spectrum which exhibit high signal to noise ratios. As a result, further away from the resonant frequency, estimates become poor in comparison with the exact Papoulis window.

Figures (2.16), (2.17) and figures (2.18), (2.19) are the respective square coherence and bias squared at $T = 150$ and $T = 300$.

——— True value.

-.-.-.-.- Optimum Papoulis window ($\rho = 0.36$).

- - - - - - Optimum Hanning window ($\rho = 0.76$).

..... Exact Papoulis.

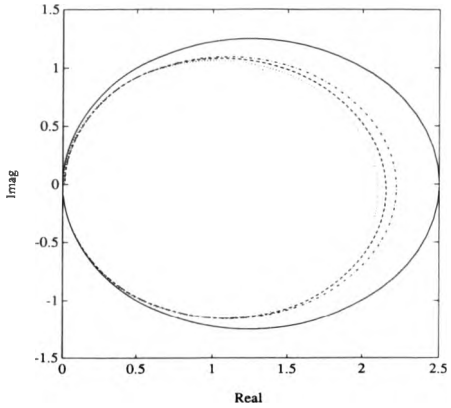

Figure 2.14: **Expected value of measured frequency function response of second order transfer function using optimum windows for $T = 150$.**

——— True value.

-.-.-.-.- Optimum Papoulis window ($\rho = 0.41$).

- - - - - - Optimum Hanning window ($\rho = 0.84$).

..... Exact Papoulis.

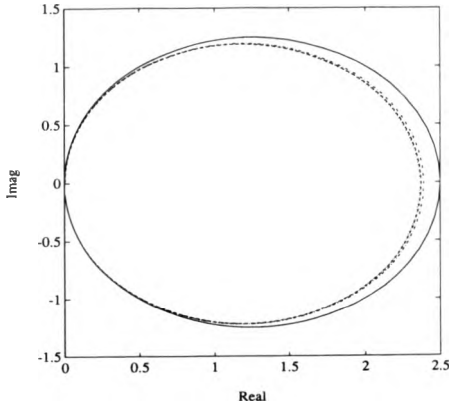

Figure 2.15: Expected value of measured frequency function response of second order transfer function using optimum windows for $T = 300$.

-.-.-.-.- Optimum Papoulis window ($\rho = 0.36$).

- - - - - Optimum Hanning window ($\rho = 0.76$).

..... Exact Papoulis.

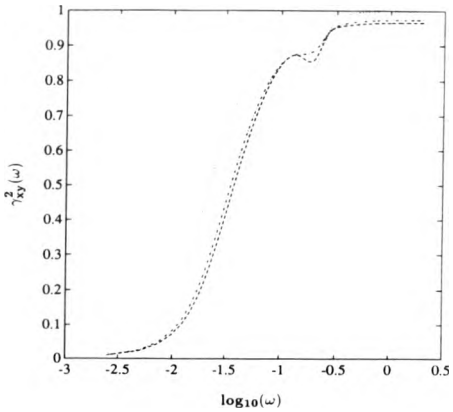

Figure 2.16: Square coherence for optimum estimates for $T = 150$.

-.-.-.-.- Optimum Papoulis window ($\rho = 0.41$).

- - - - - - Optimum Hanning window ($\rho = 0.84$).

..... Exact Papoulis.

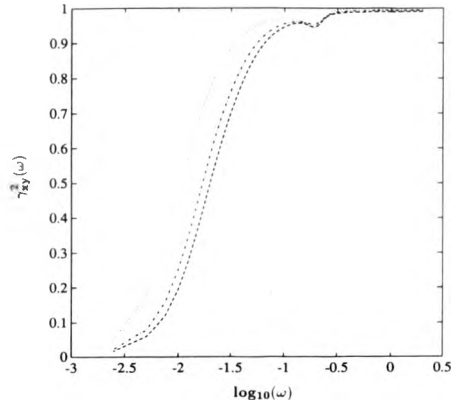

Figure 2.17: Square coherence for optimum estimates for $T = 300$.

-.-.-.-.- Optimum Papoulis window ($\rho = 0.36$).

- - - - - Optimum Hanning window ($\rho = 0.76$).

..... Exact Papoulis.

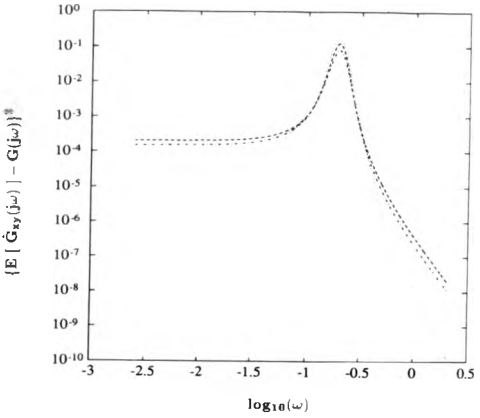

Figure 2.18: Bias squared for optimum estimates for $T = 150$.

-.-.-.-.- Optimum Papoulis window ($\rho = 0.41$).

- - - - - - Optimum Hanning window ($\rho = 0.84$).

..... Exact Papoulis.

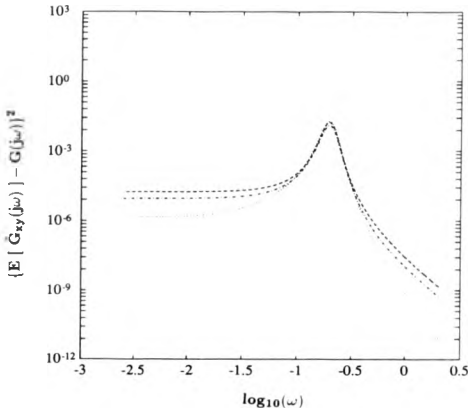

Figure 2.19: Bias squared for optimum estimates for $T = 300$.

2.7.2 Non-white noise input.

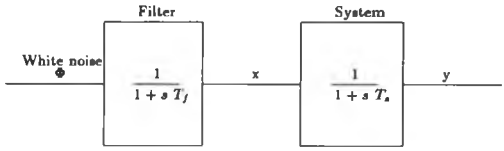

Figure 2.20: **Schematic for first order filter system arrangement.**

The preceding theory can be applied for stationary arbitrary inputs and systems. For all but the simplest cases, numerical evaluation is required throughout. A simple example is selected to demonstrate the steps involved to indicate the form of errors with various windows.

Consider the first order filter system arrangement in figure (2.20). For this, the respective correlation functions are

$$
\begin{aligned}
r_{xx}(\tau) &= \frac{1}{2T_f}\exp(-\frac{|\tau|}{T_f}), \\
r_{xy}(\tau) &= \frac{1}{2(T_f^2 - T_s^2)}[(T_f + T_s)\exp(-\tau/T_f) - 2T_s\exp(-\tau/T_s)] \quad \text{for } \tau \geq 0 \\
&= \frac{1}{2(T_f + T_s)}\exp(\tau/T_f) \quad \text{for } \tau \leq 0 \\
r_{yy}(\tau) &= \frac{1}{2(T_f^2 - T_s^2)}[T_f\exp(-|\tau|/T_f) - T_s\exp(-|\tau|/T_s)].
\end{aligned}
$$

Numerical integration is used to evaluate expectation of measured input, output and cross power spectrum.

The correlation functions for $T_f = 5$ and $T_s = 10$ are given in figure (2.21). Figures (2.22), (2.23) and (2.24) show comparison of expected frequency responses, square coherence and square of the bias for the Do-nothing, exact Hanning and exact Papoulis

window.

It is observed that, although Papoulis is overall a better estimator, the Do-nothing window performa better at low frequencies whilst the Hanning is the better at higher frequencies. Further simulation studies show that as T becomes larger, the Papoulis window exhibits increasing superiority at all frequencies. This was also found to be the case when higher order filter system arrangements were considered.

- - - - - - Input correlation $r_{xx}(\tau)$

-.-.-.-.- Output correlation $r_{yy}(\tau)$

——— Cross correlation $r_{xy}(\tau)$.

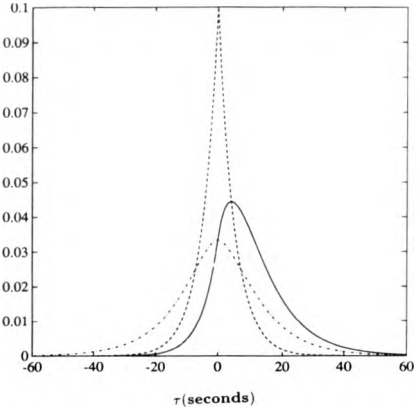

Figure 2.21: **Correlation functions for $T_f = 5$ and $T_s = 10$.**

-.-.-.-.- Exact Papoulis window ($\rho = \frac{1}{3}$).

- - - - - -Exact Hanning window ($\rho = \frac{1}{4}$).

..... Do-nothing window.

——— True.

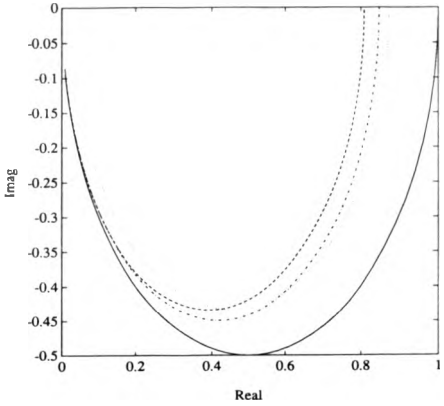

Figure 2.22: Expected value of measured frequency response for ($T_f = 5, T_s = 10, T = 60$).

- · - · - · - Exact Papoulis window ($\rho = \frac{1}{3}$).

- - - - - - Exact Hanning window ($\rho = \frac{1}{2}$).

..... Do-nothing window.

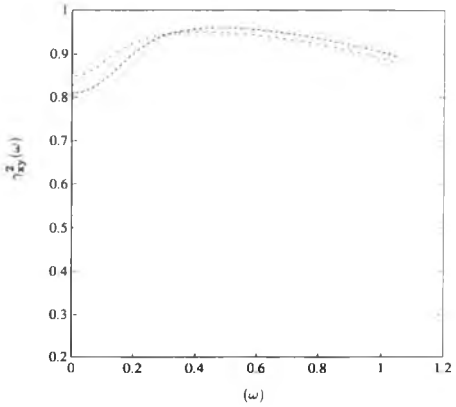

Figure 2.23: Square coherence for $T_f = 5, T_s = 10$ and $T = 60$.

-.-.-.-.- Exact Papoulis window ($\rho = \frac{1}{3}$).

- - - - - - Exact Hanning window ($\rho = \frac{1}{4}$).

..... Do-nothing window.

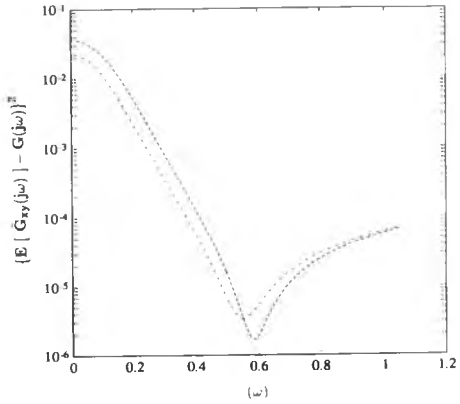

Figure 2.24: **Bias squared for $T_f = 5, T_s = 10$ and $T = 60$.**

2.8 Window design

So far it has been shown that the best window is a function of the observation time as well as the system under consideration. Several criteria which are optimum in a specific sense, have been developed in the time domain for solving the system identification problem. Amongst them are classical Least square analysis [7], and least mean square error adaptation algorithms [8]. In the frequency domain however, only very simple, suboptimal techniques have been proposed for solving the system identification problem, which have proved not to be entirely adequate for many classes of problems [9].

In this section, a qualitative evaluation of a newly proposed window design methodology is given with special consideration to short term records.

2.8.1 Differing input and output time windows.

Conventional analysis weights both input and output records with the same windows to give good estimates of individual spectra. As frequency response estimation is concerned with the ratio between the cross power spectrum and the input power spectrum, it may prove beneficial to implement on the input-output records different windows so as to improve this ratio.

2.8.2 Alignment of the cross correlation function.

Alignment is the process of time shifting the cross correlation function or the lag window so that their maximum absolute values coincide.

The process of alignment can be easily implemented when evaluating frequency responses through the estimation of sample correlation functions. The misalignment factor (say S_r) is defined as the difference in time from zero lag to the position of maximum weight of the cross correlation function and when $S \neq 0$, it is shown in [11], to lead to bias in the resulting cross power and hence coherence and frequency response estimates.

There are two methods to reduce the effects of this bias :-

(1) Align the cross correlation function and the window at zero lag.

(2) shift the window on the correlation function so that the maximum weight of the window occurs at S.

The latter will now be chosen to demonstrate the effect of misalignment on the bias of the cross power spectrum estimate.

Consider a window $w_{xy}(\tau)$ defined by

$$w_{xy}(\tau) = \frac{1}{2}[\,1 + \cos(\frac{\pi\tau}{T} - \theta)\,] \qquad \text{for} \qquad U - \frac{T}{2} \leq \tau \leq U + \frac{T}{2}$$

$$w_{xy}(\tau) = 0 \qquad \text{otherwise}$$

where

$$\theta = \frac{\pi U}{T}.$$

The above equation represents a window on the cross correlation function which has a position of maximum weight U variable over the time duration $-T \leq U \leq T$. See figure (2.25).

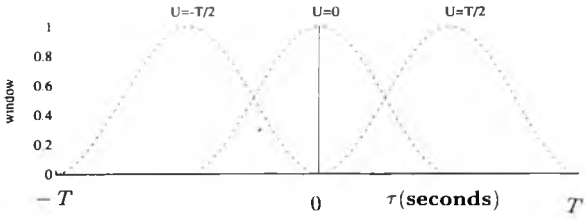

Figure 2.25: **Window on the cross correlation function with variable position of maximum weight U.**

The cross correlation function is defined for the first order filter system arrangement

of figure (2.26).

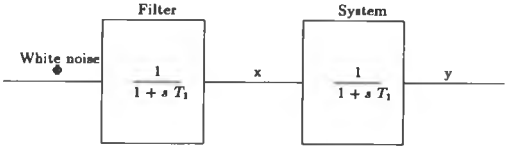

Figure 2.26: **Cross correlation function defined by first order filter system schematic.**

The signal x has auto correlation function

$$r_{xx}(\tau) = \frac{\Phi}{2T_1} \exp(-\frac{|\tau|}{T_1})$$

where Φ is the constant spectral density of the white noise input.

The system impulse response $g(t)$ is given by

$$g(t) = \frac{\exp(-t/T_1)}{T_1}$$

Using the relationship

$$r_{xy}(\tau) = r_{xx}(\tau) * g(\tau),$$

this gives

$$r_{xy}(\tau) = \frac{\Phi}{4T_1} \exp(\frac{\tau}{T_1}) \quad \text{for} \quad \tau \leq 0$$
$$r_{xy}(\tau) = \frac{\Phi}{2T_1^2}(\frac{T_1}{2} + \tau) \exp(-\frac{\tau}{T_1}) \quad \text{for} \quad \tau \geq 0$$

Figure (2.27) shows the cross correlation function calculated for $T_1 = 15$. The

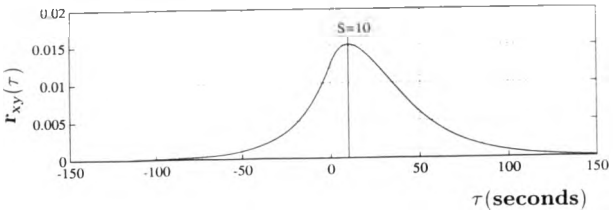

Figure 2.27: **Cross correlation function for $T_1 = 15$ seconds.**

misalignment factor $S = 10$ seconds. The amplitude and phase of the measured cross power spectrum estimates are evaluated from the expected value of the measured cross power spectrum

$$E\left[\,\hat{\Phi}_{xy}(\omega)\,\right] = \int_{-T}^{T} r_{xy}(\tau) w_{xy}(\tau) \exp(-j\omega\tau) d\tau.$$

Figure (2.28) show plots of bias in the amplitude and phase cross power estimates for value of U at $U = -10, 0, 5$ and 10. It shows that bias in amplitude and phase of these estimates is smallest at $U = S = 10$ and confirms similar observations made by Jenkins and Watts [11].

In practice this misalignment S, can be obtained from straight forward visual inspection, thus making it possible to either align the cross correlation function (so that the epoch of its peak occurs at zero lag) or to shift in time the appropriate lag window which weights this function by S in order for these peaks to coincide.

As correlation functions are not evaluated in the direct method of frequency response estimation, the alignment factor will not be observed and even if such a parameter where known, there comes the added difficulty of applying this knowledge directly to the input-output time windows.

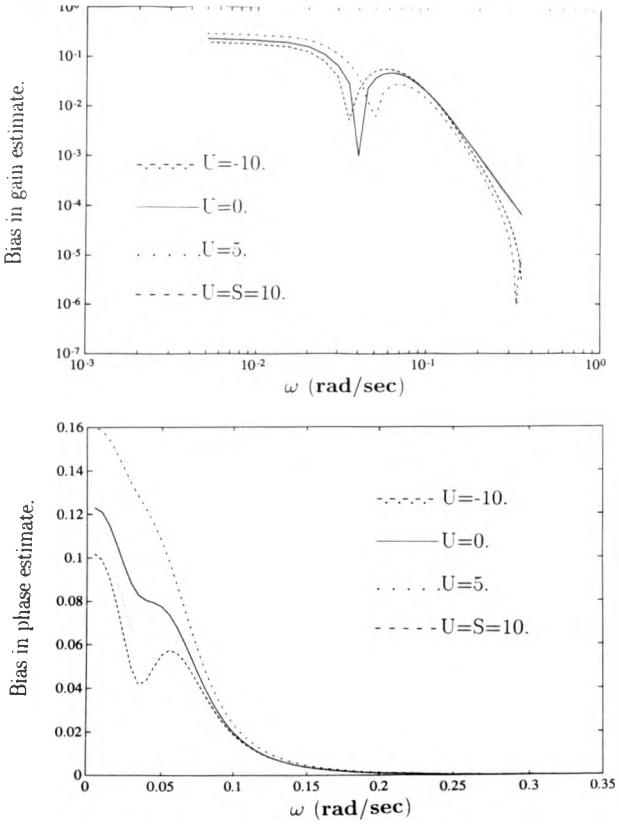

Figure 2.28: Bias in gain and phase of cross power spectral estimates for varying positions of U of $w_{xy}(\tau)$.

2.8.3 Effects of transients and external noise.

A good estimate of the frequency response of a linear systems can always be expected when the observation time is of long enough duration and there exists no extraneous noise sources to influence these records. When using short input-output records, sources of error arise due to transient effects which lead to bias and variance in the resulting frequency response estimate. **Douce and Balmer** [1], interpret the effects of transients

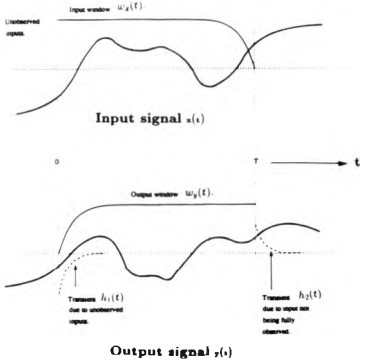

Figure 2.29: **Design of time windows to reduce transient effects.**

as the difference in output responses between an input signal $x(t)$ observed over the duration $-\infty \leq t \leq T$ and an equivalent periodic input

$$x_r(t) = x(t) \quad \text{for} \quad n = -\infty, \ldots, -1, 0.$$

This transient, may be viewed in another way.

Consider the response from $t = 0$ due to the input signal $x(t)$ observed over the time duration $-\infty \leq t \leq 0$. This 'unobserved' input, results in an output transient $h_1(t)$ that dies down as $t \longrightarrow T$ and will be part of the observed output signal $y(t)$. See figure (2.29). Similarly consider the response from $t = T$ due to the input signal $x(t)$ observed over the time duration $-\infty \leq t \leq T$. Assuming that the record length is at least greater than the settling time of the system, this transient $h_2(t)$ will be mostly due to the observed input,

$$x(t) \quad \text{for} \quad 0 \leq t \leq T,$$

and in reality should be incorporated in any spectral estimation procedure. However, it will be unobserved due to the finite duration of $y(t)$, i.e,

$$y(t) = 0 \quad \text{for} \quad t \leq 0, \quad \text{and} \quad t > T.$$

Summarising, at the start of the output record, there exist components due to unobserved inputs $h_1(t)$, and towards the finish, part of the complete response $h_2(t)$ to the observed input is not observed. Hence it is not unreasonable to give a reduced weight towards the end of the input record and also towards the beginning of the output record in order to reduce these effects.

2.8.4 Other factors to be considered.

The amount of weight to be applied on both input and output records must evidently depend on the following arguments:

(a) The observation time T.

The larger the record length T becomes, the less weight should be applied to the record, as the effects of the transients $h_1(t)$ and $h_2(t)$ will be reduced in comparison to the observed records $x(t)$ and $y(t)$.

(b) Differing window types for different systems.

It is inconceivable to imagine that a first order system described by a simple time constant will require the same shape time window pair as a second order system which is governed by both a resonant frequency and damping factor.

(c) Non-white input signals.

If any prefiltering takes place on the input record, then this must surely also influence the time windows to be applied to the record before analysis.

(d) Output noise.

In [10] it is shown that the effect of short input-output records is analogous to considering an equivalent biased system with an uncorrelated noise source. Any extra observed noise sources such as environmental or measurement noise (which are assumed to be uncorrelated with the input) can be considered for the purpose of analysis, as further increasing both the bias in the equivalent system and that of the uncorrelated noise component. Lack of information on any one of the above will inevitably lead to imperfect band limiting ability of the window [9].

2.8.5 A Priori knowledge of the system.

Here in order to show qualitatively how a priori knowledge of the system under analysis may prove to be beneficial in the system identification problem, we must give reasons as to why in the past such a concept has not been used adequately.

2.8.5.1 Reasons against

Strong criticism has been made in the past on the design of time and lag windows in advance of spectral analysis and frequency response estimation [11]. These are as follows :-

(1) Any criteria for determining optimality are case specific. Therefore each criterion will produce spectral or frequency windows which are arbitrary in that specific sense.

(2) An optimality criteria will present too rigid a mathematical formulation in the objective of spectral analysis and specific features such as width of spectral peaks or slopes of the spectrum over such bandwidths may be inadequately catered for.

(3) Optimum windows will inevitably differ for different realisations of the same system as the approach will only indicate the best window in an average sense.

(4) Any optimum window design in practical estimation methods will inevitably be a function of the unknown system under analysis and so a bad estimate of the system will always lead to bad estimate in the analysis.

It was concluded for these reasons that a more robust and flexible approach for window designs was needed in order to build a suitable empirical procedure. These procedures although simple have always lead to suboptimal techniques in solving the system identification problem, and have in general proven not to be entirely adequate for many reasonable classes of problem [9].

2.8.5.2 Optimisation criteria.

The above criticisms have been based on optimum criteria in the frequency domain. The most commonly used is the integrated mean square error criterion

$$\int_{-\infty}^{\infty} E[|\hat{G}(j\omega) - G(j\omega)|^2] d\omega, \tag{2.17}$$

where $\hat{G}(j\omega)$ and $G(j\omega)$ are the respective measured and true frequency responses at frequency ω.

Another criterion

$$\int_{-\infty}^{\infty} \frac{E[(\hat{G}(j\omega) - G(j\omega))^2]}{|G(j\omega)|^2} d\omega,$$

attempts to obtain a compromise estimate at all frequencies. This differs from (2.17) in that the expected mean square error at a particular frequency is weighted in inverse

proportion to the value of the true frequency response at that frequency and has also been indirectly proposed in [11].

It has been said that such criteria in spectral analysis are very limited and that they only serve as a useful tool in enabling windows such as the Bartlett, Hanning, Tukey, Parzen and others to be ranked according to the various criteria [11].

2.8.5.3 Reasons for

Minimum mean square error is the most obvious criterion to choose when designing input-output windows for best statistical estimates in the frequency response. This however also requires the true system $G(j\omega)$ to be known, and lack of such knowledge will result in suboptimal window design.

If external noise to the system is considered negligible or the record length is long enough to allow sufficient smoothing, choosing $w_x(t)$, and $w_y(t)$ to maximise the square coherence will prove desirable. The above is based on the following argument. In [5], it was shown that the effect of a finite record on the frequency response estimate can be considered analogous to an equivalent biased system that is subjected to an input of infinitesimal length with an uncorrelated noise source N added to the output (see figure (2.30)). Hence maximising the square coherence function is equivalent to minimising the noise to signal ratio which in turn will reduce the bias.

(1) The major criticism here is that a firm mathematical formulation to estimate these so called 'suboptimal windows' does not exist. It is for this reason that performing such analysis in the frequency domain, becomes too complex to analyse. As windows are functions of time, there exists a strong argument in performing such an optimisation directly in the time domain before analysis. This may prove beneficial from both the mathematical and qualitative view point.

(2) If a time domain approach is adopted, impulse response functions can be chosen in the optimisation criteria rather than frequency response. This allows information such as settling times, dominating time constants, static gains and time delays to be used in

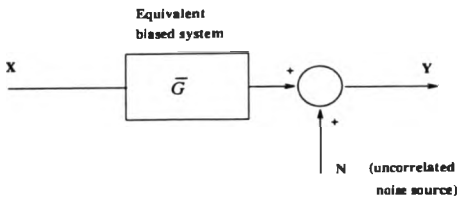

Figure 2.30: **Equivalent biased system.**

building up the initial a priori estimate in order to obtain acceptable impulse response models.

(3) Because of the ease of mapping between time and frequency domains, updates of the impulse response can be made by taking the inverse Fourier transform of the frequency response. This leads to the exciting prospect of a convergent recursive criterion for the frequency response estimate.

(4) The above arguments will make redundant the behavioral study of leakage in the corresponding spectral windows, as this information will be directly catered for in the impulse response estimate.

2.9 Example (2)

In this section, the window design concepts discussed previously will be illustrated. Consider the first order filter system arrangement

$$G_{filter}(s) = G_{system}(s) = \frac{1}{1+5s} \tag{2.18}$$

with a record length $T = 30$. The continuous transfer function is mapped to the discrete domain by using a bilinear transformation with a sampling rate of 1Hz.

The trigonometric sum type window is again used, the positions of maximum weight for the input window U_x and the output U_y are varied over the range $0 \leq t \leq T$ to illustrate the effects of alignment, and differing windows on the input-output records. The record length is chosen to be not much greater than the settling time of the system so that transient effects are not negligible.

The two optimisation criteria chosen are minimum square magnitude of the bias and maximum square coherence. In the optimisation it is required to solve

$$min \int_0^\pi \mid E \mid (\hat{G}_{xy}(j\omega) \mid - G(j\omega) \mid^2 d\omega,$$

and

$$max \int_0^\pi \gamma^2_{xy}(\omega)$$

For window pairs chosen to vary at a frequency of interest,

$$min\{E \mid (\hat{G}_{xy}(j\omega) \mid - G(j\omega))\}^2$$

and

$$max\{\gamma^2_{xy}(\omega)\}$$

are chosen. A priori judgment of the system will be dealt with in chapters 3 and 4.

For the Papoulis window, figure (2.31) is a mesh plot of the integral square of the

bias (multiplied by -1) with varying U_x and U_y.

Description of contour plot.

The contour plot of figure (2.32) compares the relative positions for the four optimised window designs. It is observed (from values of the contour lines), that both coherence criteria, lead to greater reduction in bias over the exact Papoulis window ($U_x = U_y = 15$). As expected, minimisation of the bias; either by minimising at each frequency, or by minimising over the whole range of frequencies ($0 \leq \omega \leq \pi$), produces the best results.

For the Papoulis window, figures (2.33) and (2.34) show window parameter variation of U_x and U_y with frequency for designs based on minimising square of bias and maximising square coherence.

A similar plot of contour (figure (2.35)) parameter variation of U_x and U_y with frequency (figure (2.36) and (2.37)) is also given for the Hanning window.

Simply by its nature, maximising coherence implies minimum noise to signal and hence variance. In the contour plots we observe that they are also good estimators of bias and so will lead to improved estimates when comparison is made with symmetrical windows.

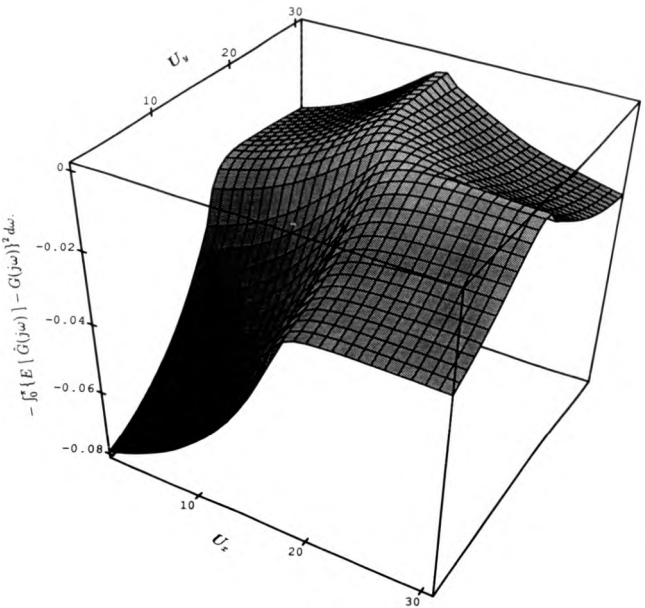

Figure 2.31: $-\int_0^\pi \{E[\hat{G}(j\omega)] - G(j\omega)\}^2 d\omega$ **with varying** U_x **and** U_y **(Papoulis window).**

$\omega = 0 - - > \cdots \omega = \pi$ Maximum square coherence

(Frequency dependent) criteria $max[\gamma^2_{xy}(\omega)]$

$\omega = 0 - - > \cdots \omega = \pi$ Minimum square of bias (Frequency dependent)

criteria $min\{E\ [\ G_{xy}(j\omega)\ ] - G(j\omega)\}^2$

□ Exact Papoulis window.

+ Maximum integrated square coherence criteria $max \int_0^\pi \gamma^2_{xy}(\omega)$.

△ Minimum integrated square of bias criteria $- \int_0^\pi \{E[\hat{G}(j\omega)] - G(j\omega)\}^2 d\omega$.

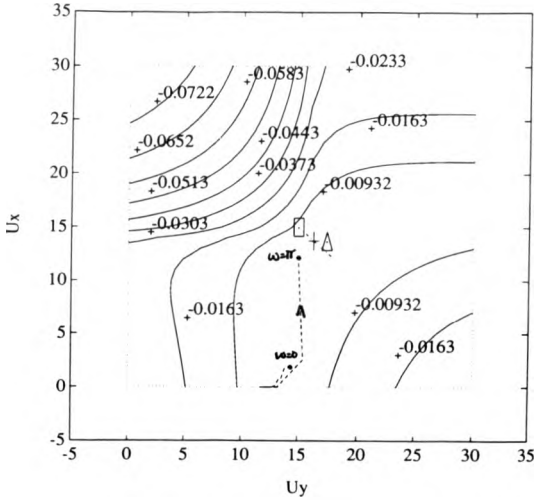

Figure 2.32: **Contour plot of $- \int_0^\pi \{E[(\hat{G}(j\omega)] - G(j\omega)\}^2 d\omega$ with varying U_x and U_y for the Papoulis window.**

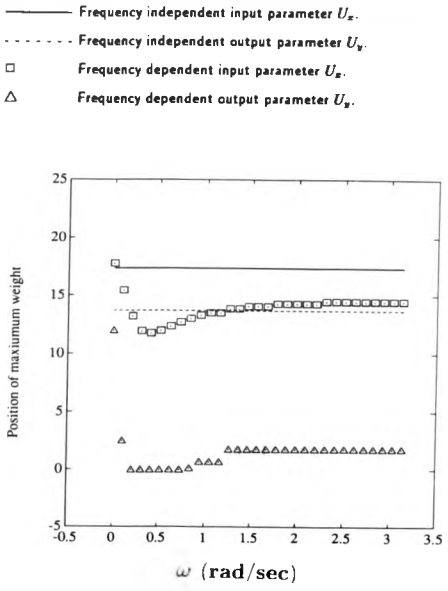

Figure 2.33: Variation of U_x and U_y using minimum bias square criterion (Papoulis window).

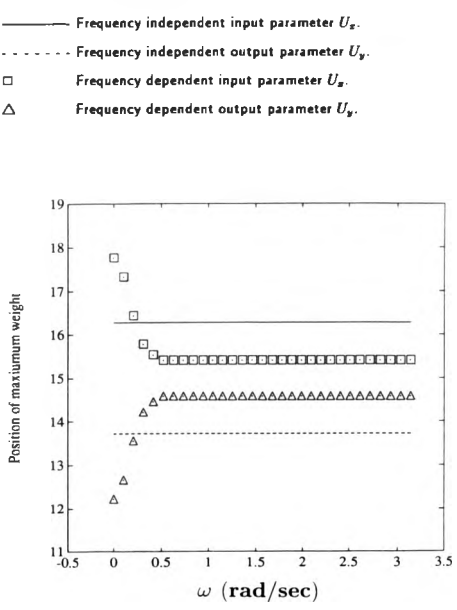

Figure 2.34: Variation of U_x and U_y using maximum square coherence criterion (Papoulis window).

$\omega = 0$ -.-.-> -.-.- $\omega = \pi$ Maximum square coherence

(Frequency dependent) criteria $max[\gamma^2_{xy}(\omega)]$

$\omega = 0$- - >- - $\omega = \pi$ Minimum square of bias (Frequency dependent)

criteria $min\{E\ [\ \hat{G}_{xy}(j\omega)\ ] - G(j\omega)\}^2$

□ Exact Papoulis window.

+ Maximum integrated square coherence criteria $max \int_0^\pi \gamma^2_{xy}(\omega)$.

△ Minimum integrated square of bias criteria $- \int_0^\pi \{E[\hat{G}(j\omega)] - G(j\omega)\}^2 d\omega$.

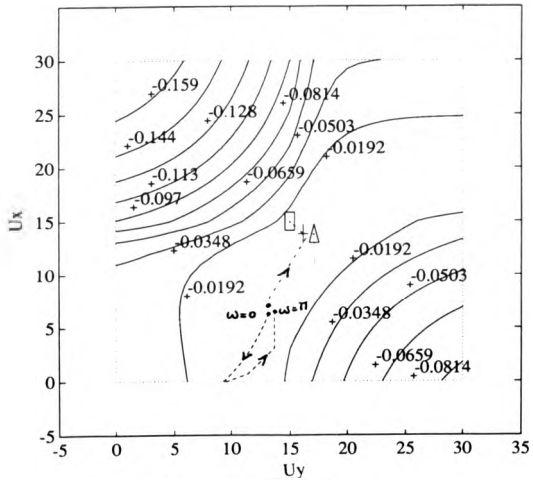

Figure 2.35: Contour plot of $- \int_0^\pi \{E[(\hat{G}(j\omega)] - G(j\omega)\}^2 d\omega$ with varying U_x and U_y for the Hanning window.

———— Frequency independent input parameter U_x.

- - - - - - - Frequency independent output parameter U_y.

□ Frequency dependent input parameter U_x.

△ Frequency dependent output parameter U_y.

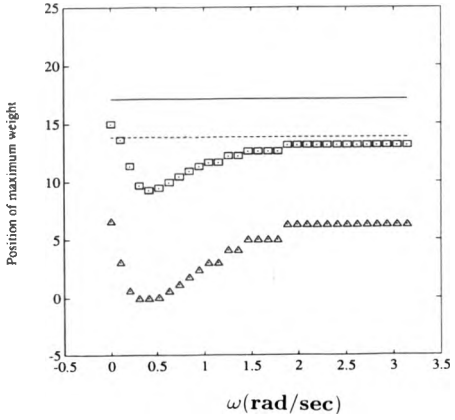

Figure 2.36: Variation of U_x and U_y using minimum bias square criterion (Hanning window).

——— Frequency independent input parameter U_x.

- - - - - - - Frequency independent output parameter U_y.

□ Frequency dependent input parameter U_x.

△ Frequency dependent output parameter U_y.

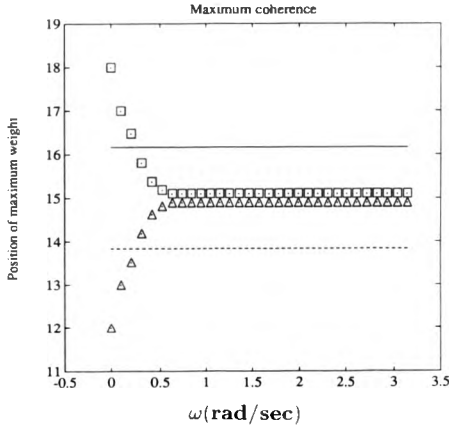

Figure 2.37: Variation of U_x and U_y using maximum square coherence criterion (Hanning window).

2.10 Summary

The introduction of parametric windows (such as Trigonometric sum type) are in themselves restricting in designing optimal windows for non-parametric spectral estimation. Ideally windows should be designed wholly in terms of either the true system or a model of the system under investigation. We have also shown that with no a priori knowledge designing windows to maximise square coherence function produces reliable estimates.

The art of window carpentry is introduced in this chapter, it is the basic building block in the design of least mean square error windows which will be introduced in the next chapter.

2.11 References for Chapter (2).

[1] **Douce. J.L. and Balmer. L.,**: 'Transient effect in spectrum estimation'. Proc,IEE.No.1,part D,pp25-29,January 1985.

[2] **Geckinli. N.C. and Yavuz. D.,**: 'Discrete Fourier transforms and its application to power spectra estimation'.Elsevier 1983.

[3] **Blackman. R.B. and Tukey. J.W.,**: 'The measurement of power spectra'. Dover Publications Inc. New York 1958.

[4] **Harris. F.J.,**: 'On the use of windows for harmonic analysis with the discrete Fourier transform'. Proc,IEEE,vol 66,No.1,January 1978.

[5] **Balmer. L.,**: 'Short term spectral estimation with applications'. Ph.D. Thesis,University of Warwick,1986.

[6] **Papoulis. A.,**: 'Minimum bias windows for high resolution spectral estimates'. Trans. IEEE, vol.IT-19,pp9-12,No. 1.January 1973.

[7] **Anderson. T.W. and Taylor. J.B.,**: 'Strong consistency of least-square estimates in dynamic models'.Ann. stat,vol 7,pp484-489,1979.

[8] **Andersson. P.,**: 'Adaptive forgetting in recursive identification through multiple models'. Int. J. Control,vol 42,pp 1175-1194,1985.

[9] **Rabiner. L.R.** : 'Short term Fourier analysis techniques for FIR systems identification and power spectrum estimation'. IEE. Trans, vol ASSP 27, No 2, April 1979.

[10] **Douce. J.L. and Balmer. L.,**: 'The statistics of frequency response estimates'. Proc. IEE. vol 137, Pt. D, No.5, September 1990.

[11] **Jenkins. G.M. and Watts. D.G.,**: 'Spectral analysis and its applications'. Holden Day,1968.

Chapter 3

Least mean square error (LMSE) window (I)

3.1 Introduction

It is not unusual to assume from the system identification viewpoint that one may have prior knowledge about certain characteristics, such as dominant time constants or dead times of the system, from which the input $x(t)$ and the output $y(t)$ are obtained. If this is the case, it may be desirable to modify $x(t)$ and $y(t)$ before analysis by choosing an appropriate input window $w_x(t)$ and output window $w_y(t)$ in order to take account of this knowledge. This in turn, may lead to an improvement in the resulting frequency response estimate.

An attractive method is presented here, where a priori knowledge of the system under analysis is assumed to be available.

Figure (3.1) illustrates a novel approach to the design of time domain windows when an a priori model of the system impulse response $g(t)$ is assumed. The object here is to minimise the time integral of the expected value of the error squared, $e^2(t)$, where the

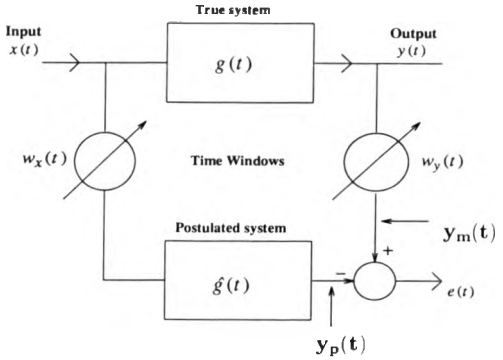

Figure 3.1: **Proposed least mean square error schematic.**

error is the difference between the windowed (or modified) system output $y_m(t)$ and the predicted response $y_p(t)$ of the given model to the windowed input.

In the following sections, we shall deal with the more generalised case when the input signal $x(t)$ is non-white. From this we will define the conditions thus enabling us to evaluate the more simplified white noise condition. This special case will be studied in section (3.8).

3.2 Coloured noise input.

Consider an input applied at time $t = t_1$. The output will be composed of responses due to excitations prior to t_1, and the response due to the input applied at time t_1.

Figure (3.1), defines the modified output $y_m(t)$ as

$$y_m(t) = w_y(t) \int_{-\infty}^{t} x(\tau) g(t-\tau) d\tau. \tag{3.1}$$

The response to the excitation $x(t)$ that is windowed by $w_x(t)$ (prior to input to the postulated system $\hat{g}(t)$) is the predicted response to the windowed input :-

$$y_p(t) = \int_0^t w_x(t) x(\tau) \hat{g}(t-\tau) d\tau. \tag{3.2}$$

Thus the function to be minimised is

$$I = \int_0^\infty E[(y_m(t) - y_p(t))^2] dt. \tag{3.3}$$

Splitting equation (3.3) into its three components and approximating the true impulse response (for the purpose of this minimisation) by assuming $g(t) = \hat{g}(t)$,

$$I = I_1 - I_2 + I_3$$

with

$$I_1 = \int_0^\infty w_y^2(t) \int_{-\infty}^{t} \hat{g}(t-\tau_2) \int_{-\infty}^{t} r_{xx}(\tau_1 - \tau_2) \hat{g}(t-\tau_1) d\tau_1 d\tau_2 dt \tag{3.4}$$

$$I_2 = 2\int_0^\infty w_y(t)\int_{-\infty}^{t}\bar{g}(t-\tau_2)\int_0^t w_x(\tau_1)r_{xx}(\tau_1-\tau_2)\bar{g}(t-\tau_1)d\tau_1 d\tau_2 dt \qquad (3.5)$$

$$I_3 = \int_0^\infty \int_0^t w_x(\tau_2)\bar{g}(t-\tau_2)\int_0^t w_x(\tau_1)r_{xx}(\tau_1-\tau_2)\bar{g}(t-\tau_1)d\tau_1 d\tau_2 dt \qquad (3.6)$$

where

$$r_{xx}(\tau_1-\tau_2) = E[x(\tau_1), x(\tau_2)]$$

A solution can be formulated by differentiating equation (3.3) separately with respect to the input and output windows at the instant $t = t_1$. Setting these derivatives to zero,

$$\frac{\partial I}{\partial w_x(t_1)} = 0, \qquad (3.7)$$

$$\frac{\partial I}{\partial w_y(t_1)} = 0. \qquad (3.8)$$

The notation $\frac{\partial I}{\partial w_x(t_1)}$ is used to denote the derivative of I with respect to the input window at $t = t_1$ and these equations must be satisfied for all t_1 in the range $0 \le t_1 \le T$.

3.3 Derivative of integral error with respect to $w_x(t_1)$.

Equation (3.7) can be written as

$$-\frac{\partial I_2}{\partial w_x(t_1)} + \frac{\partial I_3}{\partial w_x(t_1)} = 0 \qquad (3.9)$$

since I_1 does not contain terms of $w_x(t)$.

The first term in (3.9) is evaluated by differentiating I_2 with respect to $w_x(\tau_1)$ for

$\tau_1 = t_1$ and leads to

$$-2\int_0^{\infty} w_y(t)\hat{g}(t-t_1)\int_{-\infty}^{t} r_{xx}(t_1-\tau_2)\bar{g}(t-\tau_2).d\tau_2 dt \tag{3.10}$$

Essentially, in the derivative, we are assuming that the output window is a known function which is non-zero only for $0 \leq t \leq T$. Also the postulated system $\bar{g}(t)$ is physically realisable, which allows for the redefinition of the outer integral in the above equation over the range $t_1 \leq t \leq T$.

Taking this into account and substituting $u = t_1 - \tau_2$ in equation (3.10),

$$-2\int_{t_1}^{T} w_y(t)\hat{g}(t-t_1)\int_{t_1-t}^{\infty} r_{xx}(u)\hat{g}(u+t-t_1)dudt. \tag{3.11}$$

Evaluating the second term in equation (3.9) gives :-

$$2\int_{t_1}^{\infty} \hat{g}(t-t_1)\int_0^{t} w_x(\tau_2)r_{xx}(t_1-\tau_2)\hat{g}(t-\tau_2)d\tau_2 dt.$$

A change in order of integration can be realised from figure (3.2) if T is set to ∞. This results in

$$2\int_0^{t_1} w_x(\tau_2)r_{xx}(t_1-\tau_2)\int_{t_1}^{\infty} \hat{g}(t-t_1)\hat{g}(t-\tau_2)dtd\tau_2 +$$

$$2\int_{t_1}^{\infty} w_x(\tau_2)r_{xx}(t_1-\tau_2)\int_{\tau_2}^{\infty} \hat{g}(t-t_1)\hat{g}(t-\tau_2)dtd\tau_2. \tag{3.12}$$

It is however possible to restate equation (3.12) by defining the inner integral as a

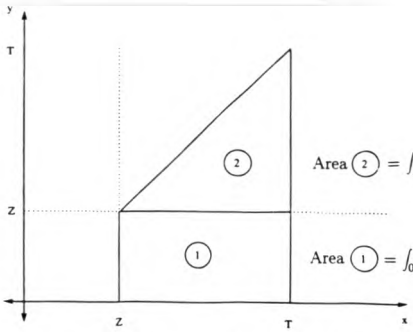

$$P(Z) = \int_Z^T \int_0^x f(x,y)dy\,dx = \text{Area}\,(1) + \text{Area}\,(2)$$

Figure 3.2: **Change of order of integration of** $P(z) = \int_z^T \int_0^x f(x,y)\,dy\,dx$.

single function

$$\begin{cases} \int_{t_1}^{\infty} \bar{g}(t-t_1)\bar{g}(t-\tau_2)dt & \text{for } t_1 \geq \tau_2 \\ \\ \int_{\tau_2}^{\infty} \bar{g}(t-t_1)\bar{g}(t-\tau_2)dt & \text{for } t_1 \leq \tau_2. \end{cases}$$

If equations (3.11) and (3.12) are substituted in equation (3.9) the generalised solution for the best least mean square input window is obtained :-

$$\int_0^{\infty} w_x(t)\gamma(t-t_1)dt = \int_{t_0}^{T} w_y(t)\varphi(t-t_1)dt \qquad (3.13)$$

where

$$\gamma(v) = r_{xx}(v) \begin{cases} \int_0^\infty \hat{g}(u)\hat{g}(u+v)du & \text{for } v \geq 0 \\ \int_0^\infty \hat{g}(u)\hat{g}(u-v)du & \text{for } v \leq 0 \end{cases} \tag{3.14}$$

and

$$\varphi(v) = \hat{g}(v) \int_v^\infty r_{xx}(u)\hat{g}(u-v)du \tag{3.15}$$

The integral in equation (3.14) is the auto correlation function to the output $y'(t)$ of the system with impulse response $\hat{g}(t)$ that is subjected to white noise excitation (See figure (3.3)). This leads to

$$\gamma(v) = r_{xx}(v) r_{y'y'}(v).$$

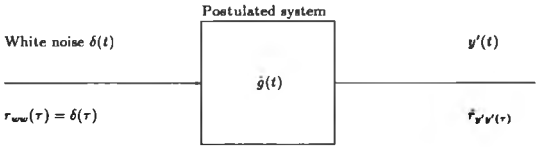

Figure 3.3: Schematic of output from postulated system subject to white noise input.

Similarly the integral in equation (3.15) is the cross correlation between the true system input $x(t)$ and the estimated system output $\hat{y}(t)$ (See figure (3.4)) and simplifies equation (3.15) to

$$\varphi(v) = \hat{g}(v)\hat{r}_{x\hat{y}}(v).$$

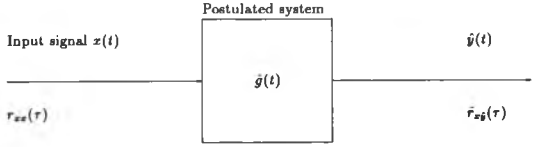

Figure 3.4: **Schematic of output from postulated system subject to input signal $x(t)$.**

3.4 Determination of $w_x(t_1)$ for a given $w_y(t_1)$.

In equation (3.13) there remains a difficulty in obtaining an exact analytical solution for $w_x(t_1)$ as the required function on the left hand side is also within an integral sign. This expression can however either be numerically evaluated or simplified by studying the behavior of function $\gamma(t - t_1)$.

METHOD 1, Numerical evaluation.

In (3.13) the required function is under the integral sign and if no assumptions are made about the left hand side of this equation, approximate solutions may be found at discrete values of t_1 by applying the theory of linear algebra. Here the integrals in equation (3.13) are essentially replaced by summations (to obtain n equations) by discretising the range of values of t_1. The linear transformation in n-dimensional space is of the form

$$f_i = \gamma_{i_1} w_{x_1} + \ \dots \ + \gamma_{in} w_{x_n} \quad \text{for} \quad i = 1, \ \dots \ , n$$

where

$$f_i = \sum_{j=1}^{n} w_{y_j} \varphi_{j,i},$$

and is characterized by the matrix formed from the transformation coefficients $\gamma_{i,j}$. This

transformation can be written in the alternative form

$$\mathbf{f} = \mathbf{\Gamma} \quad \mathbf{w_x},$$

where $\mathbf{w_x}(w_{x_1}, \ \cdots \ , \ w_{x_n})$ is the unknown vector, $\mathbf{f}(f_1, \ \cdots \ , \ f_n)$ is the transformed vector,and $\mathbf{\Gamma}$ is the matrix with coefficients $\gamma_{i,j}$.Hence the unknown can be evaluated by inverting the matrix. i.e,

$$\mathbf{w_x} = \mathbf{\Gamma}^{-1} \quad \mathbf{f}.$$

METHOD 2 - Simplifying the analysis.

In practice filters are incorporated in order to isolate the frequency range of interest in the analysis. In general the filtering is band selective and may be achieved by a frequency translation element combined with a high cut off rate, low pass filter. Such filters have bandwidths which are at least of the same order of magnitude as the system under investigation. If such a condition were not true, important spectral details would be lost when evaluating the frequency response estimate of the system.

If this assumption is valid, the function $\gamma(v)$ can be said to approximate a pulse of approximate duration $1/T$, so that for large T, it is reasonable to assume that $w_x(t_1)$ is constant over this pulse. Thus at the instant $t = t_1$, the left hand side of equation (3.13) can be approximated as

$$\int_0^\infty w_x(t)\gamma(t - t_1)dt \approx w_x(t_1)\int_0^\infty \hat{y}^2(t)dt,$$

and simplifies equation (3.13) to

$$w_x(t_1) = \lambda_x \int_{t_1}^{T} w_y(t)\varphi(t - t_1)dt \tag{3.16}$$

where

$$\lambda_x = \frac{1}{\int_0^\infty \hat{g}^2(t)dt}.$$

Experimental results has shown that even in the case when the above approximation did not strictly hold, there was no appreciable difference in the window shapes evaluated. For the reasons of accuracy of implementation, method 2 was chosen for further analysis.

3.5 Derivative of integral error with respect to $w_y(t_1)$.

Differentiating equation (3.3) with respect to $w_y(t_1)$ and using the same notation as before gives

$$\frac{\partial I_1}{\partial w_y(t_1)} - \frac{\partial I_2}{\partial w_y(t_1)} = 0 \tag{3.17}$$

since I_3 does not contain terms in w_y. The first term in equation (3.17) is

$$2w_y(t_1)\int_{-\infty}^{t_1} \hat{g}(t_1-\tau_2)\int_{-\infty}^{t_1} r_{xx}(\tau_2-\tau_1)\hat{g}(t_1-\tau_1)d\tau_1 d\tau_2. \tag{3.18}$$

Similarly the second term in equation (3.17) leads to

$$-2\int_0^{t_1} w_x(\tau_2)\hat{g}(t_1-\tau_2)\int_{-\infty}^{t_1} r_{xx}(\tau_2-\tau_1)\hat{g}(t_1-\tau_1)d\tau_1 d\tau_2 \tag{3.19}$$

Substituting $u = t_1 - \tau_1$ in equations (3.18) and (3.19) and then combining together (as in equation (3.17)) results in a generalised solution for the best Least mean square output window.

$$w_y(t_1) = \lambda_y \int_0^{t_1} w_x(t)\varphi(t_1-t)dt \tag{3.20}$$

where

$$\lambda_y = \frac{1}{\int_0^\infty \varphi(t)dt}.$$

3.6 Formulation of integral equation pairs.

Any equation containing the required function under the integral sign is defined as an Integral Equation. In equations(3.16) and (3.20) we have presented the equations to be solved for the required time windows. These can be combined to give for the input window

$$w_x(t_1) = \lambda \int_{t_1}^{T} \varphi(t - t_1) \int_0^t w_x(\tau)\varphi(t - \tau)d\tau dt \tag{3.21}$$

and for the output window

$$w_y(t_1) = \lambda \int_0^{t_1} \varphi(t_1 - t) \int_t^T w_y(\tau)\varphi(\tau - t)d\tau dt \tag{3.22}$$

where $\lambda = \lambda_x \lambda_y$.

By changing the order of integration in both equations (3.21) and (3.22),

$$\begin{aligned} w_x(t_1) &= C_0 \int_0^{t_1} w_x(\tau) \int_{t_1}^{T} \varphi(t - t_1)\varphi(t - \tau)dtd\tau \\ &+ C_0 \int_{t_1}^{T} w_x(\tau) \int_{\tau}^{T} \varphi(t - t_1)\varphi(t - \tau)dtd\tau. \end{aligned} \tag{3.23}$$

and

$$\begin{aligned} w_y(t_1) &= C_0 \int_0^{t_1} w_y(\tau) \int_0^{\tau} \varphi(t_1 - t)\varphi(\tau - t)dtd\tau \\ &+ C_0 \int_{t_1}^{T} w_y(\tau) \int_0^{t_1} \varphi(t_1 - t)\varphi(\tau - t)dtd\tau. \end{aligned} \tag{3.24}$$

By introducing a function of two variables :

$$K_x(t_1-\tau) = \begin{cases} \int_{t_1}^{T} \varphi(t-t_1)\varphi(t-\tau)dt & \text{for } 0 \le \tau \le t_1 \\ \\ \int_{\tau}^{T} \varphi(t-t_1)\varphi(t-\tau)dt & \text{for } t_1 \le \tau \le T \end{cases} \tag{3.25}$$

and

$$K_y(\tau-t_1) = \begin{cases} \int_{0}^{\tau} \varphi(t_1-t)\varphi(\tau-t)dt & \text{for } 0 \le \tau \le t_1 \\ \\ \int_{0}^{t_1} \varphi(t_1-t)\varphi(\tau-t)dt & \text{for } t_1 \le \tau \le T \end{cases} \tag{3.26}$$

equations (3.21) and (3.22) are simplified to

$$w_x(t_1) = \lambda \int_0^T w_x(\tau)K_x(t_1-\tau)d\tau. \tag{3.27}$$

and

$$w_y(t_1) = \lambda \int_0^T w_y(\tau)K_y(\tau-t_1)d\tau. \tag{3.28}$$

respectively. In mathematical terms equations (3.27) and (3.28) are known as Fredholm integral equations and a brief description of its properties, and the method by which it can be solved, will be discussed in the next section.

3.7 Fredholm equations and their solution.

Consider the integral equation of the form

$$\psi(x) - \int_a^b K(x,s)\psi(s)ds = f(x), \tag{3.29}$$

where the function $\psi(x)$ is unknown, and the functions $f(x)$ and $K(x,s)$ are assumed to be given. The limits of integration a and b are in general constants and can be finite as well as infinite; we also suppose that the variable x varies in the interval (a,b), in which the integration is to be performed.

The function $f(x)$ is called the **absolute term** of the integral equation and the function $K(x,s)$ **its kernel**. The kernel $K(x,s)$ defined in the (x,s)-plane in the square $a < x, \quad s < b$, is termed as the **basic square**, with the interval (a,b) termed as the **basic interval**. Equation (3.29) is said to be **homogeneous** if $f \equiv 0$. Evidently in this case consideration has given not one integral equation, but a family of homogeneous integral equations

$$\psi(x) - \lambda \int_a^b K(x,s)\psi(s)ds = 0. \tag{3.30}$$

The value λ, which is an arbitrary numerical quantity in equation (3.30), has a non-zero solution, and is called the **eigenvalue** of the kernel $K(x,s)$ or of the corresponding integral equation. Every non-zero solution of the equation is called an **eigenfunction** corresponding to the eigenvalue λ [1].

From the definition of the Fredholm equation it's kernel is subjected to the condition

$$\int_a^b \int_a^b \mid K(x,s) \mid^2 dxds = B^2 < \infty.$$

The solution to this Fredholm equation is considered as quadratically summable in the basic interval [1]. For such a solution, the integral

$$\int_a^b \mid \psi(x) \mid^2 dx$$

has a finite value and is said to be **unique**.

3.7.1 Method of successive approximations.

The Fredholm equation given in (3.30) may be solved by the method of successive approximations [2]. It is possible to write the above equation in the form

$$\psi(x) = \lambda K\psi$$

where the function $K\psi$ is termed as a Fredholm operator.

Given an initial guess $\psi_0(x)$, we take as a subsequent approximation, the result of the function $\psi_{n-1}(x)$ on the right hand side of the above equation, i.e,

$$\psi_n(x) = \lambda K\psi_{n-1}.$$

Which leads to the succession

$$\begin{aligned}\psi_1(x) &= \lambda K\psi_0,\\ \psi_2(x) &= \lambda^2 K^2\psi_0,\\ &\vdots\\ \psi_n(x) &= \lambda^n K^n\psi_0.\end{aligned}$$

with

$$K^n\psi_0 = \int_a^b K_n(x,s)\psi(s)ds$$

and the function

$$K_n(x,s) = \int_a^b \int_a^b \cdots \int_a^b K(x,t_1)K(t_1,t_2)\cdots K(t_{n-1},s)dt_1dt_2dt_{n-1}$$

being termed as the n^{th} iterated kernel, since it is directly expressed in terms of the original kernel $K(x,s)$. In order for the sequence of these quadratically summable

functions $\psi_n(x)$ to be convergent in the mean, it is necessary and sufficient that

$$\lim_{m,\, n \to \infty} \|\psi_m - \psi_n\| = 0.$$

3.7.2 Solution for $w_x(t_1)$ and $w_y(t_1)$.

Since the required functions appear outside as well as under the integral sign the method of successive approximations can be used to solve for $w_x(t_1)$ and $w_y(t_1)$.

Applying the results obtained to the homogeneous linear equations of (3.27) and (3.28),

$$\dot{w}_x + p(t_1)w_x = 0, \tag{3.31}$$

and

$$\dot{w}_y + q(t_1)w_y = 0. \tag{3.32}$$

The problem is said to be equivalent to finding the solution of equations (3.31) and (3.32) with the homogeneous boundary conditions,

$$w_x(0) = a \ \ , w_x(T) = 0 \ \ , w_y(0) = 0 \text{ and } w_y(T) = a. \tag{3.33}$$

This is equivalent to finding the function $w_x(t_1)$ and $w_y(t_1)$ which satisfy the integral equations given in (3.27) and (3.28).

Characteristic properties of the function kernel $K(t_1, \tau)$ are :-

(1) It is continuous in the square defined by the inequalities, $0 \leq t_1 \leq T$ and $0 \leq \tau \leq T$.

(2) Outside the diagonal, the kernel is the solution of the homogeneous equation

$$\dot{w}_x = 0$$

and

$$\tilde{w}_y = 0$$

and satisfies the boundary conditions of equation (3.33).

(3) The Kernels are symmetrical and are denoted by

$$K_x(t_1 - \tau) = K_x(\tau - t_1)$$
$$K_y(t_1 - \tau) = K_y(\tau - t_1). \tag{3.34}$$

All of the properties of the kernel follow immediately from (3.25) and (3.26). The integral equations defined by equations
(3.27) and (3.28) are called **Fredholm equations of the second kind** as they have constant limits of integration.

Equations (3.16) and (3.20) are related as the solution of one requires the solution for the other. In fact from studying their forms one can deduce that they are reflections of each other and thus have solutions which are conjugate in pairs. For these conjugate time window pairs,

$$w_x(t_1) = w_y(T - t_1) \text{ and } w_y(T - t_1) = w_x(T - t_1)$$

over the period $0 \leq t_1 \leq T$. This observation has also been confirmed by simulation studies made by the author.

Given this conjugate relationship between the input and output time windows it is possible to redefine equations (3.13) and (3.16) respectively in the form

$$w_x(t_1) = \lambda_x \int_0^{T-t_1} w_x(\tau)\varphi(T - \tau - t_1)d\tau \tag{3.35}$$

and

$$w_y(t_1) = \lambda_y \int_{T-t_1}^{T} w_y(\tau)\varphi(t_1 - T - \tau)d\tau. \tag{3.36}$$

Such equations are **Volterra equations of the second kind**. However, analytical solutions of these integral equations are usually very complicated and for the purpose of this thesis a generalised numerical evaluation will suffice.

3.7.3 Numerical solution for $w_x(t_1)$ and $w_y(t_1)$.

When the unknown functions also appears outside the integral sign one can numerically apply the method of successive approximations to obtain solutions to the equations. Assuming the criterion is to solve for $w_x(t_1)$ in equations (3.27) and (3.35), the following evaluation steps should be implemented :

(i) Evaluate the steady state input and estimated output correlation defined by

$$r_{xx}(\tau) = \int_0^\infty \hat{g}(u)\hat{g}(u+\tau)d\tau, \quad \hat{r}_{xy}(\tau) = \int_\tau^\infty r_{xx}(u)\hat{g}(u-\tau)d\tau,$$

and

$$\varphi(\tau) = \hat{g}(\tau)\hat{r}_{xy}(\tau).$$

(ii) Evaluate either the kernel $K_x(t_1 - \tau)$ if (3.27) is used, or the function $\varphi(T - \tau - t_1)$ if (3.35) is to be used.

(iii) Evaluate the current approximation for the input window from either

$$w_{x_i}(t_1) = \int_0^T K_x(t_1 - \tau)w_{x_{i-1}}(\tau)$$

or

$$w_{x_i}(t_1) = \int_0^{T-t_1} \varphi(T - t_1 - \tau)w_{x_{i-1}}(\tau),$$

(iv) On normalising the current input window estimate, apply the method of successive approximation and compute the error

$$F = \int_0^T \mid w_{x_i}(t_1) - w_{x_{i-1}}(t_1) \mid^2 dt_1.$$

The index i and $i-1$ are the current and previous estimates of the input window to be evaluated.

(v) Repeat steps (iii) and (iv) until an acceptable level of convergence ϵ is obtained. Termination is accepted in the procedure if $F \leq \epsilon$. From experience ϵ is found to be 10^{-10}.

(vi) Finally compute $w_y(t_1)$ by making the substitution,

$$w_y(t_1) = w_x(T - t_1) \text{ for } 0 \leq t_1 \leq T$$

3.8 White noise input.

An exact analytical solution can be obtained when the input to the system $x(t)$ is white, i.e ,

$$r_{xx}(v) = \begin{cases} 1 & \text{if } v = 0 \\ 0 & \text{otherwise} \end{cases} \tag{3.37}$$

Substituting this into equation (3.13) and subsequently in to equation (3.16) leads to,

$$w_x(t_1) = \lambda_x \int_{t_1}^T w_y(t)\hat{g}^2(t - t_1)dt. \tag{3.38}$$

Similarly equation (3.20) reduces to,

$$w_y(t_1) = \lambda_y \int_0^{t_1} w_x(t)\hat{g}^2(t_1 - t)dt \tag{3.39}$$

where

$$\lambda_x = \lambda_y = \int_0^\infty \bar{g}^2(t)dt. \tag{3.40}$$

A unique analytical equation in terms of $w_x(t_1)$ can be obtained by substituting equation (3.39) into (3.38) to give,

$$w_x(t_1) = \lambda_x^2 \int_{t_1}^{T} \bar{g}^2(t-t_1) \int_0^t w_x(\tau)\bar{g}^2(t-\tau)d\tau dt. \tag{3.41}$$

Similarly for the output window the result is

$$w_y(t_1) = \lambda_y^2 \int_0^{t_1} \bar{g}^2(t_1-t) \int_t^T w_y(\tau)\bar{g}^2(\tau-t)d\tau dt \tag{3.42}$$

Changing the order of integration, leads to exact analytical solutions for the least mean square input and output window :

$$w_x(t_1) = \lambda_x^2 \int_0^T w_x(\tau)K(t_1-\tau)d\tau \tag{3.43}$$

$$w_y(t_1) = \lambda_y^2 \int_0^T w_y(\tau)K(\tau-t_1)d\tau \tag{3.44}$$

where

$$K(t_1-\tau) = \begin{cases} \int_{t_1}^T \bar{g}^2(t-t_1)\bar{g}^2(t-\tau)dt \text{for } 0 \le \tau \le t_1 \\ \\ \int_\tau^T \bar{g}^2(t-t_1)\bar{g}^2(t-\tau)dt \text{for } t_1 \le \tau \le T \end{cases} \tag{3.45}$$

and

$$K(t_1-\tau) = K(\tau-t_1). \tag{3.46}$$

It should be noted that the difference between the above formulation for the white noise and that for the non-white noise cases, lies in the evaluation of the kernel. Equation (3.25) contains knowledge of the cross correlation between the true input and the predicted (or postulated) output and enables the window to conform to this shape. Although equation (3.46) also contains information on this function, it is well known that, for white noise, the cross correlation function is zero for negative lags and takes the shape of the impulse response estimate for positive lags. It is not surprising therefore that equation (3.46) is a function only of the postulated impulse response.

As in equations (3.35) and (3.36) the least mean square input-output windows may be defined as Volterra equations of the second kind by writing :-

$$w_x(t_1) = \lambda_x \int_0^{T-t_1} w_x(\tau)\hat{g}^2(T-\tau+t_1)d\tau \tag{3.47}$$

$$w_y(t_1) = \lambda_y \int_{T-t_1}^{T} w_y(\tau)\hat{g}^2(t_1-T+\tau)d\tau. \tag{3.48}$$

3.9 Examples.

Having developed the theoretical work, it is necessary to consider some specific examples. The evaluation is concerned with numerical computation of the integral square error of the bias $G_b(j\omega)$, i.e.

$$\int_0^{\pi} \mid G_b(j\omega) \mid^2 d\omega$$

where

$$G_b(j\omega) = E\ [\ \hat{G}_{xy}(j\omega)\ ] - G(j\omega)$$

and the integral error of the noise to signal ratio $NS_{xy}(j\omega)$ is,

$$\int_0^{\pi} NS_{xy}(j\omega)d\omega$$

for

$$NS_{xy}(j\omega) = \frac{E\,[\,\bar{\Phi}_{yy}(\omega)\,]}{E\,[\,\bar{\Phi}_{xx}(\omega)\,]} - |\,G_s(j\omega)\,|^2\,.$$

Steady state input, output and cross correlation functions (for predefined time window pairs) are used to evaluate the expected value of the measured frequency response function and the least mean square error windows are compared with the

(i) Do-nothing window,

(ii) Bartlett window,

(iii) Hanning window,

(iv) Hamming window,

(v) Blackman window.

Comparison for least mean square windows is also made when the postulated system is different from the true system under investigation.

Three systems are chosen to illustrate the theoretical work developed and all continuous transfer functions are mapped into their discrete equivalent via the bilinear transformation.

Example (1).

A first order filter and system with an open-loop transfer function

$$G_f(s) = G_s(s) = \frac{1}{1 + T_c s}$$

with impulse response

$$g_f(t) = g_s(t) = \frac{\exp(-t/T_c)}{T_c},$$

where $T_c = 5$ seconds. The observation time of $T = 30$ seconds is chosen to be of the same order of magnitude as the setting time of the system $G_s(s)$, with a sampling frequency of $F_s = 1$ Hz.

Example (2).

A second order filter and system with an open-loop transfer function,

$$G_f(s) = G_s(s) = \frac{\omega_o}{(s+\alpha)^2 + \omega_o^2}$$

with impulse response,

$$g_f(t) = g_s(t) = \exp(-\alpha t)\sin(\omega_o t),$$

where $\alpha = 1/T_c$, $T_c = 2.5$ seconds, $\omega_o = \pi/2$ and a sampling frequency of $F_s = 4$ Hz. The observation time ($T = 12.5$ seconds) is again chosen to be of the same order as the settling time of the system.

Example (3).

A first order system $G_s(s)$ that is subjected to white noise input.

3.9.1 First order filter-system.

Figure (3.5) shows the expected value of the measured frequency response for the least mean square error window when the postulated system $\bar{g}(t)$ is assumed to be the same as the true system $g(t)$. Comparisons are made with two conventional windows (in this case, that of the Bartlett and Hanning). Frequency spacing of 1/30Hz is given in order to compare points along the locus of the frequency response estimate.

Figures (3.6) and (3.7) are the respective bias square and the noise to signal ratio plots for the windows described in figure (3.5).

Figure (3.8) shows the computed least mean square error input and output windows. It shows that the windows are reflections of each other about $T/2$, and that the positions of their peaks are automatically chosen so that the position of maximum weight, in the resulting cross correlation lag window, coincides with the the maximum of the theoretical cross correlation function.

Table (3.1) makes comparisons for the integral square of the bias between the LMSE

window and conventional windows, as well as that when the true system time constant is under estimated ($T_c = 2.5$ seconds) and over estimated ($T_c = 7.5$ seconds) by 50%.

Figure (3.9) show expected value of measured frequency response for the different estimates of the system time constant, and it is observed that even with such bad estimates of impulse responses, significant improvements in bias still result, see figure (3.10).

Finally figure (3.11) illustrates the effect on the time window with the different levels of a priori judgment.

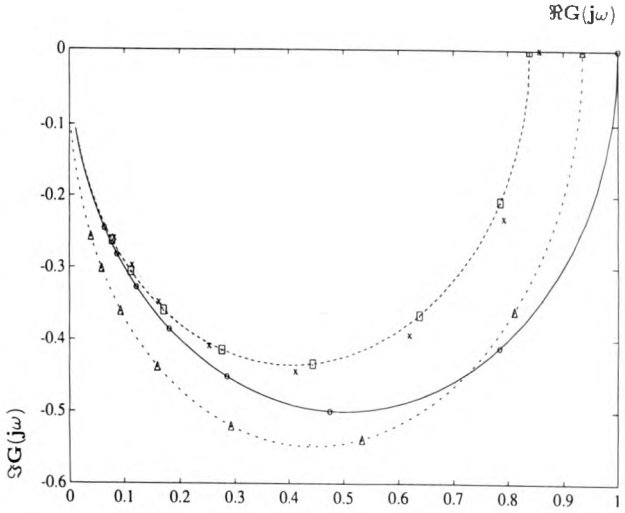

Figure 3.5: **Expected value of measured frequency response for first order filter-system $G_f(S) = G_s(S) = 1/(1 + T_c S)$, $T_c = 5$.**
– ⊟ – ⊟ –⊟ True plots at harmonic frequencies of 1/30 (Hz).
· × · × · × · × Bartlett Window.
–△ – △ – △ Least mean square error window, $T_c = 5$.
□ · □ · □ · □ · □ Hanning Window.

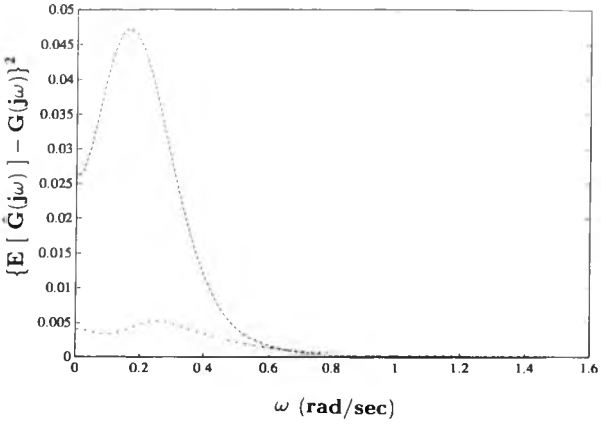

Figure 3.6: **Square of bias for first order filter-system.**

..... **Bartlett Window.**
– – – – – **Hanning Window.**
– · – · – **LSME Window.**

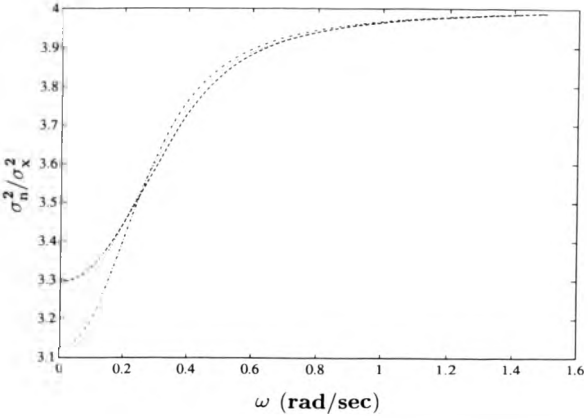

Figure 3.7: **Noise to signal ratio for first order filter-system.**

..... **Bartlett Window.**
– – – – – – **Hanning Window.**
– · – · – · – **LSME Window**

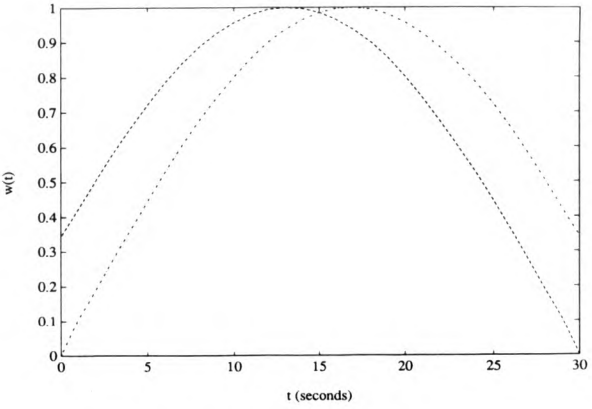

Figure 3.8: **Least mean square error windows for first order filter-system.**

– – – – – – **Input window $w_x(t)$**
– · – · – · – **Output window $w_y(t)$**

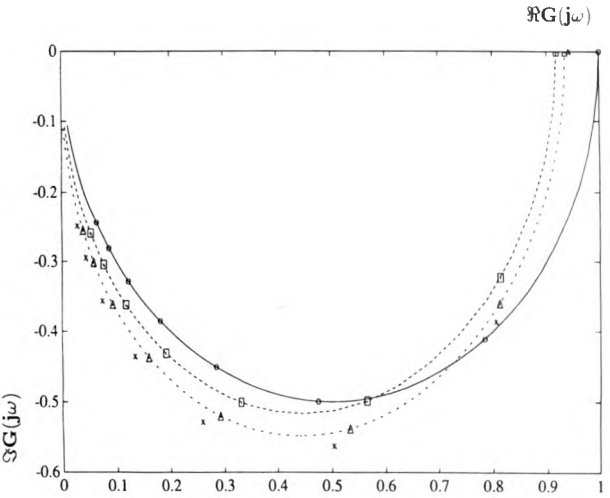

Figure 3.9: **Expected value of measured frequency response for least mean square error windows with different levels of a priori assumptions $G_f(S) = G_s(S) = 1/(1 + T_cS)$, $T_c = 5$.**

$-\ominus-\ominus-\ominus$ **True plots at harmonic frequencies of 1/30 (Hz).**
$\cdot\times\cdot\times\cdot\times\cdot\times$ $T_c = 2.5$.
$\square\cdot\square\cdot\square\cdot\square\cdot\square$ $T_c = 5$.
$-\triangle-\triangle-\triangle$ $T_c = 7.5$.

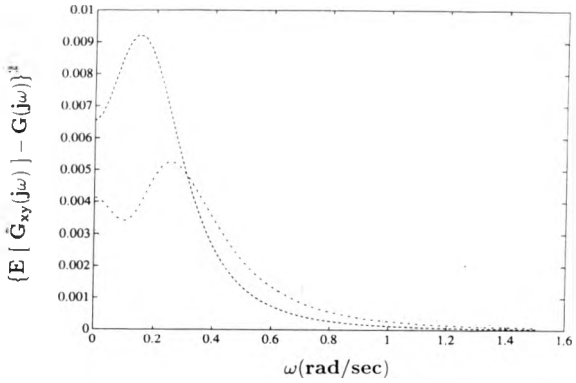

Figure 3.10: **Square of bias for least mean square error windows with different levels of a priori assumptions.**

..... $T_c = 2.5$.
-·-·-·- $T_c = 5$.
– – – – – $T_c = 7.5$.

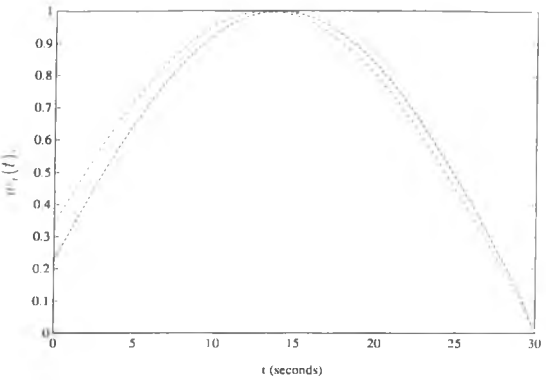

Figure 3.11: **Least mean square error input time windows with different levels of a priori assumptions.**
..... $\mathbf{T_c = 2.5}$.
- · - · - · - $\mathbf{T_c = 5}$.
– – – – – – $\mathbf{T_c = 7.5}$.

Window Type	Integral square error in bias	Improvement
Do-nothing	0.01949	1.00
Bartlett	0.01063	1.83
Hanning	0.01468	1.33
Hamming	0.01112	1.76
Blackman	0.02189	0.89
LSME $T_c = 5.0$	0.002487	7.84
LSME $T_c = 7.5$	0.003145	6.20
LSME $T_c = 2.0$	0.002882	6.76

Table 3.1: **Comparison of square error for differing window types, and accompanying factors of improvement.**

3.9.2 Second order filter system.

Figures (3.12) and (3.13) show the expected value of the measured amplitude squared and phase response. Comparisons are made between :

(i) Least mean square error window when $\bar{g}(t) = g(t)$,

(ii) Do-nothing window,

(iii) Bartlett window.

For this second order filter system arrangement, Do-nothing and Bartlett windows were used as they produced best estimates of mean square error out of the other classical windows chosen for comparison. See section (3.9).

In this case, Do-nothing was found to be a better mean square error than the Hanning window. Figures (3.14) and (3.15) show plots of bias squared and signal to noise ratio for the above windows. The optimum windows are shown in figure (3.16). Figure (3.17) makes comparison of bias with different levels of a priori knowledge of the impulse response model. The Least mean square error windows evaluated for these are shown in figure (3.18). Finally Table (3.2) compares integral square of bias with accompanying improvement factors.

Based on results carried out in this section and simulation studies of other filter system arrangements, the following conclusions are made.

(1) The use of LMSE windows significantly reduces bias and variance in the resulting frequency response estimates.

(2) Factors of improvement result from this new window over conventional windows range from 50 % to 900 % when using mean square as the error criterion.

(3) Evaluating these windows based on an in exact a priori estimate, will still lead to significant improvements the mean square error of the frequency response estimates.

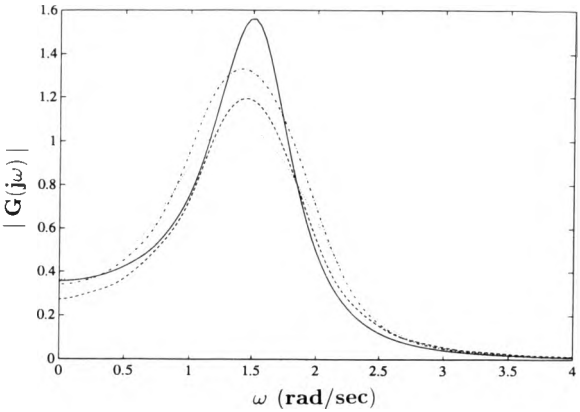

Figure 3.12: **Expected value of amplitude response for second order filter-system.**

$$\mathbf{G_f(S) = G_s(S) = \omega_o/((S+\alpha)^2 + \omega_o^2)\alpha = 1/T_c,}$$

where $\mathbf{T_c = 5}$ **and** $\omega_o = \pi/2$

True amplitude spectrum.
Bartlett Window.
Do-nothing Window.
LSME Window $\mathbf{T_c = 5}$.

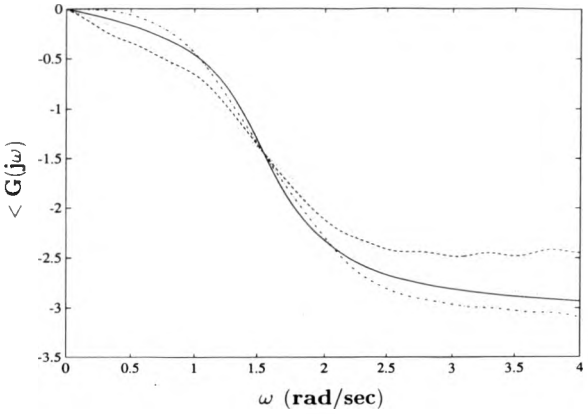

Figure 3.13: **Expected value of phase response for second order filter-system.**

$$G_f(S) = G_s(S) = \omega_o/((S+\alpha)^2 + \omega_o^2)\alpha = 1/T_c,$$

where $T_c = 5$ **and** $\omega_o = \pi/2$

——————— **True phase spectrum.**
..... **Bartlett Window.**
. . . . . **Do-nothing Window.**
..... **LSME Window** $T_c = 5$.

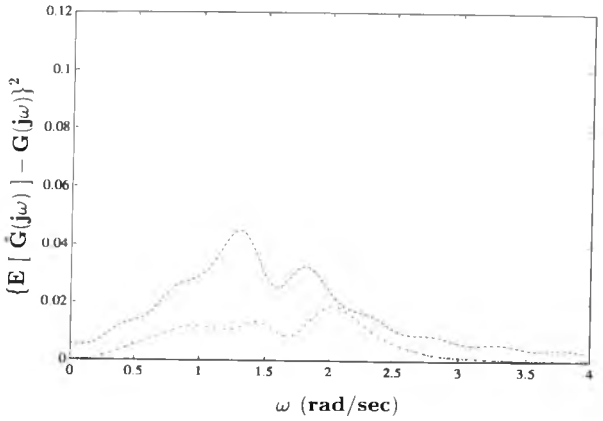

Figure 3.14: **Square of bias for second order filter-system.**

$$G_f(S) = G_s(S) = \omega_o/((S+\alpha)^2 + \omega_o^2)\alpha = 1/T_c,$$

where $T_c = 5$ **and** $\omega_o = \pi/2$

..... **Bartlett Window.**
- - - - **Do-nothing Window.**
..... **LSME Window** $T_c = 5$.

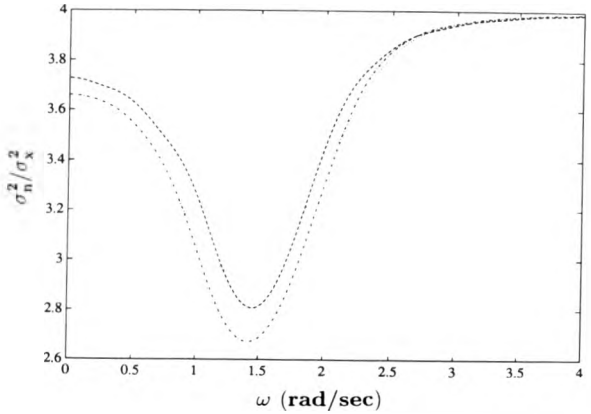

Figure 3.15: Noise to signal ratio for second order filter-system.

$$G_f(S) = G_s(S) = \omega_o/((S+\alpha)^2 + \omega_o^2)\alpha = 1/T_e,$$

where $T_e = 5$ and $\omega_o = \pi/2$

..... Bartlett Window.
- - - - - - - Do-nothing Window.
-.-.-.-.-.-.-LSME Window $T_e = 5$.

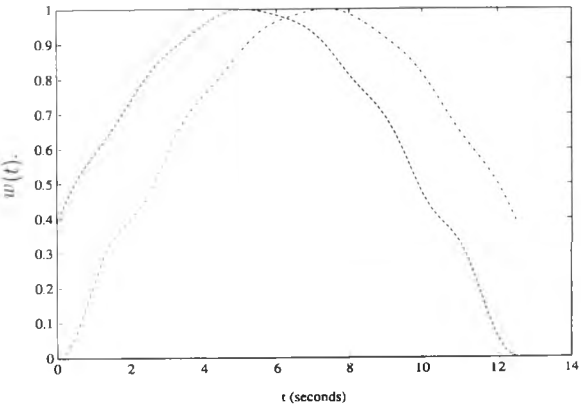

Figure 3.16: **Least mean square error windows for second order filter-system.**

– – – – – – **Input window $w_x(t)$**
·–·–·–·– **Output window $w_y(t)$**

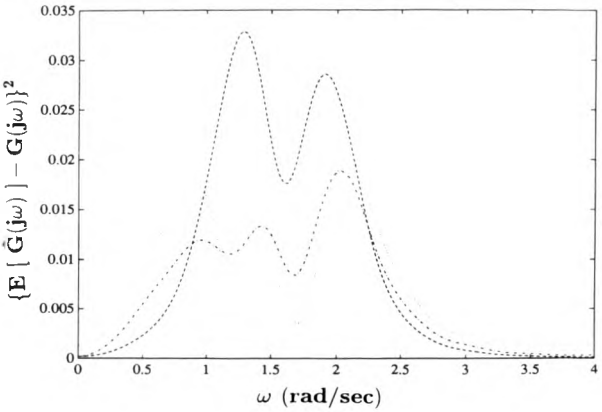

Figure 3.17: **Square of bias of second order filter-system for least mean square error windows with different levels of a priori assumptions.**

..... $T_c = 1.25, \quad \omega_0 = 5\pi/8.$
-.-.-.-.- $T_c = 2.50, \quad \omega_0 = \pi/2.$
——— $T_c = 3.75, \quad \omega_0 = 3\pi/8.$

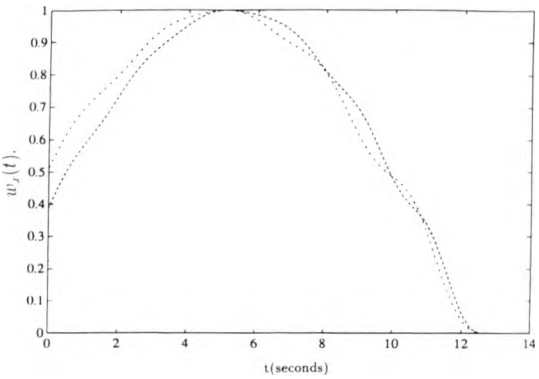

Figure 3.18: **Least mean square error windows of first order filter-system with different levels of a priori assumptions.**

..... $T_c = 1.25,\ \omega_0 = 5\pi/8.$
-.-.-.- $T_c = 2.50,\ \omega_0 = \pi/2.$
——— $T_c = 3.75,\ \omega_0 = 3\pi/8.$

Window Type	Integral error in bias	Improvement
Do-nothing	0.01778	3.18
Bartlett	0.02960	1.93
Hanning	0.04017	1.42
Hamming	0.03145	1.82
Blackman	0.05718	1.00
LMSE $T_c = 1.25,\ \omega_0 = 5\pi/8$	0.006656	8.59
LMSE $T_c = 2.50,\ \omega_0 = \pi/2$	0.009515	6.01
LMSE $T_c = 3.75,\ \omega_0 = 3\pi/8$	0.007277	7.86

Table 3.2: Second order filter, system comparison of square errors for differing window types, and accompanying factors of improvement.

3.9.3 First order system subject to white noise input.

It has already been mentioned that obtaining an exact analytical solution for the least mean square window, even for the most simple of cases, can prove to be very difficult. However, a parametric model has been formulated for the trivial case of a first order system subjected to white noise input.

The LMSE windows evaluated are parametised using a first order trigonometric sum type window.

The trigonometric sum type window defined by

$$w(t) = \sum_{k=-1}^{1} \sigma_k \cos(\alpha_k t + \beta_k) \tag{3.49}$$

where

$$\alpha_k = \begin{cases} \frac{-k\pi}{2[T-U]} & \text{for } U \leq T/2 \\ \\ \frac{-k\pi}{2U} & \text{for } U \geq T/2, \end{cases}$$

and

$$\beta_k = -\alpha_k U$$

is used to minimise the difference between itself and the evaluated least mean square window, for varying T/T_c. The optimisation used is a Nelder Mead simplex algorithm obtained in matlab with a precision of 10^{-8}.

It was found that the coefficients of the trigonometric sum type window where of a fixed value with

$$\sigma_{-1} = \sigma_1 = 0.5 \quad \sigma_0 = 0.0.$$

Substitution of these fixed coefficients in to equation (3.49) leads to

$$w(t) = \cos \alpha_1 (t - U). \tag{3.50}$$

The position the of maximum weight of the windows are

$$U = \begin{cases} KT & \text{for the input window} \\ (1-K)T & \text{for the output window} \end{cases}$$

with

$$K = 0.14628\frac{T}{T_c}\exp(-0.28823T/T_c) + (1 - \exp(-0.17040T/T_c))/2.$$

Figure (3.19) is a mesh plot of the parametised input window as a result of varying T_c from 1 to 100 whilst keeping the record length constant at $T = 100$. The output window is identical with the input window with t replaced by (T-t).

We observe that asymptotically as $T/T_c \longrightarrow \infty$ the window tends to

$$w_x(t) = w_y(t) = \sin(\pi t/T). \tag{3.51}$$

This window is in fact known as a Papoulis window.

Papoulis describes this as being minimum mean square error for systems requiring high resolution spectral estimates [4]. It is interesting that the above analysis agrees with conventional practice in that for long observation times the input and output window become identical and are symmetrical. This has been demonstrated for a first order system subject to a white noise input. In fact further simulation studies have shown that the time window pairs for higher order systems, subject to white noise inputs, and large observation times, lead to equation (3.51).

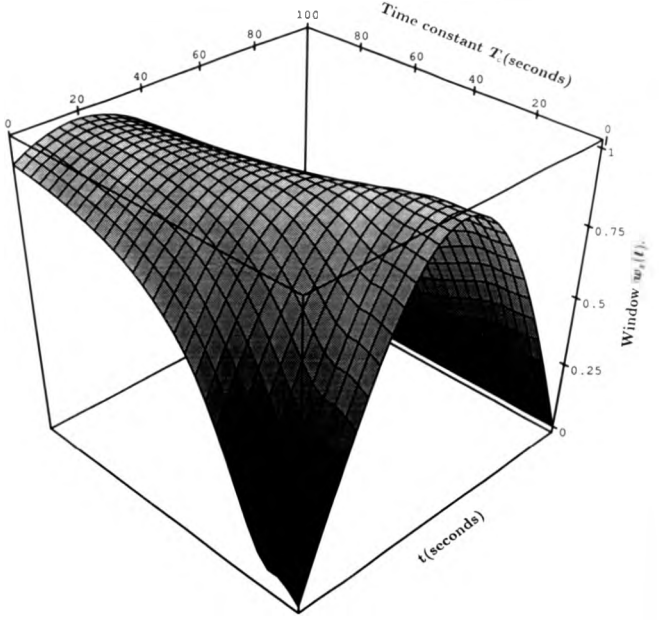

Figure 3.19: **Parameterised least mean square input windows for first order system.**

3.10 Summary

In this chapter the author has shown that designing time and correlation windows based on *priori* knowledge of the system under analysis has lead to significant reductions in the statistical errors of the measured frequency response estimate. When comparison is made with conventional windows, such factors of improvement are shown to range from 2 to 10. It is also shown that underestimating or overestimating the postulated impulse response structure still results in comparable improvements. The theorems developed, are an attempt to introduce a firm and more robust mathematical formulation to the design of time and correlation windows for non-parametric spectral analysis. As a result, it makes redundant the study of leakage in designing optimum and sub-optimum spectral windows. In the next chapter procedures are produced by which this technique can be adapted to automatically design time and correlation windows based on single realisation of input and output records.

3.11 References for Chapter (3).

[1] **Pogorzelski. W.,**: 'Integral equations and their applications'. Volume 1. Pergamon Press. Warszaiva, Poland.

[2] **Delves. L.M. and Walsh. J.,**: 'Numerical solution of integral equation'. Claridon Press. Oxford, England, 1974.

[3] **Jenkins. G.M. and Watts. D.G.,**: 'Spectral analysis and its applications'. Holden Day,1968.

[4] **Papoulis. A.,**: 'Minimum bias windows for high resolution spectral estimates'. Trans. IEEE, vol.IT-19,pp9-12,No. 1.January 1973.

Chapter 4

Least mean square error windows (II)

4.1 Introduction.

In this chapter, simulation results of frequency response estimates (based on single realisations input-output records) is analysed and comparison of these estimates are made between LMSE windows and conventional windows.

These comparisons will be given for :-

(1) The indirect method, in which frequency response estimates are computed from windowed sample covariance functions.

(2) The direct method, in which frequency response estimates are based on the segmental averaging of input-output records.

Section (4.2) describes the procedure by which frequency response estimates based on the indirect method are evaluated [1]. The definitions of biased covariance functions are given based on N samples of an input-output record, from which smoothed (or windowed) auto and cross spectral estimates are computed. The Gain and phase of the estimate, with accompanying confidence intervals, coherence and output noise spectrums, are also defined.

The empirical procedure for determining a suitable bandwidth for the spectral window, which has been extensively described in [1] and [4], is summarised in section (4.2.1). Section (4.3) compares directly, the frequency response estimate from windowed covariance functions computed from a single realisation input-output time series. The comparison is made between the Tukey window and LMSE windows derived in chapter (3).

Section (4.4) describes the method of frequency response estimates based on non-overlapping segment averaging. In section (4.4.2) comparison of this estimate (based on the Hanning and LMSE windows) is made of windowed segments from a single realisation input-output time series.

It should be stated that in the analysis undertaken in chapter (3), the LMSE windows were evaluated for the noise free case. An attempt (so far unsuccessfully) has been made to incorporate a measure of output noise into the analysis and is still a subject of further research by the author.

4.2 Frequency response estimates based on sample covariance functions.

One of the most established procedures of time series analysis is the method of power spectrum analysis through windowed sample covariance sequences. The importance of this method of power spectrum estimation, of which a schematic account is given in [5], further increased when it was extended to the estimation of frequency response functions through estimates of auto and cross power spectra. The secret to the success of this method lies entirely in the application of the windowing procedure. This transforms the original sample covariance sequences into windowed covariance sequences by multiplication with an appropriately chosen numerical factor that constitutes the correlation window [1]. Thus, the effectiveness of the windowing procedure is most evident when the appropriately windowed sample covariance sequences provide a better estimate of

the covariance functions than the original sample covariance sequences.

When viewed as a method of estimation of a covariance sequence, this windowing procedure is obviously a very naive one, unless it is supplied with some rules for the adaptive selection of the correlation window. Using information supplied by the observed sample covariance sequences demonstrates the significance of LMSE window selection for this method of non-parametric frequency response estimation. Figure (4.1) is a schematic presentation by which LMSE time windows are evaluated from computation of the sample cross covariance function and knowledge of the postulated impulse response of the system. In section (4.3), comparison of frequency response estimates between LMSE window selection and the Tukey window will be given. The Tukey window is given for comparison in section (4.3) as this was extensively used by Jenkins and Watts in their evaluation of frequency response estimates from sample covariance function [1].

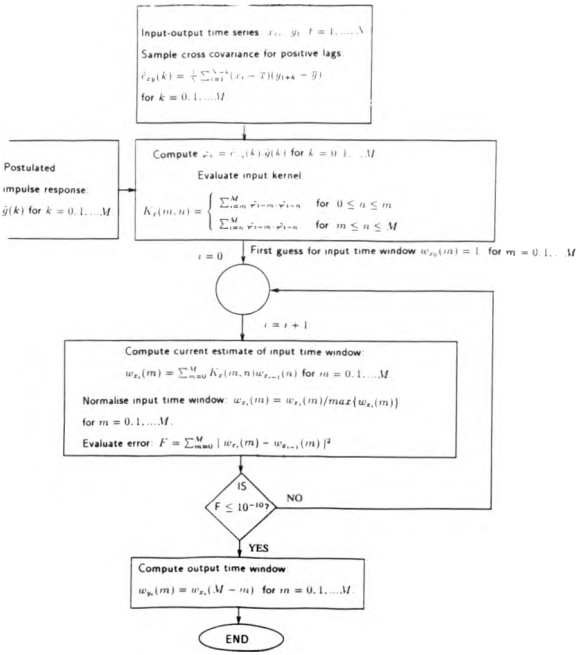

Figure 4.1: **A schematic for the evaluation of LMSE time windows based on single realisations of an input-output record.**

All theory so far has been formulated with the assumption that the record $x(t)$ and $y(t)$ are continuous. In practice these records are discrete and a digital procedure is required since most spectral analysis is implemented using computers. This sampling process is well documented and a detailed analysis of its effects on correlation analysis is given in [2].

Let the sampling records of the input and output records be represented respectively by $x_t, \quad t = 1, \ldots, N$ and $y_t, \quad t = 1, \ldots, N$ at a sampling interval Δ, and have mean values given by

$$\bar{x} = \frac{1}{N}\sum_{t=1}^{N} x_t \quad \text{and} \quad \bar{y} = \frac{1}{N}\sum_{t=1}^{N} y_t.$$

The biased auto and cross-covariance functions are defined by

$$\hat{c}_{xx}(k) = \frac{\Delta}{N}\sum_{t=1}^{N-k}(x_t - \bar{x})(x_{t+k} - \bar{x}), \quad 0 \le k \le (N-1)$$

$$\hat{c}_{yy}(k) = \frac{\Delta}{N}\sum_{t=1}^{N-k}(y_t - \bar{y})(y_{t+k} - \bar{y}), \quad 0 \le k \le (N-1)$$

and

$$\hat{c}_{xy}(k) = \frac{\Delta}{N}\begin{cases} \sum_{t=1}^{N-k}(x_t - \bar{x})(y_{t+k} - \bar{y}) & \text{for } 0 \le k \le (N-1) \\ \sum_{t=1}^{N-k}(y_t - \bar{y})(x_{t+|k|} - \bar{x}) & \text{for } -(N-1) \le k \le 0. \end{cases}$$

Another covariance function in common use is obtained by replacing $\frac{\Delta}{N}$ with $\frac{\Delta}{N-|k|}$ in the above equations. The latter are unbiased covariance functions and would seem, at first, to be the better choice. However, the biased estimator has a lower variance and in general will produce a lower mean square error [1].

Computing discrete Fourier transforms of the windowed covariance functions, leads to the smoothed auto and cross spectral estimates :-

$$\bar{R}_{xx}(f) = \Delta \sum_{k=-(M-1)}^{M-1} w_{xx}(k)\hat{c}_{xx}(k)\exp(-j2\pi fk\Delta), \quad 0 \le f \le \frac{1}{2\Delta}, \qquad (4.1)$$

$$\overline{R}_{yy}(f) = \Delta \sum_{k=-(M-1)}^{M-1} w_{yy}(k)\hat{c}_{yy}(k)\exp(-j2\pi fk\Delta), \quad 0 \le f \le \frac{1}{2\Delta}, \tag{4.2}$$

and

$$\overline{R}_{xy}(f) = \Delta \sum_{k=-(M-1)}^{M-1} w_{xy}(k)\hat{c}_{xy}(k)\exp(-j2\pi fk\Delta), \quad 0 \le f \le \frac{1}{2\Delta}, \tag{4.3}$$

where $w_{xx}(k)$, $w_{yy}(k)$, $w_{xy}(k)$ are the windows on the correlation function with truncation point M that are only defined at discrete time points $u = k\Delta$.

Its has been suggested in [3] that the measured spectral estimates should be computed at values of frequency corresponding only to $f = 0, \frac{1}{T\Delta}, \frac{2}{T\Delta}, \ldots, \frac{1}{2\Delta}$. However, in [1], it is stated that such frequency spacings are normally too great and the spectral estimates should be evaluated at a fraction of this spacing. For simulation studies undertaken in [1], frequency values are computed at a spacing of $\frac{1}{KT\Delta}$, where K is 2 or 3 times M. A similar procedure will also be adopted by the author.

Defining the real and imaginary components of the smoothed cross spectral estimates

$$\overline{L}_{xy}(f) = \Re\,[\overline{R}_{xy}(f)] \quad \text{and} \quad \overline{Q}_{xy}(f) = \Im\,[\overline{R}_{xy}(f)]$$

leads to the smoothed gain, phase, square coherence, and output noise power spectra,

$$|\,\overline{G}_{xy}(f)\,| = \frac{\sqrt{\overline{L}_{xy}^2(f) + \overline{Q}_{xy}^2(f)}}{\overline{R}_{xx}(f)},$$

$$\overline{F}_{xy}(f) = \arctan\left(\frac{\overline{Q}_{xy}(f)}{\overline{L}_{xy}(f)}\right),$$

$$\overline{\gamma}_{xy}^2(f) = \frac{\overline{L}_{xy}^2(f) + \overline{Q}_{xy}^2(f)}{\overline{R}_{xx}(f)\overline{R}_{yy}(f)}$$

and

$$\overline{R}_{vv}(f) = \overline{R}_{yy}(f)(1 - \overline{\gamma}_{xy}^2(f)).$$

Jenkins and Watts [1] have studied the sampling distribution of frequency response estimators, and have shown that the function $(\overline{R}_{xx} \mid \overline{G}_{xy} - G_{xy} \mid (\overline{R}_{xx})^{-1})$ is approximately Fisher distributed. The approximate confidence interval (100 $(1-\alpha)$%) for the gain and phase estimates were shown to be :-

$$\mid \overline{G}_{xy}(f) \mid (1 \pm \sqrt{\frac{2}{\nu-2}\mathrm{f}_{2,\nu-2}(1-\alpha)\frac{1-\overline{\gamma}^2_{xy}(f)}{\overline{\gamma}^2_{xy}(f)}})$$

and

$$\overline{F}_{xy}(f) \pm \arcsin \sqrt{\frac{2}{\nu-2}\mathrm{f}_{2,\nu-2}(1-\alpha)\frac{1-\overline{\gamma}^2_{xy}(f)}{\overline{\gamma}^2_{xy}(f)}}.$$

The quantity

$$\nu = \frac{2M}{\sum_{k=0}^{M-1} w_{xy}(k)}$$

is the number of degrees of freedom associated with the smoothing of the spectrum spectral estimates and $\mathrm{f}_{2,\nu-2}(1-\alpha)$ is the upper 100 $(1-\alpha)$% point on the $\mathrm{F}_{2,\nu-2}$ distribution.

In the indirect method of spectral analysis, the window closing procedure, chosen by suitable truncation points M, will adjust itself to the local smoothing properties of the frequency response function. However, the window carpentry technique (i.e. the most appropriate shape for the window) is chosen in an inexact manner.

An advantage of LSME windows is that this information is readily evaluated from the postulated system characteristics. As any optimum window will inevitably be a function of the unknown system characteristics, this does not seem too surprising. For this reason, it is suggested that the grey box methodology implied by LMSE windows will always yield better estimates than any previously developed non-parametric method, as was shown to be the case in chapter (3).

4.2.1 Window closing.

The technique of window closing involves computing windowed spectral estimates with an initially large bandwidth and then reduction of the bandwidth until significant and relevant features in the frequency response estimate are observed [1]. The optimum truncation point M is thus a function of both the frequency response estimate and the window used. This optimum value is evaluated in [4] to be

$$M_{opt}(f) = \left(\frac{4M_1^2 \mid P(f) \mid^2 R_{xx}(f)}{M_2 R_{yy}(f)}\right)^{1/5} \cdot N^{1/5} \tag{4.4}$$

where

$$P(f) = \frac{1}{2}\frac{d^2 G_{xy}(f)}{df^2} + \frac{dG_{xy}(f)}{df} \cdot \frac{dR_{xx}(f)}{df} \cdot \frac{1}{R_{xx}(f)},$$

$$M_1 = \int_{-\frac{1}{2\Delta}}^{\frac{1}{2\Delta}} f^2 W_{xy}(f) df, \quad M_2 = \int_{-\frac{1}{2\Delta}}^{\frac{1}{2\Delta}} W_{xy}^2(f) df.$$

Here, as M increases, the frequency window $W_{xy}(f)$ becomes narrower and M_1 decreases as M_2 increases. If $W_{xy}(f)$ is wide, then a greater number of frequencies will be weighed together, which should lead to a small variance in $\overline{G}_{xy}(f)$. At the same time a wide window will involve frequency estimates further from the frequency of interest and therefore cause a large bias. The frequency dependent optimum value $M_{opt}(f)$, however, cannot be realised, since it contains several unknowns. A typical empirical procedure would be to start by taking M=N/20 and then compute and compare plots for corresponding estimates of $\overline{G}_{xy}(f)$ for various values of M. On increasing M more detail in the estimate should appear due to a decreased bias but this will also result in an increased variance (spurious, random peaks). The procedure should be halted when emerging details in the frequency response estimate become predominately spurious.

4.3 Simulation studies.

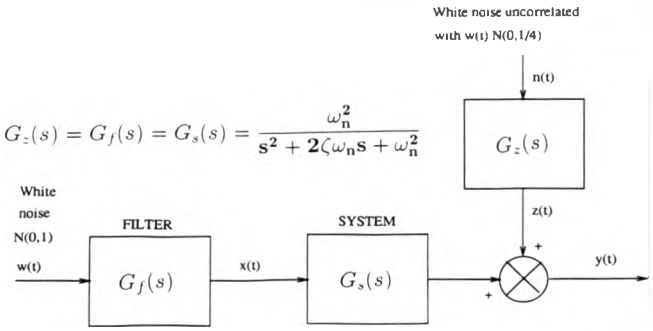

Figure 4.2: **Schematic of experimental simulation for frequency response estimates based on windowed sample correlation functions.**

In this section comparison will be made between LSME and conventional windows using the developed windowing procedure in [1].

Figure (4.2) represents a linear second order filter system chosen for the experiment with $\omega_n = \pi/5$ and $\zeta = 0.4$. The input $x(t)$ to the system is obtained by passing white noise N(0,1) through the filter. Similarly, the output $y(t)$ is obtained by passing $x(t)$ through the system and adding the filtered noise input $z(t)$ to it.

A total observation period of 400 seconds was chosen with a sampling interval $\Delta =$ 0.5 second. The first 100 samples are not considered in order to allow for the initial transients, thus leaving a total of N=700 samples for analysis.

4.3.1 Computations and display

(a) The sample auto and cross covariance functions are computed for truncation points $M = 50, 60, 70, 80, 90$ and 100.

(b) The two auto spectra $\overline{R}_{xx}(f)$, $\overline{R}_{yy}(f)$, the noise spectra $\overline{R}_{ss}(f)$, square coherence $\overline{\gamma}^2_{xy}(f)$ and the gain and phase spectra based on aligned covariance functions are computed for the range of truncation points in (a).

(c) The gain estimate on a logarithmic scale at each value of M is plotted against frequency (Hz). The phase, square coherence and output noise spectra are all plotted against frequency (Hz).

(d) All gain and phase plots are accompanied by 95 % confidence intervals and their true theoretical values.

4.3.2 Computation of spectral estimates for Tukey window.

The auto, gain, phase, coherence, and noise spectra for the different truncation points M are based on a Tukey window

$$w_{xx}(k) = w_{yy}(k) = w_{xy}(k) = \frac{1}{2}\left(1 + \cos\frac{\pi k}{M} \right) \text{ for } -M \leq k \leq M,$$

which is applied directly to the input, output and cross covariance functions. Figure (4.3) shows the sample auto and cross correlations functions of the simulated system for $M = 60$. Alignment between this window and $\hat{c}_{xy}(\tau)$ is implemented before spectral analysis for reasons which were given in chapter (2), section (2.8.2).

Evaluation of results.

In the window closing procedure, the gain estimate showed significant changes on increasing M from 50 to 60 but little change on increasing M further. Figures (4.4), (4.5) and (4.6) show plots of gain, phase, square coherence and noise spectra for $M = 50, 60$ and 100. The decision to accept $M = 60$ was based on the phase estimates, as these were found to fluctuate violently above $M = 60$, for $f > 3.5Hz$.

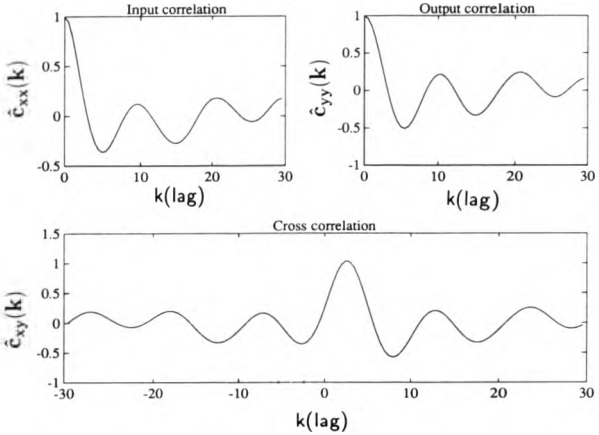

Figure 4.3: **Sample auto and cross covariance function based on $M = 60$.**

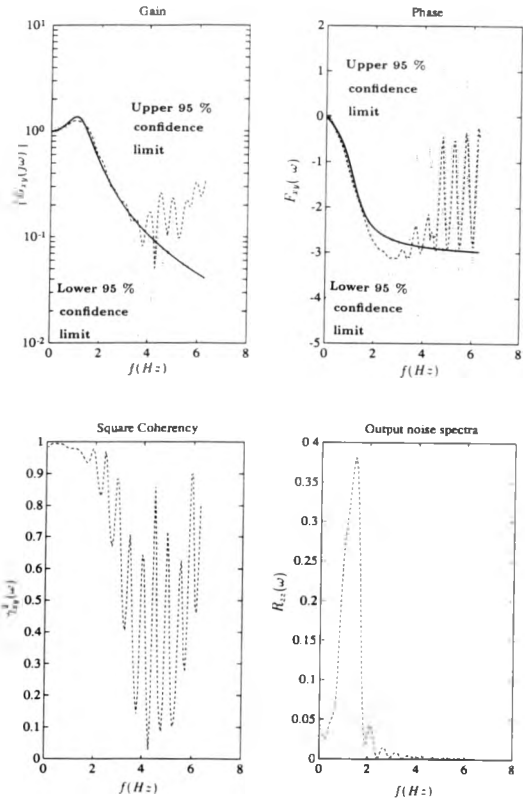

Figure 4.4: **Tukey estimates of gain, phase, square coherence and output noise spectra of simulated system for $M = 50$.**

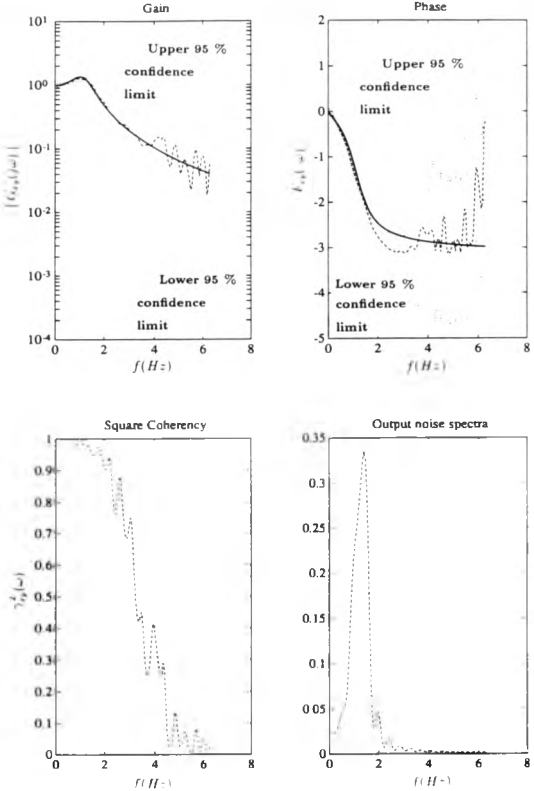

Figure 4.5: **Tukey estimates of gain, phase, square coherence and output noise spectra of simulated system for $M = 60$.**

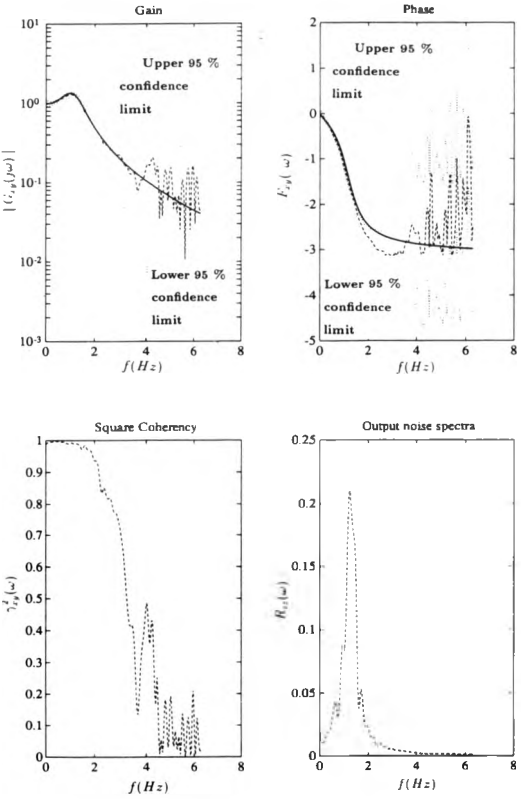

Figure 4.6: **Tukey estimates of gain, phase, square coherence and output noise spectra of simulated system for $M = 100$.**

4.3.3 Computation of spectral estimates for LMSE windows.

In the schematic for evaluating LMSE input-output time windows of figure (4.1), two requirements are needed :

(i) An estimate of the cross covariance function,

(ii) The postulated impulse response of the system.

The first requirement can easily be evaluated by computing the sample cross covariance function between the x_t and y_t.

There exist two options for evaluating an impulse response directly from its measured frequency response data. These are :-

(1) To compute (as in [1]) the impulse response by evaluating the inverse Fourier transform of the frequency response. i.e,

$$\hat{g}(t) = \int_0^{\frac{1}{2\Delta}} \frac{L_{xy}(f)}{R_{xx}(f)} \cos(2\pi f t) df - \int_0^{\frac{1}{2\Delta}} \frac{Q_{xy}(f)}{R_{xx}(f)} \sin(2\pi f t) df$$

for $t = 0, \Delta, 2\Delta, \ldots, M\Delta$.

(2) To implement a least square analysis that performs a best fit on the frequency response data.

In practice method (2) is preferred because of its ability to perform such an analysis over any desired frequency range or spacing. This enables any undesirable portion of the frequency response data to be ignored or given a reduced weight in the analysis. Figure (4.7) shows the impulse response estimates of the above two methods for the Tukey window at $M = 60$ and the least square curve fit based on the frequency response data over the range

$$0 \leq f \leq 3.5(Hz).$$

Neither method gives an exact representation of the true impulse and both lead to an over estimation of the damping factor. The principles of least square curve fitting to

frequency response data have been extensively studied and documented in [5]. Using the above estimates as postulated impulse responses in the computation of LMSE windows, both the resulting frequency response estimates were found to be superior to that of the Tukey window, with the impulse response estimate of method (2) yielding slightly better results.

This was also found to be the case at different truncation points M and different filter system arrangements. The simulation results presented in this section however are on estimates of the impulse response obtained by method (1).

Figure (4.8) shows the LMSE windows evaluated for $M = 60$ after alignment with the sample cross covariance function $\hat{c}_{xy}(\tau)$ superimposed. Figures (4.9) and (4.10) show plots of gain, phase, coherence and noise spectra for $M = 50$ and 60 using aligned LMSE windows on the cross correlation function.

Evaluation of results.

It is evident that the evaluation of the spectral estimates leads to a substantial reduction in variability when comparison is made with the Tukey window estimates of figures (4.4) and (4.5). By strictly abiding with the window closing procedure in [1], $M = 80$ was chosen as the best LMSE window (see figure (4.11)).

From these and numerous simulation studies of other filter system arrangements, two conclusions are made :-

(1) Least mean square error windowing reduces some of the undesired spurious details.

(2) The reduction in variability, allows for larger truncation points M and so leads to reduced bias in the estimate.

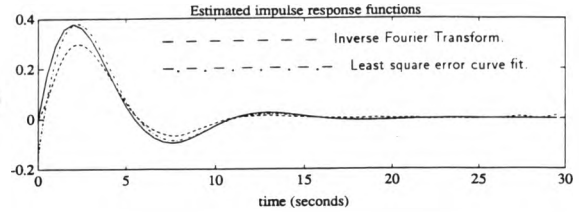

Figure 4.7: **Impulse response estimates based on inverse Fourier transformation and least square curve fit for the Tukey window estimate of the frequency response function based on $M = 60$.**

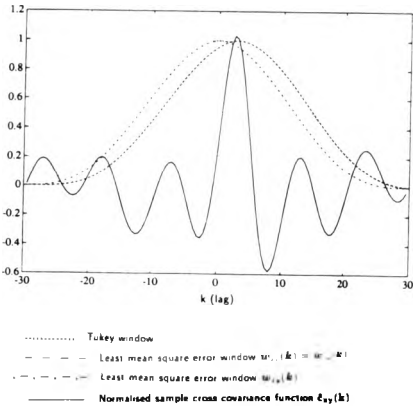

Figure 4.8: **Least mean square error window based on postulated impulse response from the Tukey estimate at $M = 60$.**

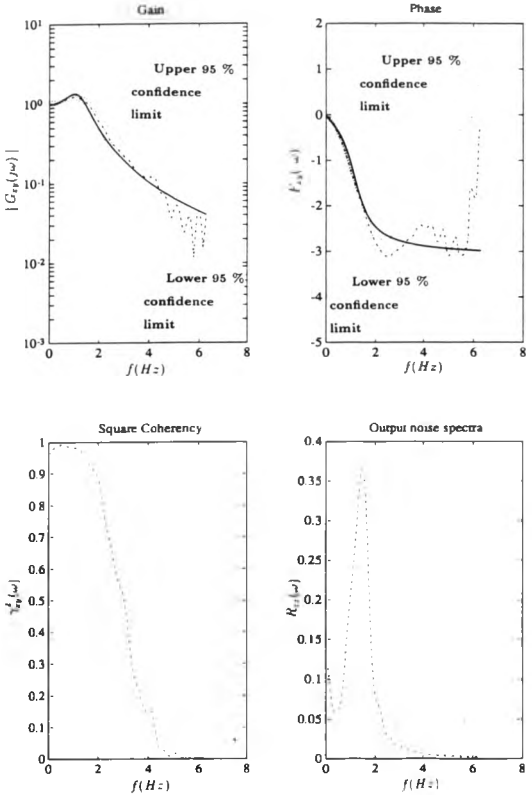

Figure 4.9: **Least mean square error window estimates of gain, phase, square coherence and output noise spectra of simulated system for** $M = 50$.

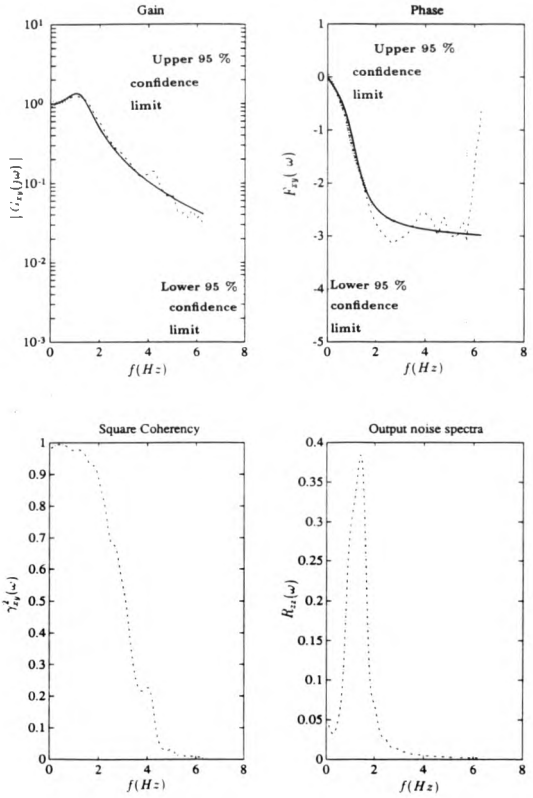

Figure 4.10: **Least mean square error window estimates of gain, phase, square coherence and output noise spectra of simulated system for** $M = 60$.

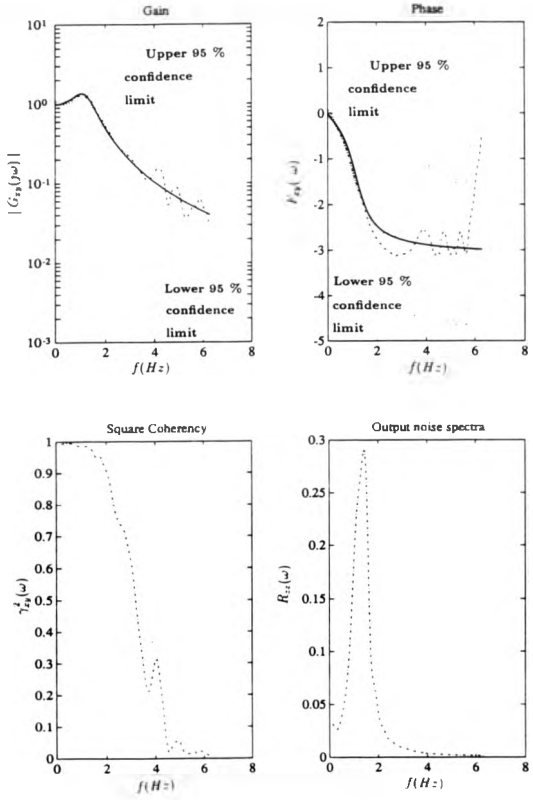

Figure 4.11: **Least mean square error window estimates of gain, phase, square coherence and output noise spectra of simulated system for** $M = 80$.

4.4 Estimation of frequency response functions by segmental averaging.

The estimation of frequency response functions can also be based on averaging over short, modified periodograms. An advantage of this method is that it involves fewer computations than the direct method. The procedure has been extensively documented in [6].

4.4.1 Method of segmental averaging.

Let $x(i)$ and $y(i)$, $i = 0, 1, 2, ..., N-1$ represent samples of the input and output from a stationary process $G(j\omega)$, $|\omega| \leq \pi/\Delta$.

By taking L segments (each of length M), we can define as follows

$$x_n(i) = x(i + M(n-1)) \quad \text{and} \quad y_n(i) = y(i + M(n-1))$$

for $i = 0, 1, 2, ..., M-1$ and $n = 1, ..., L$.

Here we are assuming that L is such that the condition $ML = N$ is true. The L segments will then cover the entire records of $x(i)$ and $y(i)$.

Selecting the appropriate input-output time windows,

$$w_x(i) \quad \text{and} \quad w_y(i), \quad \text{for} \quad i = 0, 1, 2, ..., M-1$$

forms the sequences

$$x_n(i)w_x(i) \quad \text{and} \quad y_n(i)w_y(i)$$

$$\text{for} \quad i = 0, 1, 2, ..., M-1 \quad \text{and} \quad n = 1, ..., L.$$

Discrete finite Fourier transforms of the above windowed sequences gives

$$X_n(k) = \frac{1}{M}\sum_{i=0}^{M-1} x_n(i)w_x(i)\exp(-j2kni/M) \tag{4.5}$$

and

$$Y_n(k) = \frac{1}{M}\sum_{i=0}^{M-1} y_n(i)w_y(i)\exp(-j2kni/M). \tag{4.6}$$

for $k = 0, 1, ..., \frac{M}{2}$.

From equations (4.5) and (4.6), the modified periodograms of the input and output are given by :-

$$\hat{P}^n_{xx}(\omega_k) = \frac{\Delta M}{q_x} \mid X_n(k) \mid^2$$

$$\hat{P}^n_{yy}(\omega_k) = \frac{\Delta M}{q_y} \mid Y_n(k) \mid^2$$

$$\hat{P}^n_{xy}(j\omega_k) = \frac{\Delta M}{q_{xy}} X_n(k)Y^*_n(k)$$

where

$$q_x = \frac{1}{M}\sum_{i=0}^{M-1} w_x^2(i),$$

$$q_y = \frac{1}{M}\sum_{i=0}^{M-1} w_y^2(i),$$

$$q_{xy} = \frac{1}{M}\sum_{i=0}^{M-1} w_x(i)w_y(i),$$

and

$$\omega_k = \frac{2\pi k}{\Delta M} \quad \text{for} \quad k = 0, 1, ..., \frac{M}{2}.$$

Finally by averaging the modified periodograms evaluated from the segments, we obtain the smoothed modified periodograms

$$\overline{P}_{xx}(\omega_k) = \frac{1}{L}\sum_{i=1}^{L} \hat{P}^{(i)}_{xx}(\omega_k),$$

$$\overline{R}_{yy}(\omega_k) = \frac{1}{L}\sum_{i=1}^{L} \hat{R}_{yy}^{(i)}(\omega_k),$$

$$\overline{R}_{xy}(j\omega_k) = \frac{1}{L}\sum_{i=1}^{L} \hat{R}_{xy}^{(i)}(j\omega_k).$$

The above equations lead to expressions for frequency response and coherence estimates defined respectively by

$$\overline{G}_{xy}(j\omega_k) = \frac{\overline{R}_{xy}(j\omega_k)}{\overline{R}_{xx}(\omega_k)}$$

and

$$\overline{\gamma}_{xy}^2(\omega_k) = \frac{|\,\overline{R}_{xy}(j\omega_k)\,|^2}{\overline{R}_{xx}(\omega_k)\overline{R}_{yy}(\omega_k)}.$$

4.4.2 Example of frequency response estimate based on segmental averaging.

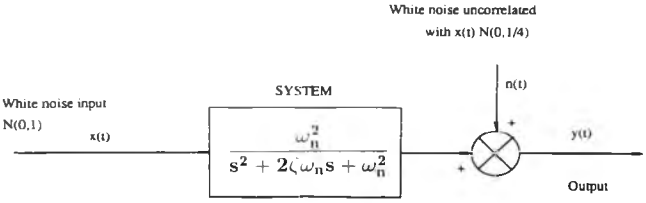

Figure 4.12: Schematic of experimental simulation for segmental averaging.

Figure (4.12) represents a linear second order system chosen for this experiment with $\omega_n = \pi$ and $\zeta = 0.4$. The white noise input N(0,1) is passed into the system and the output is then corrupted by additive white noise N(0,0.25) that is uncorrelated with $x(t)$. With an observation time of T = 1600 seconds at a sampling interval of $\Delta = 0.025$, the corresponding input and output records are then divided into $L = 250$ segments of length $M = 256$. From figure (4.13) we observe that $M\Delta = 6.4$ is chosen so that its

value is of the same order of magnitude as the system settling time.

From the input and output records that result, the method of segmental averaging is applied to give smoothed modified periodograms at a frequency spacing of $\omega_s = 0.9856$ radians per second.

Figure (4.14) shows plots of frequency response estimates based on the Hanning and LMSE windows. The postulated system is computed by the inverse Fourier transform of the frequency response estimate using the Hanning window. Figure (4.14) makes comparisons between the square of error in the resulting frequency response estimates. Both plots are shown for the first 8 harmonic frequencies and figure (4.13), is accompanied by the true system frequency response.

Evaluation of results.

The coherence plot in figure (4.14) further emphasises the superiority of LMSE windows. We observe that whilst these windows show dramatically improved coherence estimates at low frequencies, at high frequencies, the Hanning (which in practice gives exceptionally good estimates,) does not differ significantly from the estimates based on the LMSE windows. Finally figure (4.15) shows the time windows evaluated for the segmental averaging process.

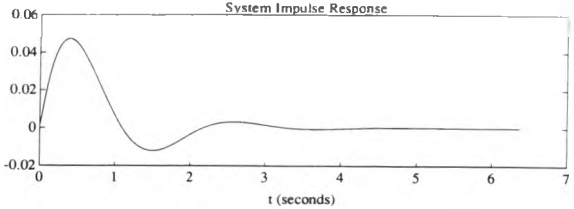

Figure 4.13: **Impulse response model of system under investigation**

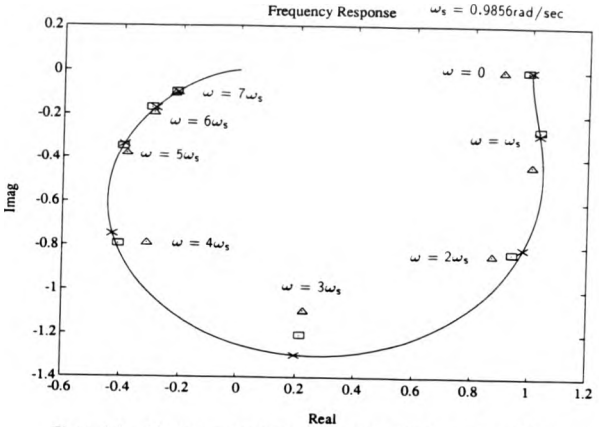

Figure 4.14: **Frequency response estimates of Hanning and Least mean square error windows for L=250,M=256.**

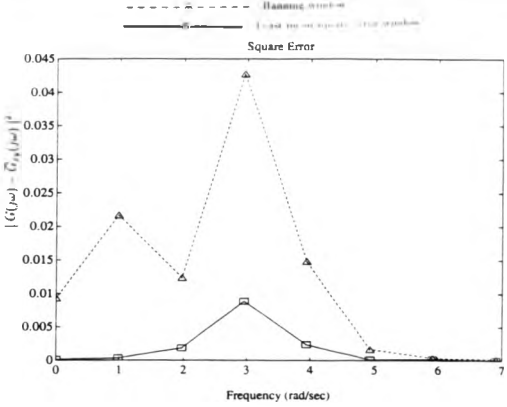

Figure 4.15: Square of error between estimates and true frequency response.

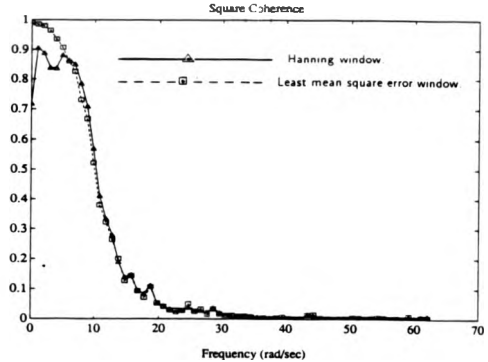

Figure 4.16: Comparison for coherence estimates of Hanning and Least mean square error windows

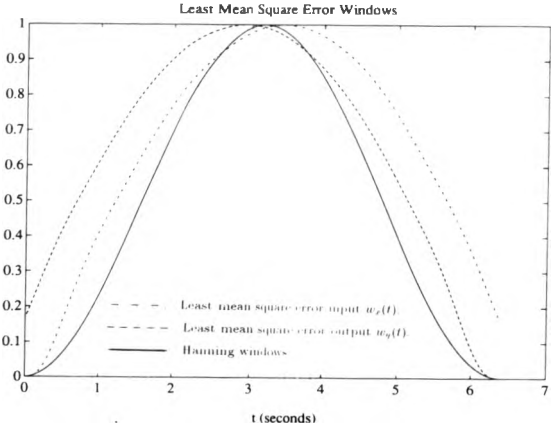

Figure 4.17: **Plots of Least mean square error and Hanning windows.**

4.5 Summary

In this chapter a more generalised schematic was introduced to design time and correlation windows based on single realisations of input-output records. These windows are robust and are found not to vary significantly for different realisations of the same system. The advantage of this method is apparent in that it allows engineers to design optimum windows which are based wholly on the input-output record available. As a result it removes any uncertainty which may exist in choosing the numerous forms of other classical windows. In the next chapter, window carpentry is again used to design time windows for power spectral analysis. The example used is taken from ambient response data of the Humber Suspension bridge and is shown to further emphasize the significance of the Papoulis window.

4.6 References for chapter (4).

[1] **Jenkins. G.M. and Watts. D.G..:** 'Spectral analysis and its applications'. Holden Day,1968.

[2] **Cochran. W.T. et al.,** ' What is the Fast Fourier Transform ? ' IEEE Trans. Audio and Electroacoustics, Vol. Au-15, No.2,p.45,June 1967.

[3] **Rabiner. L.R. and Rader. C.M.,:** 'Signal and linear system'. 'Digital signal processing', IEEE, Press.

[4] **Ljung. L.,:** 'System identification: Theory for the user'. Prentice-Hall, 1987.

[5] **Parks. T.W. and Burrus. C.S.,:** 'Digital Filter Design'. John Wiley and Sons, 1987.

[6] **Piersol. A.G. and Bendat. J.S.,:** 'Engineering applications of correlation and spectral analysis'. Wiley, New York (1980).

[7] **Blackman. R.B. and Tukey. J.W.,:** 'The measurement of Power spectra'. Dover, 1958.

Chapter 5

Modelling of spectral estimates from high Q bridge dynamics.

5.1 Introduction

Careful mathematical modelling is always required in the design of modern suspension bridges, as these models are used to predict free vibrations and asynchronous excitation responses [1]. However, in order to validate any assumptions made in the modelling and accuracy of the model parameters, full scale testing procedures need to be undertaken.

Such tests are usually in the form of :-

(1) Measurement of dynamic responses from ambient excitation.

(2) Forced vibration response measurement.

The term ambient is used to describe all forms of uncontrollable inputs such as excitation caused by wind, waves and vehicle vibration.

This chapter is concerned with modelling power spectral data computed from ambient response data of the Humber suspension bridge.

To investigate problems that arise in fitting such models to the auto power spectrum, consideration is given to the over-estimation of the damping factor ζ due to :-

(i) The finite length of data given for analysis.

(ii) The frequency resolution at which the spectral data and modelling procedure is performed.

(iii) The number of averages that are performed on the spectral data to reduce variability, in order to produce smooth spectral estimates for the model fitting procedure.

(iv) The type of time window that is applied to the ambient response before spectral analysis in order to reduce the effects of spectral leakage due to this finite length of data.

To reduce the above effects we will :-

(a) Investigate the concept of the integrated power spectrum in order that the modelling procedure is implemented with the highest possible frequency resolution based on the data.

(b) Review the use of time windows in order to achieve minimum bias in the spectral data.

Main advantages of ambient vibration testing are :-

(a) There is no need for eccentric mass excitors or hydraulic actuators, as these simplified test procedures require the use of data acquisition equipment only. As a result they are less disruptive to normal operations in the structure.

(b) As data is analysed, it is easier to return to the structure to run additional tests.

(c) Advances in computer hardware and software makes it possible to obtain rapid on-site multi-channel spectral analysis, thereby reducing the complexity of the systems identification problem for the engineer [1].

The main disadvantage of this method is that the non-stationary random process of the excitation and the extraction of model properties is made more difficult by the varying and sometimes negligible participation of some structural response modes [4].

In the majority of cases, some knowledge of mathematical structure of the unknown system is available and the problem of system identification becomes that of determining unknown parameters within the structure in accordance with a stated identification criterion.

5.1.1 General comments on the testing and modelling of large structures.

The fundamental motivation for testing large structures is to obtain information which will help to produce in an economical manner, structures which are safer for their intended function. More specifically, one may wish to verify or improve the modelling or analysis techniques. Knowledge of certain characteristics is often imperative, and such characteristics as damping factors or nonlinearities which are difficult to predict by analytical means, often play an important role in determining how the structure will behave under loads. Thus testing can provide a signature of the system which can be used to identify changes in the system resulting from damage caused by severe loads such as earthquakes, hurricanes and fatigue damage [2].

The system identification problem can be divided into three parts [1] :

(1) SYSTEM STRUCTURE IDENTIFICATION- This is the selection from experience of differential equations (or transfer functions) for the assumed model, from which unknown parameters within the structure may be determined.

(2) CRITERION FUNCTION IDENTIFICATION- The mathematical criterion which is optimised in order to accomplish identification and the goodness of fit of the models response to the actual system inputs.

(3) SYSTEM PARAMETER IDENTIFICATION- The alogrithm used to adjust and identify the unknown parameters in which the system identification criterion is minimised.

5.2 System identification structure.

The first step in the identification scheme is to simplify the representation of the suspension bridge model structure. Initially the non-linearities in the system and its time dependent characters are often ignored [1]. As a result, in the analysis it is assumed that the structure is linear with constant coefficient differential equations [2]. The formulation can be further simplified by the fact that large bridge structures exhibit light damping factors [3], which allows identification to be typically reduced to finding a system's lower natural frequencies and modal damping factors.

Given the above assumptions, this identification scheme (based on a system of light damping and multiple degrees of freedom [1]), can be closely approximated by a single degree of freedom system with an appropriate natural frequency and damping factor in the region near each of the system's natural frequencies.

5.3 Criterion function identification.

The fundamental relationship which enables spectral analysis to be used in estimating a system's frequency response is given by

$$P_{yy}(\omega) = \mid G(j\omega) \mid^2 \; P_{xx}(\omega) \tag{5.1}$$

where

$P_{xx}(\omega)$is the power spectral density of the input to the system,

$G(j\omega)$ is the frequency response of the system,

$P_{yy}(\omega)$is the power spectral density of the output of the system.

The most severe restriction in the use of this formulation is that the system must be linear with constant coefficients and the response must be stationary and ergodic [2]. In equation (5.1) the ratio $P_{xx}(\omega)/P_{yy}(\omega)$ provides the desired estimate for the amplitude squared of the frequency response.

In the analysis of the Humber suspension bridge $P_{xx}(\omega)$ cannot be measured accurately, but as $P_{xx}(\omega)$ can be assumed to be constant in each of the regions surrounding the natural frequencies of interest, the magnitude of the frequency response can be obtained on replacing it with a multiplicative constant [3].

The error criterion used in the modelling of such data is the integrated error between the measured and modelled output power spectral data around each natural frequency of interest

$$M_e = \int_{\omega_1}^{\omega_2} [P_{yy}(\omega) - \hat{P}_{yy}(\omega)]^2 d\omega. \tag{5.2}$$

The parameters ω_2 and ω_1 represent the upper and lower limits of integration bounding the natural frequency of interest.

Typical transfer function models chosen are of the form :-

$$G(s) = \frac{K.w_n^2}{s^2 + 2\zeta w_n s + w_n^2}, \tag{5.3}$$

$$G(s) = \frac{K.w_n^2.s}{s^2 + 2\zeta w_n s + w_n^2} \tag{5.4}$$

where K, ζ and w_n are the gain, damping factor and resonant frequency respectively.

To fit these models to the resulting power spectral data it is assumed that :-

(1) the exciting force spectrum is flat over the frequency range of interest.

(2) there exists minimum cross coupling (or interference) between successive frequency modes.

For equation (5.3) the output power is readily evaluated and gives

$$P_{yy}(\omega) = \frac{K^2\omega_n^4}{\omega_n^4 - 2\omega_n^2\omega^2(1 - 2\zeta^2) + \omega^4}. \tag{5.5}$$

The object here is to relate the characteristics of the measured spectral estimates to the structural parameters (K, ω_n, ζ) by minimising the error function M_e in equation (5.2). This least squares curve fitting procedure can be implemented with any optimisation package. A Matlab Optimisation Toolbox has been written by Bangor University (Wales) and although not commercially available, the author would like to take this opportunity to thank Professor P.J. Fleming and his group for permitting the use of this package.

Another error criterion, proposed by Professor J.L. Douce, is minimum integrated square error between the measured and modelled cumulative spectral data

$$IM_e = \int_{\omega_1}^{\omega_2} [IP_{yy}(\omega) - \hat{IP}_{yy}(\omega)]^2 d\omega. \tag{5.6}$$

The cumulative spectrum is defined by

$$IP_{yy}(\omega) = \int_{\omega_1}^{\omega} P_{yy}(\omega_2) d\omega_2. \tag{5.7}$$

This criterion is believed to be reliable in the identification scheme; as for record lengths T, significantly larger than the systems settling time, large fluctuations in the measured spectral estimate will be effectively reduced by its averaging out (or smoothing) effect.

In previous analyses [3-5], minimisation of equation (5.2) has been used to model the measured spectrum density around the natural frequencies of interest and in order to reduce large fluctuation (variability), smoothing of the spectral estimate is achieved by segmental averaging of the response data [2] , or by averaging unsmoothed spectral estimates over frequencies [5].

The curve fitting procedure adopted has been designed for unsmoothed spectral estimates obtained from computing the Fast Fourier Transform of the response data. Reliable initial estimates for model parameters are always required in order to improve the efficiency of any least squares curve fitting procedure and a review of this will be made in section (5.4.1).

The advantages of this procedure are that bias errors associated with smoothed spectral estimates are reduced, maximum frequency resolution is obtained and the statistics of each spectral estimate are well defined enabling a criterion to be developed for the selection of the analysis interval [1]. Also the data can be fitted directly to higher order systems thus allowing for closely spaced spectral peaks to be identified [2].

In this chapter, both curve fitting criteria are applied to the Humber suspension bridge data and they are found to yield estimates differing consistently from earlier results [4]. In particular estimates of damping factor are shown to be very much smaller than those based on smoothed spectral density measurements.

5.4 The model cumulative spectrum and its properties.

Performing the integration in equation (5.6) for $\zeta < 1$, leads to the cumulative spectrum

$$\begin{aligned} IP_{yy}(\omega) &= C_0(\sin(\frac{\alpha}{2})\log[\frac{\omega^2 + 2\omega_n\omega\cos(\alpha/2) + \omega_n^2}{\omega^2 - 2\omega_n\omega\cos(\alpha/2) + \omega_n^2}] \\ &+ 2\cos(\frac{\alpha}{2})\arctan[\frac{\omega^2 - \omega_n^2}{2\omega_n\omega\sin(\alpha/2)}]) + C \end{aligned} \tag{5.8}$$

where

$$\begin{aligned} C = &- C_0(\sin(\frac{\alpha}{2})\log[\frac{\omega_1^2 + 2\omega_n\omega_1\cos(\alpha/2) + \omega_n^2}{\omega_1^2 - 2\omega_n\omega_1\cos(\alpha/2) + \omega_n^2}] \\ &- 2\cos(\frac{\alpha}{2})\arctan[\frac{\omega_1^2 - \omega_n^2}{2\omega_n\omega_1\sin(\alpha/2)}]), \end{aligned}$$

$$C_0 = \frac{K.\omega_n}{4\sin(\alpha)}, \alpha = \arccos(1 - 2\zeta^2) \text{ and } \zeta < 1.$$

In practice, performing a least square curve fit on the cumulative spectra will lead to a superior estimate for the following reasons :-

(1) The cumulative spectrum by definition performs a smoothing operation on the raw auto spectral data and thus will lead to a more consistent estimate of K, ω_n and ζ. However, this consistency will be subject to the particular realisation.

(2) The effects of nearby resonant modes will be to broaden the bandwidth of the spectral peak under consideration. This problem can be reduced (although not eliminated) by fitting the cumulative spectra in equation (5.8) over the range

$$\omega_- \leq \omega \leq \omega_+,$$

where ω_- and ω_+ are the half power bandwidth frequencies.

(3) From straightforward visual inspection of the cumulative spectra it becomes easier to make estimates of ω_n, ω_-, and ω_+ in order to define the frequency range over which the model is to be fitted and so produce initial estimates for the damping factor.

5.4.1 Initial model parameter estimates.

In any optimisation routine, reliable initial estimates of the model parameters are required to assure that the global minimum is found. A brief explanation (as found in [1]) will be given in this section to the methods used in providing initial estimates of gains, damping factors and resonant frequencies that are evaluated at each resonant mode.

Initial gain estimate. Employing a least square estimate, the estimate $\hat{K}$ is chosen in such a way that the loss function

$$L_f = \int_{\omega_1}^{\omega_2} \mid P_{yy}(\omega) - \hat{P}_{yy}(\omega) \mid d\omega$$

is a minimum. $\hat{P}_{yy}(\omega)$ and $P_{yy}(\omega)$ are the respective experimental and modelled auto spectral data around the resonant frequency of interest. This leads to the common least

square notation

$$\hat{K} = \frac{\int_{\omega_1}^{\omega_2} P_{yy}(\omega).\hat{P}_{yy}(\omega)d\omega}{\int_{\omega_1}^{\omega_2} P_{yy}^2(\omega)d\omega}.$$

Initial damping estimate.

For small values of damping, computation shows the 'Log' term to be much smaller than the 'Arctan' term in equation (5.8). At the resonant frequency $\omega \approx \omega_n$, an initial estimate of the damping can be evaluated by setting the 'Arctan' term in equation (5.8) to zero. i.e,

$$\omega^2 - 2\omega\omega_n \sin(\frac{\alpha}{2}) - \omega_n^2 = 0,$$

which leads to the solution

$$\omega = \omega_n \sin(\frac{\alpha}{2}) \pm \omega_n\sqrt{1 + \sin^2(\alpha/2)}. \tag{5.9}$$

In particular, for values of damping, $\zeta(\ <\ 0.1\ )$,

$$\sin(\frac{\alpha}{2}) \approx \zeta, \text{ and } \zeta^2 << \zeta,$$

and equation (5.9) can be approximated by

$$\omega = \omega_n(1 + \zeta). \tag{5.10}$$

At the resonant frequency ($\omega = \omega_n$),

$$P_{yy}(\omega_n) = \frac{1}{4\zeta^2},$$

and at the half power frequency $u_{\pm} = \omega_{\pm}^2/\omega_n^2$ is given by

$$\frac{1}{8\zeta^2} = \frac{1}{u^2 - 2u(2\zeta^2 - 1) + 1} \tag{5.11}$$

has solution $u = \pm 2\zeta$.

From equation (5.10),

$$(\frac{\omega_{\pm}^2}{\omega_n^2})^2 = 1 \pm 2\zeta + \zeta^2. \tag{5.12}$$

Assuming that $\zeta^2 \approx 0$, equations (5.11) and (5.12) leads to an initial estimate for the damping factor :-

$$\zeta = \frac{\omega_+^2 - \omega_-^2}{4\omega_n^2}.$$

Initial estimate of resonant frequency. Initial estimates of resonant frequency can be readily obtained from straight forward visual inspection of the auto spectral or cumulative spectral data. On the auto spectral data, this estimate is found from the spectral peak and at each resonant mode, and on the cumulative spectral data, the estimate is obtained from the approximate point of inflexion around each resonant mode.

5.5 Simulation studies.

To illustrate the advantage of implementing this least square curve fitting procedure on the cumulative spectrum, consider figure (5.1) for $n = 5$.

The gain,damping and resonance frequency for the 5 modes are set to

$$\begin{aligned} K &= [0.500, 0.600, 0.250, 0.130, 0.120], \\ \zeta &= [0.0250, 0.0398, 0.0136, 0.0109, 0.0098], \\ \omega_n &= [0.425, 0.071, 0.100, 1.356, 1.700], \end{aligned}$$

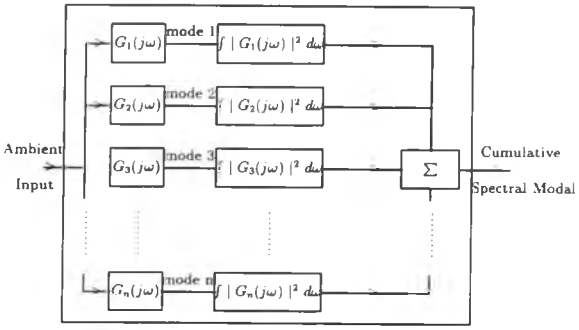

Figure 5.1: **Schematic of an n-mode cumulative spectral modal**

These parameters are chosen to best illustrate (visually) the type of power spectral structure observed from the Humber suspension bridge data taken from [4].

5.5.1 Method.

(1) The overall transfer function of the system is evaluated by summing the 5 modal transfer function models. This gives

$$G(s) = \frac{a_8 s^8 + a_7 s^7 + a_6 s^6 + a_5 s^5 + a_4 s^4 + a_3 s^3 + a_2 s^2 + a_1 s + a_0}{b_{10} s^{10} + b_9 s^9 + b_8 s^8 + b_7 s^7 + b_6 s^6 + b_5 s^5 + b_4 s^4 + b_3 s^3 + b_2 s^2 + b_1 s + b_0} \tag{5.13}$$

where

$$\begin{aligned} a_8 &= 0.157, a_7 = 0.00683, a_6 = 0.0818, a_5 = 0.00265, \\ a_4 &= 0.0121, a_3 = 0.000258, a_2 = 0.000547, \\ a_1 &= 0.00000569, a_0 = 0.00000617. \end{aligned}$$

and

$$\begin{aligned} b_{10} &= 1, b_9 = 0.0549, b_8 = 0.743, b_7 = 0.0322, \\ b_6 &= 0.170, b_5 = 0.00549, b_4 = 0.0137, b_3 = 0.000291, \\ b_2 &= 0.000347, b_1 = 0.00000356, b_0 = 0.00000355. \end{aligned}$$

(2) Equation (5.13) is excited by white noise with sampling interval $\Delta = 1$ second.

(3) The resulting output of the system of record length $T = 2^{17}$ windowed by a Papoulis weight is Fast Fourier Transformed and multiplied with its complex conjugate to obtain the unsmoothed power spectral estimate.

(4) A least square curve fitting procedures is implemented on the power spectrum as well as its cumulate.

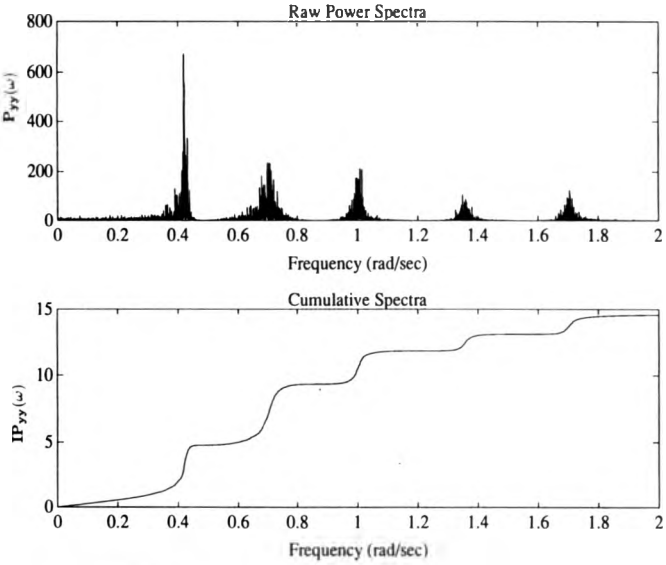

Figure 5.2: **Raw power spectrum and its cumulate for 5 modal model.**

5.5.2 Results.

Figure (5.2) show plots of the raw auto power and cumulative spectral estimate. Theoretically, there is no distinction between the two curve fitting procedures, but for realisations of the true output, use of the cumulative spectrum reduces the effects of variability and sharp spikes in the raw spectrum and thus should improve the accuracy of the curve fit.

Tables (5.1) gives comparison between the model fit on the raw power spectrum and its cumulate. Table (5.2) show the standard deviation in gains, damping factors and resonant frequency in comparison to the true values.

	Optimisation on $P_{xx}(\omega)$			Optimisation on $\int P_{xx}(\omega)d\omega$		
Mode no.	ω_n (rad/sec)	ζ	K	ω_n (rad/sec)	ζ	K
(1)	0.4209	0.0194	0.4535	0.4206	0.0251	0.5447
(2)	0.7061	0.0333	0.5479	0.7046	0.0359	0.5786
(3)	1.0051	0.0142	0.2271	1.0013	0.0139	0.2247
(4)	1.3565	0.0108	0.1187	1.3568	0.0109	0.2096
(5)	1.7037	0.0107	0.1121	1.7034	0.0102	0.1088

Table 5.1: **Estimates of resonant frequency, gain and damping factor for simulated model.**

	Optimisation on $P_{xx}(\omega)$			Optimisation on $\int P_{xx}(\omega)d\omega$		
Mode no.	ω_n (%)	ζ (%)	K (%)	ω_n (%)	ζ (%)	K (%)
(1)	0.96	22.4	9.3	1.03	0.4	8.9
(2)	0.87	16.3	8.7	0.57	2.3	3.6
(3)	0.15	4.4	9.2	0.13	2.2	10.1
(4)	0.37	0.9	8.5	0.59	0.9	6.9
(5)	0.22	11.2	6.7	0.20	1.1	9.3

Table 5.2: **Comparison of standard(%) for simulated model**

Figure (5.3) is a graphical representation for the two model fitting procedures at mode 2. The curves marked (-.-.-.-) represent the modelled data resulting from a least square curve fit on the unsmoothed power spectrum. Also the curves marked (– – – –) represent the modelled data resulting from a least square curve fit on the unsmoothed cumulative power spectrum.

Brief summary of above results

It is found that estimates of ω_n show favourable agreement with the true model parameters and for the damping factors ζ, curve fitting of the cumulative spectra lead to consistently improved estimates. This was shown to be the case for studies of other realisation and system arrangements.

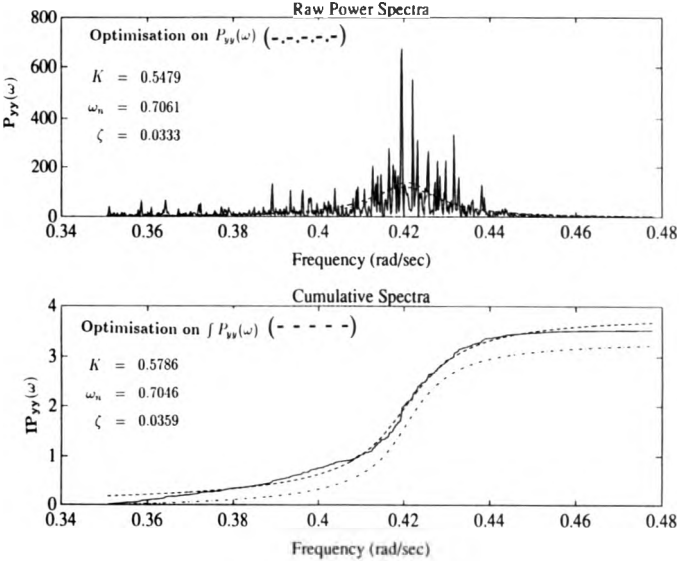

Figure 5.3: Model fitting procedure at Mode 2.

5.6 Humber Suspension Bridge.

Previous to the ambient vibration tests undertaken on the Humber bridge by the Bristol University group only one series of tests has been carried out on suspension bridges with slender towers,inclined hangers and box-girder (Boshporus bridge). The Humber bridge tests describe measurements of wind and traffic induced vibrations to determine vertical, lateral and torsional acceleration characteristics of the desk and tower.

Figure (5.4), reproduced from reference [4], is a schematic representation of the Humber suspension bridge with travelling accelerometers positioned to measure relative accelerations in the vertical mode. The accelerometer I1 positioned at either R1 or R2 is used as a reference. I2 and I3 are used as travelling accelerometers along the bridge between measurements in order for the sum I2+I3 in this position to produce a measure of the vertical response. The calibrated accelerometers are Schaevitz force balance servo-accelerometers with operating ranges $\pm 0.25g$ in the frequency range 0-30Hz. Measurements of the vertical mode are made at R1 and R2 over averaging periods of 13 hours to relate measurements with a common reference R2 and to obtain the highest possible quality over all relative measurements.

Vertical response data from the Humber bridge at positions R1 and m16 have been presented to the author for analysis with permission of the Bristol University group. It must be stated here that in analysis undertaken by Bristol group, full scale testing of the response data at vertical, torsional, lateral, longitudinal tower, lateral span modes have been undertaken and the main purpose in this section is simply to justify the use of the new modelling procedure described in the previous sections. If the results are deemed satisfactory then it is hoped that similar analysis will be undertaken on the response data at the other modes.

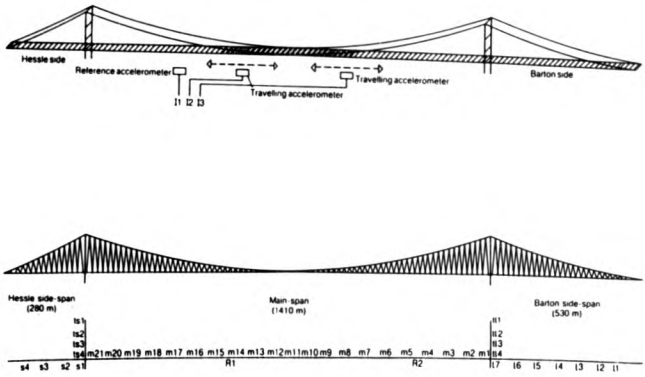

Figure 5.4: **Schematic of Humber Suspension bridge and measurement positions.**

5.6.1 Data processing procedure from the Humber bridge response data.

From recorded acceleration signals, estimates of resonance frequency, damping and spectral amplitude at each resonance mode up to an appropriate frequency limit is evaluated by the use of a Winograd discrete Fourier transform twin channel Spectral analyser. The 'auto power' facility in the analyser automatically applies a Hanning window before spectral analysis and gave averaged 501 frequency data point after analysis.

Around each resonance mode a least squares curve fitting procedure of the auto power spectral response data is implemented with a single degree of freedom (SDOF) oscillator and in the curve fitting procedure it was hoped that the resulting smoothed response would reduce the effect of bias error and so obtain reliable estimates of natural frequencies, amplitude and damping ratios [4]. In [4] it was however concluded that damping estimates obtained by fitting SDOF response curves to the windowed and averaged auto power spectra are probably higher than the values that would be obtained from forced vibration testing.

5.7 Examination of results.

In this section an examination of the results obtained from least square curve fitting of the raw power and cumulative spectral data is made and comparison with results obtained by the Bristol group is given.

The vertical mode response data supplied was recorded from the accelerometers with gain 100V/g and was attenuated by 10 on recording. Data was replayed at 64 times the recording speed, amplified by a factor of 50 and passed through a high order low-pass anti-aliasing filter with a cut-off frequency of 160 Hz. The resulting signals were digitised at 512Hz for 420 seconds to give 215040 samples with a time interval of $\Delta = 0.00195$ seconds.

The A/D convertor output

$$y_d(i) \quad \text{for} \quad i = 1, ..., 215040,$$

is obtained in the form 0-4095 and corresponds to a range of $\pm$ 10V. The original data is obtained by computing

$$y(i) = ((y_d(i) - 2048)/204.8)/500 \quad \text{for} \quad i = 1, ..., 215040,$$

with $\Delta = \Delta \times 64$ results in a Nyquist frequency of 4Hz.

Figure (5.5) shows the resulting unsmoothed power spectrum at position R1 evaluated using 'Matlab' from a Sun 4 workstation. Performing the Fast Fourier Transform took approximately 90 seconds under normal operating multi-user conditions and the original data for vertical mode at positions R1 and m16 were weighted with a Papoulis window before spectral analysis. The full significance of this will be made apparent in the next section.

In figure (5.5), the spike labelled (a) was not considered to be a resonance mode on closer inspection of its detailed structure. Typical bounce frequencies of vehicles are in the frequency range

$$1.8Hz \leq f \leq 2.5Hz$$

[1], and so all response data above 1.8 Hz is ignored.

Tables (5.3) and (5.4) gives estimates of resonant frequencies, damping factor (as a percentage of critical) and gains for the two curve fitting procedures. Figures (5.6) and (5.7) are graphical representations of results obtained for modes R1V2 and m16V1. As in figure (5.3), in figures (5.6) and (5.7), the curves marked (-.-.-.-) represent the modelled data resulting from a least square curve fit on the unsmoothed power spectrum. Also the curves marked (– – – –) represent the modelled data resulting from a least square curve fit on the unsmoothed cumulative power spectrum.

In Figure (5.8) comparison is made between the modelled damping estimates (against frequency) from the above experiment and those obtained by the Bristol group and figure (5.9) shows a plot of the model power spectral output for position R1.

It is found that all of the damping estimates from the authors analysis and particularly those obtained by least square curve fit on the cumulative power spectra, shows significant reductions over those obtained by the Bristol group [4].

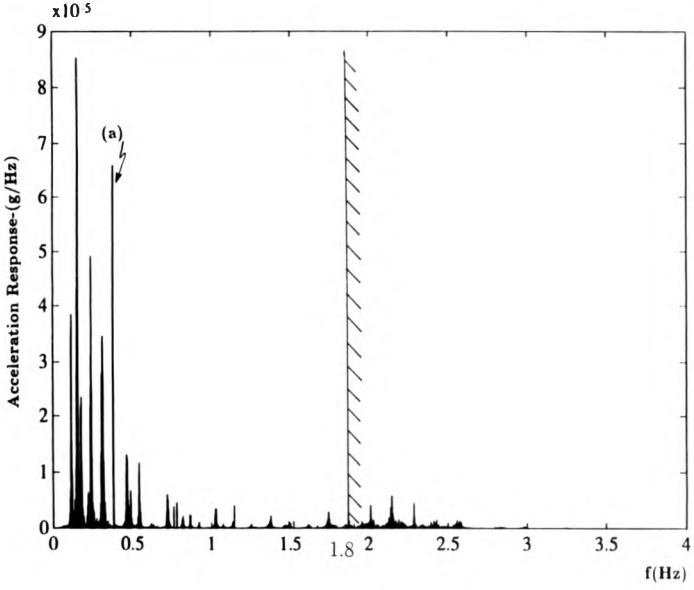

Figure 5.5: **Unsmoothed power spectrum of Humber suspension bridge at vertical mode position R1.**

Mode no.	Optimisation on $\int P_{zz}(\omega)d\omega$			Optimisation on $P_{zz}(\omega)$		
	f_n (Hz)	ζ (%)	K (10^{-7})	f_n (Hz)	ζ (%)	K (10^{-7})
R1V1	0.1167	2.77	1526	0.1166	2.77	1526
R1V2	0.1569	2.09	1923	0.1571	1.23	1307
R1V3	0.1789	2.59	1124	0.1791	2.71	1159
R1V4	0.2415	1.43	901	0.2417	1.45	908
R1V5	0.3129	1.55	890	0.3130	1.69	950
R1V6	0.4662	1.14	456	0.4663	1.11	443
R1V7	0.4861	1.16	311	0.4863	1.23	325
R1V8	0.5438	0.76	214	0.5436	0.71	201
R1V9	0.7243	0.71	180	0.7238	0.75	188
R1V10	0.8184	0.65	98	0.8184	0.64	97
R1V11	0.8653	0.66	76	0.8654	0.73	82
R1V12	0.9200	0.46	42	0.9200	0.47	43
R1V13	1.0250	0.48	93	1.0259	0.53	100
R1V14	1.0743	0.76	54	1.0742	0.83	56
R1V15	1.1347	0.65	67	1.1344	0.64	65
R1V16	1.2505	0.48	40	1.2507	0.53	43
R1V17	1.3700	0.63	80	1.3701	0.60	77
R1V18	1.7473	0.48	77	1.7473	0.49	78

Table 5.3: **Estimates for vertical modes at position R1.**

Mode no.	Optimisation on $\int P_{zz}(\omega)d\omega$			Optimisation on $P_{zz}(\omega)$		
	f_n (Hz)	ζ (%)	K (10^{-5})	f_n (Hz)	ζ (%)	K (10^{-5})
m16V1	0.1572	2.13	4680	0.1568	1.25	3193
m16V2	0.1799	2.43	7280	0.1801	1.99	6174
m16V3	0.2023	2.23	1786	0.2023	1.95	1553
m16V4	0.3134	1.69	2875	0.3123	1.70	2874
m16V5	0.3861	1.29	1840	0.3856	1.09	1588
m16V6	0.4676	1.34	1010	0.4670	1.09	833
m16V7	0.4852	1.52	1372	0.4852	1.30	1205
m16V8	0.5439	0.94	351	0.5442	0.76	303
m16V9	0.6321	0.63	596	0.6321	0.67	624
m16V10	0.6547	0.93	436	0.6547	1.02	475
m16V11	0.7245	0.64	533	0.7244	0.64	536
m16V12	0.8189	0.74	194	0.8191	0.72	191
m16V13	0.9202	0.49	170	0.9202	0.46	164
m16V14	1.0266	0.51	309	1.0265	0.54	322
m16V15	1.0756	0.74	222	1.0754	0.86	250
m16V16	1.1345	0.57	282	1.1374	0.56	277
m16V17	1.2764	0.63	168	1.2766	0.64	160
m16V18	1.3717	0.53	152	1.3719	0.52	149
m16V19	1.4926	0.48	296	1.4924	0.45	283
m16V20	1.6193	0.64	263	1.6188	0.66	286

Table 5.4: **Estimates for vertical modes at position m16.**

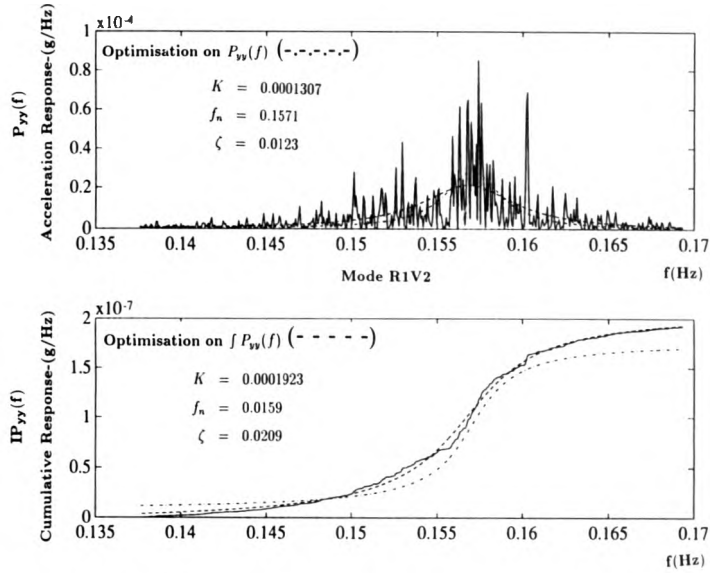

Figure 5.6: Model fitting procedure for vertical mode at position R1V2.

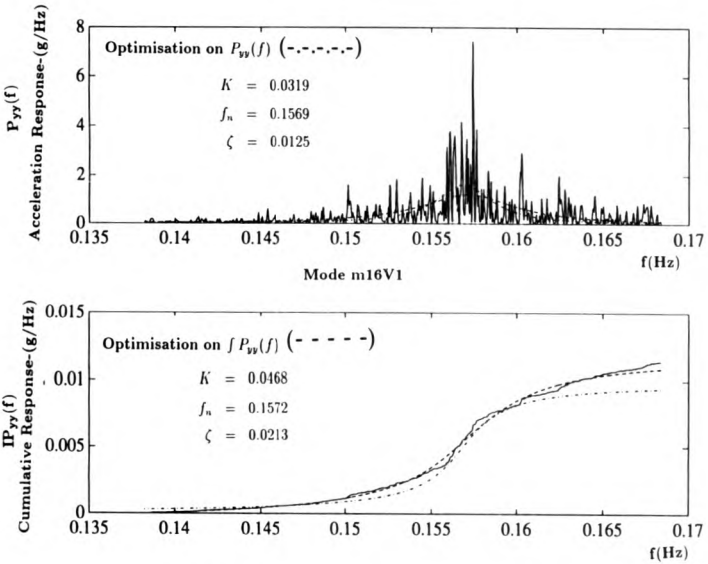

Figure 5.7: **Model fitting procedure for vertical mode at position m16V1.**

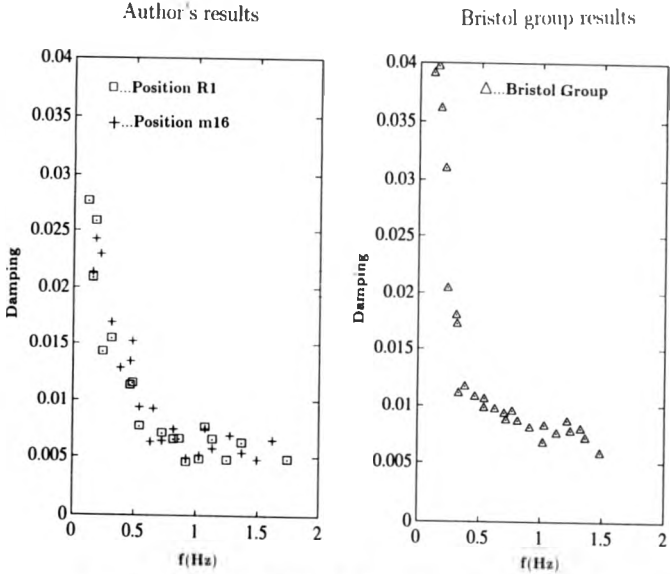

Figure 5.8: **Comparison of damping factors between new and previous design procedure.**

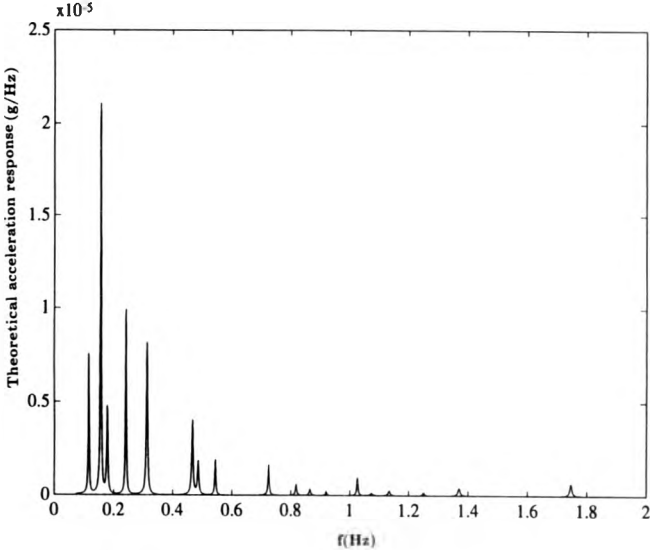

Figure 5.9: **Model power spectral output of vertical mode at position R1.**

5.8 Evaluation of errors due to windowing and averaging over segments.

An attempt is now made to illustrate the accuracy of results obtained in the previous section. Also, a more precise analysis of resulting errors in the damping estimates due to the windowing and averaging process in [4] is given.

The effects on the expected value of the smoothed output power spectrum for the Papoulis and Hanning windows have been studied in chapter (2) section (2.5). For the exact Hanning window this value is evaluated as :

$$\begin{aligned} E\,[\,\hat{\Phi}_{yy}(\omega)\,] &= \frac{1}{2}C_{yy}(\omega) - \frac{1}{2M}\frac{dS_{yy}(\omega)}{d\omega} \\ &+ \frac{1}{4}C_{yy}(\omega+\omega_0) + \frac{3\pi}{16}S_{yy}(\omega+\omega_0) - \frac{1}{2M}\frac{dS_{yy}(\omega+\omega_0)}{d(\omega+\omega_0)} \\ &+ \frac{1}{4}C_{yy}(\omega-\omega_0) - \frac{3\pi}{16}S_{yy}(\omega-\omega_0) - \frac{1}{2M}\frac{dS_{yy}(\omega-\omega_0)}{d(\omega-\omega_0)} \end{aligned} \quad (5.14)$$

where M is the segment length and $\omega_0 = 2\pi/M$.

The terms $C_{yy}(\omega)$, $S_{yy}(\omega)$ are the cosine and sine transforms of the output auto correlation function $r_{yy}(\tau)$ and are defined by :-

$$C_{yy}(\omega) = \int_0^\infty r_{yy}(\tau)cos(\omega\tau)d\tau$$

and

$$S_{yy}(\omega) = \int_0^\infty r_{yy}(\tau)sin(\omega\tau)d\tau.$$

Also for the Papoulis window

$$\begin{aligned} E\,[\,\hat{\Phi}_{yy}(\omega)\,] &= \frac{1}{2}\{C_{yy}(\omega+\omega_0) + \frac{1}{\pi}S_{yy}(\omega+\omega_0) - \frac{1}{M}\frac{dS_{yy}(\omega+\omega_0)}{d(\omega+\omega_0)}\} \\ &+ \frac{1}{2}\{C_{yy}(\omega-\omega_0) - \frac{1}{\pi}S_{yy}(\omega-\omega_0) - \frac{1}{M}\frac{dS_{yy}(\omega-\omega_0)}{d(\omega+\omega_0)}\} \end{aligned} \quad (5.15)$$

where $\omega_0 = \pi/M$.

Although averaging a record of length T over L segments will improve variability, such an effect will also lead to an increase in bias caused by the unavoidable reduction of the segment length from $M = T$ to $M = T/L$.

Assuming the author's evaluation of the bridge data to be a reasonable representation of the bridge dynamics, it should be possible to quantify the error caused by the combination of windowing and reduction of the record length due to the segmental averaging in [4].

To illustrate this, the cosine, sine and differentiated sine transforms of the theoretical output correlation function derived at each mode, are substituted into equation (5.14) to give the expectation of the measured output power spectrum for the Hanning window. An overall power spectral structure is achieved by summing the individual spectrums at each mode. A similar substitution into equation (5.15) gives the expectation of the measured output power spectrum for the Papoulis window.

From the i^{th} mode impulse response

$$g_i(t) = \frac{c_i}{b_i}\exp(-a_i t)\sin(b_i t), \quad \text{where} \quad a_i = \zeta_i\omega_{n_i}, \quad b_i = \omega_{n_i}\sqrt{1-\zeta_i^2}, \quad \text{and} \quad c_i = K_i\omega_{n_i}^2,$$

the output auto correlation function is evaluated using

$$r_{yy_i}(\tau) = \int_0^\infty g_i(t)g_i(t+\tau)dt = \frac{c_i^2}{b_i^2}\exp(-a_i t)[d_i\cos(b_i t) + e_i\sin(b_i t)]$$

where

$$d_i = \frac{1}{4}[\frac{1}{a_i} - \frac{a_i}{a_i^2 + b_i^2}] \quad \text{and} \quad e_i = \frac{b_i}{4(a_i^2 + b_i^2)}.$$

The cosine, sine and derivative of sine transforms at each mode is given by

$$\begin{aligned} C_{yy_i}(\omega) &= \frac{a_i c_i^2 d_i}{2b_i^2}[\frac{1}{a_i^2 + 4(b_i+\omega)^2} + \frac{1}{a_i^2 + 4(b_i-\omega)^2}] \\ &+ \frac{c_i^2 e_i}{b_i^2}[\frac{b_i+\omega}{a_i^2 + 4(b_i+\omega)^2} + \frac{b_i-\omega}{a_i^2 + 4(b_i-\omega)^2}] \end{aligned}$$

$$S_{yy}(\omega) = \frac{c_i^2 d_i}{b_i^2}\left[\frac{b_i+\omega}{a_i^2+4(b_i+\omega)^2}+\frac{\omega-b_i}{a_i^2+4(\omega-b_i)^2}\right] + \frac{a_i c_i^2 e_i}{2b_i^2}\left[\frac{1}{a_i^2+4(b_i+\omega)^2}-\frac{1}{a_i^2+4(b_i-\omega)^2}\right] \quad (5.16)$$

and

$$\frac{dS_{yy}(\omega)}{d\omega} = \frac{c_i^2 d_i}{b_i^2}\left[\frac{a_i^2-4(b_i+\omega)^2}{[a_i^2+4(b_i+\omega)^2]^2}+\frac{a_i^2-4(\omega-b_i)^2}{[a_i^2+4(\omega-b_i)^2]^2}\right] + \frac{a_i c_i^2 e_i}{b_i^2}\left[\frac{4(b_i+\omega)}{[a_i^2+4(b_i+\omega)^2]^2}+\frac{4(b_i-\omega)}{[a_i^2+4(b_i-\omega)^2]^2}\right].$$

In Brownjohn et al [4], given a frequency resolution of 0.003125 Hz, L=100 and results in a record length of T=26880 seconds. Thus, averaging over 100 segments will result to a segment length of M=2688 seconds.

For the Hanning window, the theoretical power spectrum at M=2688 is evaluated from equation (5.14). Similarly the theoretical power spectrum for the Papoulis window at M=2668 is evaluated from equation (5.15). For the above results, figure (5.11) shows theoretical power spectrums for the first tnree modes. On comparison, it is shown that :

(1) windowing with the Hanning weight,

(2) averaging over 100 segment of length M=2668,

will yield unacceptable bias in the power spectrum estimate and in particular, model estimates of damping factor will be too high. It is also noted that the weighting with a Papoulis window yields a better spectral estimator than the Hanning window.

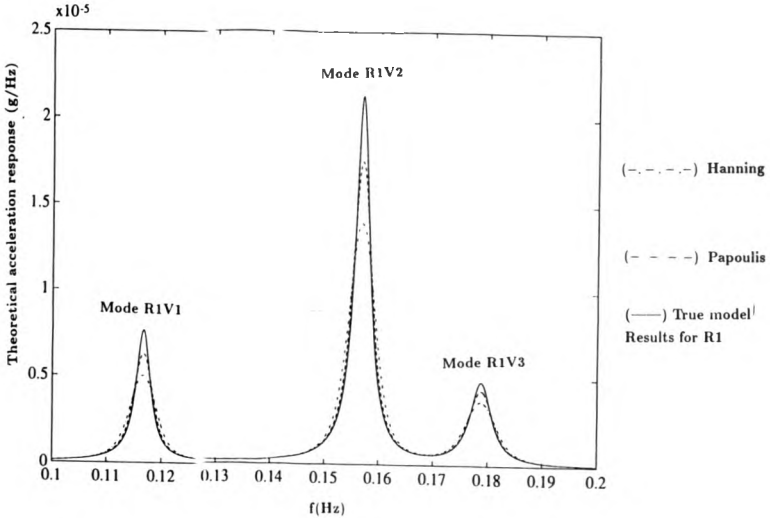

Figure 5.10: Expected value of auto power spectral estimates for M=2688 seconds.

5.9 Summary

Evidence suggests that in order to obtain the best possible model due to ambient testing of the bridge data :-

(i) Averaging over segments should not be implemented so that highest possible frequency resolution can be obtained.

(ii) All acceleration response data should be given a Papoulis weight before spectral analysis and so keep the bias in the resulting estimate to a minimum.

(iii) The least square curve fitting procedure should be adopted on the smoother cumulative power spectrum instead of the unsmoothed power spectrum estimate.

5.10 References for chapter (5).

[1] **Pilkey. W.D. and Cohen. R.,**: 'System identification of vibrating structures - Mathematical models from test data'. The American Society of Mathematical Engineers. New York, 1972.

[2] **Bendat. J.S. and Piersol. A.G.,**: 'Engineering applications of correlation and spectral analysis'. Wiley, New York, 1980.

[3] **Nieman. R.E., Fisher. D.G. and Seborg. D.E.,**: 'A review of process identification and Parameter estimation techniques'. International Journal of Control, April 1971, pp 209-264.

[4] **BrownJohn. J.M. et al.**: 'Ambient vibration measurements of the Humber suspension bridge and comparison with calculated characteristics'. Proc. Instn Civ. Engrs, Part 2,1987, 83, September, pp 561-600.

[5] **Blackman. R.B. and Tukey. J.W.,**: 'Measurement of Power Spectra'. Dover, New York, 1958.

Chapter 6

Conclusions

This chapter summarises the results presented in the thesis, draws conclusions and suggests, possible areas for future research.

Chapter (1) defined from basic principles the frequency response function of open-loop time invariant systems. As well as a brief historical perspective of non-parametric spectral analysis, it discussed qualitatively the effects of windows on spectral estimates.

There exists for review an extensive literature on the statistics of frequency response estimates [1-3]. Reference [3] was chosen for review in this thesis because it gives a clear and concise evaluation of these statistics, whilst at the same time minimising the number of approximations made in error analysis. It also gave a qualitative understanding of the problem from which possible methods of reduction of these statistical errors could be discussed.

As a result, the motivation for the use of asymmetrical windows for open-loop frequency response estimation was proposed in [4] and developed by the author.

Chapter (2) discussed extensively the concept of differing windows on the input and output. In particular, it introduced a general class of window functions (termed Trigonometric sum type windows) which as a subset encompasses a majority of the conventional windows. These new windows were used to evaluate theoretical frequency

response and coherence functions in order to study the effects of different window shapes on bias and variance in the resulting frequency response estimate. Also, for the Hanning and Papoulis family of windows, exact theoretical expressions of auto and cross power spectral estimates (in terms of record length T) were derived and compared.

Many authors recommend the Hanning window because of its excellent variance reduction and relatively good bias properties [4-5] . Little attention in the past has been paid to the minimum bias window developed by Papoulis [6] . This, however, is shown (by the author) to be statistically the superior window.

Factors found to greatly influence the statistics of the measured frequency response function are :-

(1) The record length T.

(2) The position of maximum weight of the input and output windows $w_x(t)$ and $w_y(t)$.

(3) The shape and sharpness of the windows.

(4) The asymmetrical properties of the windows.

(5) The true (or postulated) filter and system transfer function characteristics.

It was also shown that these windows could be chosen to be dependent on a frequency or on a frequency range of interest. In particular, choosing the trigonometric sum type input-output windows by maximising the square coherence function led to improvements in the resulting frequency response estimate. In order to include the above factors, a new procedure based on a priori knowledge of the system characteristics was introduced in chapter (3). Originally proposed by Douce (1987), this novel concept has been extensively developed by the author and has led to the evaluation of **least mean square error windows**.

The methods developed in chapter (3) were applied in chapter (4) to computer simulated realisations of input and output data. These experiments confirmed the predicted

improvement of these least mean square error over conventional windows.

In chapter (5) the Papoulis minimum bias window was used in the modelling of the high Q dynamics of a modern suspension bridge.

It was shown that applying the Papoulis window over the whole record before spectral analysis, and implementing the curve fit on the smooth cumulative spectrum, led to significant reduction in bias when evaluating the model parameters corresponding to each spectral peak.

6.1 Proposals for future work.

The range of application for least mean square error windows introduced in this thesis is by no means exhaustive. Some possible areas of future investigation are now outlined.

6.1.1 Closed-loop systems

Consider the general closed loop system in figure (6.1).

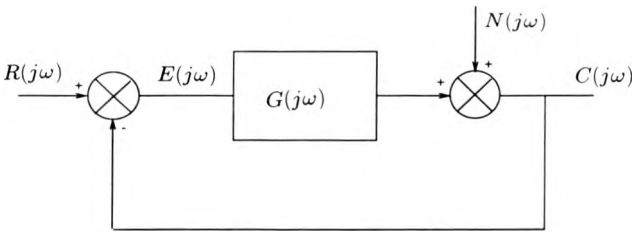

Figure 6.1: **Schematic of closed-loop system**

In the presence of a noise term $N(j\omega)$, it has been shown that the open-loop fre-

quency response estimate based on

$$\overline{G}(j\omega) = \frac{\sum_{i=1}^{L} \Phi_{ec}(j\omega)}{\sum_{i=1}^{L} \Phi_{ee}(j\omega)},$$

is biased [7].

In order to reduce this bias, the estimator used in closed loop conditions is

$$G(j\omega) = \frac{\sum_{i=1}^{L} \Phi_{rc}(j\omega)}{\sum_{i=1}^{L} \Phi_{re}(j\omega)}.$$

It is explained in [4] that transients in closed-loop systems are due to feedback present in both the output and input of the forward path.

The estimation of the closed-loop frequency response will be based on the Fourier transform of $r(t).w_r(t)$, $c(t).w_c(t)$, and $e(t).w_e(t)$, where $w_r(t)$, $w_c(t)$ and $w_e(t)$ are the time windows applied to the reference, output and error signals in the closed-loop schematic.

It is proposed that least mean square error windows of $w_r(t)$, $w_c(t)$ and $w_e(t)$, should be evaluated by considering the control ratio

$$\frac{C(j\omega)}{R(j\omega)} = \frac{G(j\omega)}{1 + G(j\omega)},$$

and the error ratio

$$\frac{E(j\omega)}{R(j\omega)} = \frac{1}{1 + G(j\omega)}.$$

The object would be to :-

(1) Design windows $w_r(t)$ and $w_c(t)$ based on the postulated impulse response

$$\hat{g}_{rc}(t) = \int_0^{\pi} \frac{\hat{G}(j\omega)}{1 + \hat{G}(j\omega)} \exp(j\omega t) d\omega,$$

where $\hat{G}(j\omega)$ is the postulated frequency response of the system. See figure (6.2).

(2) Design window $w_e(t)$ based on the postulated impulse response

$$\hat{g}_{er}(t) = \int_0^\infty \frac{1}{1 + \hat{G}(j\omega)} \exp(j\omega t) d\omega,$$

under the assumption that $w_r(t)$ is the optimum window on the reference signal. See figure (6.3).

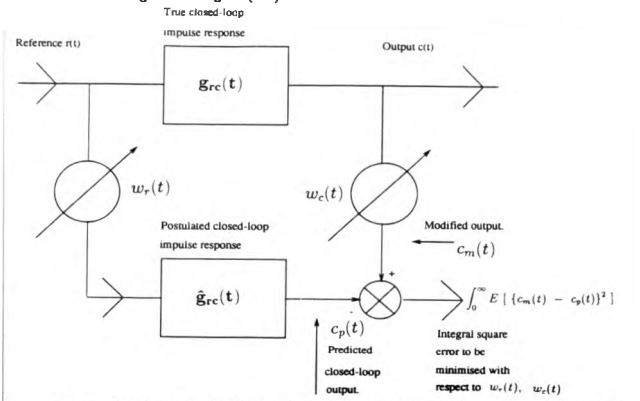

Figure 6.2: Proposed schematic of Least mean square error reference and output windows based on postulated closed-loop transfer function.

6.1.2 Frequency dependent windows.

A further range of possibilities is opened if windows are chosen optimally to vary with the frequency at which the gain is to be determined. The main disadvantage here is that each frequency will require the evaluation of an optimum window pair thus leading to added computation. However it could be possible to design these optimum windows over a specified range of frequencies and so reduce computation time.

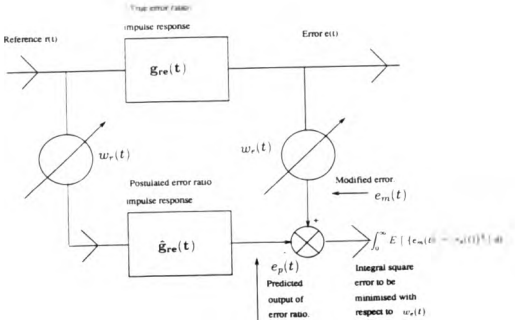

Figure 6.3: **Proposed schematic of Least mean square error window based on postulated error ratio transfer function.**

It was felt that some mention of this work should be made in order to give the reader an appreciation of the complexity of the problem that remains to be solved. Although formulation is only given for white noise input, it must be stated that the author's work on this topic also assumes non-white input, and that the white noise case is only considered here for simplicity.

Figure (6.4) represents the the proposed schematic for the evaluation of frequency dependent least mean square error windows.

6.1.3 Formulation

Consider an excitation applied at time $t = t_1$ such that $0 \leq t_1 \leq T$. We assume that the input is modelled as a series of independent impulses of strength h $N(0, \sigma^2)$, where $\sigma^2 = E[h^2] = \Phi$, with Φ the constant power spectral density of the input signal. The response to this excitation lasts for infinite time but can only be measured over the

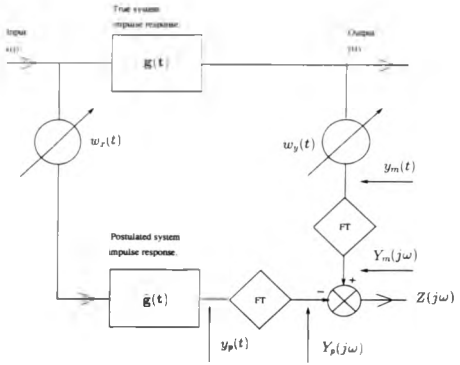

Figure 6.4: **Schematic for frequency dependent Least mean square error windows.**

observation time $0 \leq t \leq T$ of the record due to the unavoidable windowing of the response by $w_y(t)$. Assuming $g(t) = \hat{g}(t)$ the modified system output is

$$y_m(t) = h.\hat{g}(t - t_1)w_y(t)$$

and the short term Fourier transform of $y_m(t)$ is given by

$$Y_m(j\omega) = h.\int_{t_1}^{T} \hat{g}(t - t_1)w_y(t)\exp(-j\omega t)dt$$

For the estimated system output, the input excitation is weighted by $w_x(t_1)$ before it is passed through the postulated system $\hat{g}(t)$ and is given by

$$y_p(t) = h.w_x(t_1)\hat{g}(t - t_1).$$

This response, unlike $y_s(t)$, is observed over $t_1 \leq t \leq \infty$, and when Fourier transformed leads to

$$Y_p(j\omega) = h.w_x(t_1) \int_{t_1}^{\infty} \hat{g}(t-t_1) \exp(-j\omega t) dt.$$

Substituting $u = t - t_1$,

$$\begin{aligned} Y_p(j\omega) &= h.w_x(t_1) \int_0^{\infty} \hat{g}(u) \exp(-j\omega(u+t_1)) du \\ &= h.w_x(t_1) \exp(-j\omega t_1) \hat{G}(j\omega), \end{aligned} \tag{6.1}$$

where $\hat{G}(j\omega)$ is the postulated system frequency response.

The error between the postulated and modified system output is given by

$$\begin{aligned} Z(j\omega) &= h.[\int_{t_1}^{T} \hat{g}(t-t_1) w_y(t) \exp(-j\omega t) dt \\ &- \exp(-j\omega t_1) w_x(t_1) \hat{G}(j\omega)] \\ &= h.[(R_m(\omega) - jI_m(\omega)) - (R_p(\omega) - jI_p(\omega))], \end{aligned}$$

where

$$\begin{aligned} R_m(\omega) &= \int_{t_1}^{T} \hat{g}(t-t_1) w_y(t) \cos(\omega t) dt, \\ I_m(\omega) &= \int_{t_1}^{T} \hat{g}(t-t_1) w_y(t) \sin(\omega t) dt, \\ R_p(\omega) &= w_x(t_1)(\hat{G}_r(\omega) \cos(\omega t_1) + \hat{G}_i(\omega) \sin(\omega t_1)), \end{aligned}$$

and

$$I_p(\omega) = w_x(t_1)(\hat{G}_r(\omega) \sin(\omega t_1) - \hat{G}_i(\omega) \cos(\omega t_1)).$$

Dropping the dependence on ω, the function to be minimised is

$$\begin{aligned} I &= E[Z.Z^*] \\ &= \Phi.[R_m^2 + I_m^2] - 2\Phi.[R_p R_m + I_p I_m] + \Phi.[R_p^2 + I_p^2]. \end{aligned} \tag{6.2}$$

The solution for a frequency dependent input window is achieved by setting

$$\frac{\partial I}{\partial w_x(t_1)} = 0.$$

In equation (6.2),

$$\begin{aligned} R_p^2 + I_p^2 &= \Phi.w_x^2(t_1)[\bar{G}_r^2 \cos^2(\omega t_1) + \bar{G}_i^2 \sin^2(\omega t_1) \\ &+ \bar{G}_r^2 \sin^2(\omega t_1) + \bar{G}_i^2 \cos^2(\omega t_1)] \\ &= w_x^2(t_1).\Phi.[\bar{G}_r^2 + \bar{G}_i^2], \end{aligned}$$

the derivative of which is given by

$$\frac{d[\bar{G}_r^2 + \bar{G}_i^2]}{dw_x(t_1)} = 2w_x(t_1).\Phi.[\bar{G}_r^2 + \bar{G}_i^2]. \tag{6.3}$$

Differentiating the second term in equation (6.2) gives

$$\Phi.(\bar{G}_r \cos(\omega t_1) + \bar{G}_i \sin(\omega t_1)) \int_{t_1}^{T} \bar{g}(t - t_1) w_y(t) \cos(\omega t) dt$$

$$+ \Phi.(\bar{G}_r \sin(\omega t_1) - \bar{G}_i \cos(\omega t_1)) \int_{t_1}^{T} \bar{g}(t - t_1) w_y(t) \sin(\omega t) dt. \tag{6.4}$$

The combination of equations (6.3) and (6.4) leads to the least square frequency

dependent input window.

$$w_x(t_1) = \frac{\hat{G}_r}{\hat{G}_r^2 + \hat{G}_i^2} \int_{t_1}^{T} \hat{g}(t - t_1) w_y(t) \cos(\omega(t - t_1) dt + \frac{\hat{G}_i}{\hat{G}_r^2 + \hat{G}_i^2} \int_{t_1}^{T} \hat{g}(t - t_1) w_y(t) \sin(\omega(t - t_1) dt. \quad (6.5)$$

Similar consideration for the output window however, leads to a solution of the form

$$\int_0^T w_y(t) f_y(\hat{g}, \hat{G}_r, \hat{G}_r, \omega) = \int_0^T w_x(t) f_x(\hat{g}, \hat{G}_r, \hat{G}_r, \omega),$$

where f_x and f_y are functions related to the postulated systems characteristics.

As the required window $w_y(t)$ is also within an integration, an analytical solution could not be found. It was also found that conditions by which $w_y(t)$ could be taken out of this integral, could not be satisfied.

However in chapter (3), we note that the least mean square error window pairs are mirror images of each other about time T/2. If this assumption is made also for frequency dependent windows, a solution would lead to,

$$w_y(t_1) = \frac{\hat{G}_r}{\hat{G}_r^2 + \hat{G}_i^2} \int_0^{t_1} \hat{g}(t_1 - t) w_y(t) \cos(\omega(t_1 - t) dt + \frac{\hat{G}_i}{\hat{G}_r^2 + \hat{G}_i^2} \int_0^{t_1} \hat{g}(t_1 - t) w_y(t) \sin(\omega(t_1 - t) dt. \quad (6.6)$$

Substituting equation (6.5) into (6.6) and equation (6.6) into (6.5) will lead to formulation of the two Fredholm integral equation pairs to be solved :-

$$w_x(t_1) = \int_0^T w_x(\tau) K_x(t_1, \tau, \omega) d\tau, \quad (6.7)$$

$$w_y(t_1) = \int_0^T w_y(\tau) K_y(t_1, \tau, \omega) d\tau. \tag{6.8}$$

where

$$K_x(t_1, \tau, \omega) = \begin{cases} \int_{t_1}^{T} \varphi(t - t_1, t - \tau, \omega) dt & \text{for } 0 \leq \tau \leq t_1 \\ \\ \int_{\tau}^{T} \varphi(t - t_1, t - \tau, \omega) dt & \text{for } t_1 \leq \tau T \end{cases},$$

$$K_y(t_1, \tau, \omega) = \begin{cases} \int_0^{\tau} \varphi(t_1 - t, \tau - t, \omega) dt & \text{for } 0 \leq \tau \leq t_1 \\ \\ \int_0^{t_1} \varphi(t_1 - t, \tau - t, \omega) dt & \text{for } t_1 \leq \tau T \end{cases},$$

and

$$\begin{aligned} \varphi(t - t_1, t - \tau, \omega) &= \frac{1}{\hat{G}_c^2 + \hat{G}_s^2} [\hat{G}_c^2 \gamma_c(t - t_1)\gamma_c(t - \tau) \\ &+ \hat{G}_c \hat{G}_s \hat{g}(t - t_1)\hat{g}(t - \tau) \sin \omega(2t - t_1 - \tau) \\ &+ \hat{G}_s^2 \gamma_s(t - t_1)\gamma_s(t - \tau)], \end{aligned}$$

$$\gamma_c(t - t_1) = \hat{g}(t - t_1) \cos \omega(t - t_1),$$

$$\gamma_c(t - \tau) = \hat{g}(t - \tau) \cos \omega(t - \tau),$$

$$\gamma_s(t - t_1) = \hat{g}(t - t_1) \sin \omega(t - t_1),$$

and

$$\gamma_s(t - \tau) = \hat{g}(t - \tau) \sin \omega(t - \tau).$$

In sections (3.8) and (3.10) of chapter (3), a solution for the least mean square windows was evaluated through the method of successive approximation. However a particular problem arises when applying this method for least mean square windows that

are dependent on the frequency of interest. The introduction of the cosine and sine terms in the evaluation of the kernels, leads to a inability to apply the constraint of absoluteness in the evaluation of the window function. By this we mean that the solution for any least mean square error window must satisfy the condition

$$w_x(t) \geq 0, \quad \text{and} \quad w_y(t) \geq 0, \quad \text{for} \quad 0 \leq t \leq T.$$

Under the condition of absoluteness, the solution will be uniformly (or absolutely) convergent [8]. If this constraint is violated, the the solution is said to be weakly convergent. To ensure absolute convergence in the solution , the kernel defined in the square

$$0 \leq t_1 \leq T, \text{ and } 0 \leq \tau \leq T,$$

must take either all positive or negative values. Therefore a modification of the function defining the kernels K_x and K_y will need to be made. These modification are defined by

$$K_x(t_1, \tau, \omega) = \begin{cases} \int_{t_1}^{T} \mid \varphi(t - t_1, t - \tau, \omega) \mid dt & \text{for} \quad 0 \leq \tau \leq t_1 \\ \\ \int_{\tau}^{T} \mid \varphi(t - t_1, t - \tau, \omega) \mid dt & \text{for} \quad t_1 \leq \tau T \end{cases}$$

and

$$K_y(t_1, \tau, \omega) = \begin{cases} \int_{0}^{\tau} \mid \varphi(t_1 - t, \tau - t, \omega) \mid dt & \text{for} \quad 0 \leq \tau \leq t_1 \\ \\ \int_{0}^{t_1} \mid \varphi(t_1 - t, \tau - t, \omega) \mid dt & \text{for} \quad t_1 \leq \tau T \end{cases}.$$

To date the author has not been able to apply the constraints of absoluteness prior to the formulation of the problem. Applying such a constraint after formulation as been adopted with some success. In some systems, estimation of frequency responses based

on such windows have been found to be better than their conventional and frequency independent counterparts. But for other systems and at some frequencies, the resulting estimates are very poor indeed. From this, it must be assumed that applying the constraint of absoluteness prior to analysis is not the same or equivalent to applying this constraint after.

Many other techniques and procedures have been adopted by the author and it is believed that in time, and with contributions from other readers, a solution will be found.

6.2 References for chapter (6).

[1] **Akaike. H. and Yamanouchi. Y.,**: 'On the statistical estimation of frequency response functions'. An. Inst. Statistical Mechanics,. Vol 14, No 1, 1962, pp 23-56.

[2]. **L.Ljung**: 'System identification: Theory for the user'. Prentice-Hall information and system sciences series. 1987.

[3] **Douce. J.L. and Balmer. L.,**: 'The statistics of frequency response estimates'. Proc,IEE., vol 137,Pt.D,No 5,September 1990.

[4] **Balmer. L.,**: 'Short term spectral estimation with applications'. Ph.D. Thesis,University of Warwick,1986.

[5] **Bendat. J.S. and Piersol. A.G.,**: 'Engineering applications of correlation and Spectral analysis. Wiley, New York, 1980.

[6] **Papoulis. A.,**: 'Minimum bias windows for high resolution spectral estimates'. Trans. IEEE, vol.IT-19,pp9-12,No. 1.January 1973.

[7] **Wellstead. P.E.,**: 'Aspects of real-time digital spectral analysis'. Ph.D Thesis, University of Warwick, 1970.

[8] **Pogrzelski. W.,**: 'Integral equations and applications'. Graylock press. Rochester, New York, 1957.